NASA CR-72653
ALRC-2100-3

FINAL REPORT NO. 2
(FOLLOW-ON PROGRAM)

COATINGS FOR REGENERATIVE ENGINES

by

W. J. LEWIS

AEROJET LIQUID ROCKET COMPANY
SACRAMENTO, CALIFORNIA 95813

Prepared for

NATIONAL AERONAUTICS AND SPACE ADMINISTRATION

NASA Lewis Research Center
Contract NAS 3-7955
Rudy Duscha, Project Manager

NASA CR-72653

ALRC-2100-3

FINAL REPORT NO. 2

(Follow-On Program)

COATINGS FOR REGENERATIVE ENGINES

Prepared for

NATIONAL AERONAUTICS AND SPACE ADMINISTRATION

6 July 1970

CONTRACT NAS 3-7955

Prepared by:

AEROJET LIQUID ROCKET COMPANY
P. O. Box 13222
Sacramento, California 95813

AUTHOR: W. J. Lewis
Project Engineer

APPROVED: V. Frick
Project Manager

Technical Management:

NASA LEWIS RESEARCH CENTER
21000 Brookpark Road
Cleveland, Ohio 44135

APPROVED: Rudy Duscha
Project Manager
Chemical Rocket Division

FOREWORD

This final report is a summary of the follow-on work conducted by the Aerojet Liquid Rocket Company, Sacramento, California, under Contract NAS 3-7955. It covers the period 1 July 1968 through 30 January 1970. The contract was sponsored by the Lewis Research Center of the National Aeronautics and Space Administration and was administered under the technical direction of the Chemical Rocket Division with Mr. Rudy Duscha as Project Manager.

The author wishes to acknowledge the significant contributions of Mr. A. Oare, who designed the injector and chamber for the coating evaluation and Mr. L. Schoenman, who conducted the heat transfer analysis.

ABSTRACT

Plasma-sprayed thermal barrier coatings were evaluated for the flame surface of a regeneratively-cooled chamber operating with flox/hydrocarbon propellants. The coatings were subjected to laboratory screening tests using a plasma torch to simulate the thermal environment. Coatings also were placed into the exhaust stream of a flox/propane rocket engine to simulate the chemical environment. Concurrently, an injector and rectangular chamber were designed to operate with flox/methane propellants. Two, replaceable, cooled test panels formed the convergent-divergent contour of the chamber. Plasma-sprayed coatings were applied to the test panels and evaluated in the exhaust stream at the chamber, throat, and exit areas. These tests revealed that the coating system consisting of a flame liner of tungsten (>95% density) provided the lowest regression rate.

TABLE OF CONTENTS

TABLE OF CONTENTS (cont.)

LIST OF TABLES

LIST OF FIGURES

LIST OF FIGURES (cont.)

I. SUMMARY

Thermal barrier coatings were developed for the flame surface of a regeneratively-cooled chamber operating with flox/hydrocarbon propellants. Previous studies (Ref. 2), wherein tube specimens were exposed to the exhaust of a flox/propane engine, have shown that the lowest regression rates were obtained with flame liners containing 100% W, Mo or ZrC. In the program being reported, the coatings studied were modified by increasing the flame liner density through additions to the liner material and by altering the plasma-arc spraying procedures.

The modified coatings were subjected to laboratory screening tests using a plasma torch to simulate the thermal environment only. Tests also were conducted with coated five-tube specimens placed into the exhaust stream of a flox/propane rocket engine to simulate the chemical environment. During these tests, the specimens were cooled similarly to tubes in a regeneratively-cooled chamber.

Increasing the density of the plasma-sprayed tungsten flame liner resulted in significantly lower regression rates. The regression rate of 87% dense, plasma-sprayed, tungsten flame liners was 0.4 mils/sec (1.016×10^{-5} m/sec) as compared to less than 0.1 mils/sec (2.54×10^{-6} m/sec) for 95% dense tungsten. Improved carbides and silicide additives in the coatings offered no significant improvement in regression. Therefore, the dense tungsten flame liner was recommended for further evaluation for subscale testing in the rectangular test chamber using flox/methane as the propellants.

Concurrent with the coating evaluation, an injector and rectangular chamber were designed and fabricated to operate with flox/methane propellants. The chamber was designed so that two, replaceable, cooled test panels formed the convergent-divergent contour of the chamber. These panels were exposed to the flox/methane exhaust gases at the throat, chamber, and exit areas. The thrust chamber and test specimen were designed to be water-cooled by separate manifolds.

Reversed triplet (O-F-O) element injectors were designed with a rectangular grid, cross-drilled manifold for the oxidizer circuit and a "flooded-back" manifold for the fuel circuit. A nickel rigimesh injector face, cooled with methane, was required to prevent the injector face from overheating.

Satisfactory operation was obtained with the injector and test chamber for mixture ratios from 3.9 to 5.8, chamber pressures from 336 to 470 psia, (23.2×10^5 to 32.4×10^5 N/m^2) and durations of up to 30 sec. Oxidizer streaks were experienced along the chamber wall, but these were eliminated by utilizing a mixer section between the injector and chamber.

Plasma-sprayed coatings, consisting of an underlayer of 5 mils (12.7×10^{-5} m) of 55% W and 45% Al_2O_3 to provide a thermal resistance of 180 in.^{2} sec-°F/Btu (6.12×10^{-5} m^2 sec °K/J) with top coats of tungsten for the flame liner,

were evaluated in the rectangular tester. The regression rate of the tungsten coatings (95% density) in the non-streaked areas was 0.02 mils/sec (5×10^{-7} m/sec) for 45 sec of total exposure. The regression rate of the tungsten with a density of 80% was 0.1 mils/sec (2.54×10^{-6} m/sec). In the oxidizer-streaked areas, the coatings were completely eroded down to the primer.

Spalling was also observed in the coatings of these cooled specimens. This spalling occurred between the tungsten flame liner and tungsten-Al_2O_3 layer. At this interface, the tungsten liner is deposited on the layer which contained 55% tungsten by weight or 70% by volume. In plasma-sprayed coatings, the metal does not adhere as well to a ceramic substrate as to a metal substrate. To minimize spalling, the coating should be graduated with increasing metal content from the substrate to the surface which would provide a metal-rich substrate for the application of the 100% tungsten flame liner.

II. INTRODUCTION

This program was conducted to develop thermal barrier coatings for the flame surface of regeneratively-cooled thrust chambers operating with flox/hydrocarbon propellant combinations. The coating would provide sufficient thermal resistance (thickness/thermal conductivity) to reduce the heat flux to the coolant while remaining compatible with the exhaust gas environment of the engine.

In the previous program (Ref. 1), W, Mo, Al_2O_3, ZrO_2, and ZrC coatings were evaluated by exposing coated five-tube specimens to the exhaust stream of a flox/propane rocket engine. These specimens were water-cooled during the tests to simulate regeneratively-cooled tubes in a chamber. The exhaust environment was more severe than at the throat of the chamber because of air entrainment as evidenced by the severe regression in the graphite shields.

Because of the air entrainment, the regression data were not directly related to actual service; however, the data were adequate for comparative purposes. With the severe exhaust environment, regression rates of 0.4 mil/sec (1.016×10^{-5} m/sec) were obtained with flame liners consisting of pure W, Mo, and ZrC/C. Regression rates increased as the ceramics Al_2O_3 and ZrO_2 were added to the flame liners.

Based upon these studies, the subject program was conducted to improve coating performance by both refining the coating system and evaluating the coating in an environment representative of actual service. Coating refinement was accomplished by increasing the density of the flame barrier from the existing 88% to greater than 95% of theoretical density. This increased density resulted in a decreased regression rate in solid rocket motor firings made under controlled conditions (Ref. 1). In these firings, regression rates of 5 mils/sec (12.7×10^{-5} m/sec) were obtained with densities of 65% dense tungsten as compared to 4 mils/sec (10.16×10^{-5} m/sec) for 75% dense tungsten and zero regression for 100% dense tungsten.

To provide an environment simulating those conditions actually existing in a rocket engine, a rectangular chamber was designed and fabricated wherein test panels were exposed to the combustion gas at the throat, chamber, and exit cone areas.

The coating improvement evaluation, the design and fabrication of the rectangular test chamber, and the coating evaluation are reported herein.

III. MATERIAL SELECTION AND EVALUATION IN FLOX/PROPANE ENVIRONMENT

A. BACKGROUND

The method of selecting materials for the thermal barrier coating was detailed in the final report of the original program (Ref. 2). Selection was based upon the use of a theoretical 5000 lb (2270 Kg) thrust engine operating at 100 psia (689×10^3 N/m^2) chamber pressure and at a flox/propane mixture ratio of 4.5. With this engine, the coating was required to have a thermal resistance (thickness/thermoconductivity) of 1400 in.^{2} sec-F/Btu (5.2×10^{-4} m^2 sec °K/J), and operate at a surface temperature of 3000°F (1922°K). The exhaust-gas environment at the throat of the engine was calculated to be 55.7% HF, 24.7% CO, 9.5% H_2, 10% F, and 0.1% C_2F_2.

Thermodynamic calculations were made for the candidate materials and the exhaust gas species using available free-energy data (Ref. 2). It was assumed that complete equilibrium was reached and that the reaction occurred at 70 psia (482×10^3 N/m^2), at temperatures of 3000°F (1922°K), 4000°F (2480°K) and 5000°F (3033°K).

Table I is a summary of thermodynamic analysis results for the compatibility of the refractory metals with the exhaust gas species. At 3000°F (1922°K), all of the metals, except hafnium, are compatible with HF, but all of the metals react with F_2. Tungsten and iridium are compatible with CO. Carbon is compatible with HF but reacts with both H and F.

Table II is a summary of thermodynamic analysis results for the compatibility of the ceramic materials with the exhaust gas species at 3000°F (1922°K). The ceramic materials are compatible with CO but, generally, are not compatible with the fluorine gas species or hydrogen. Only Al_2O_3 and SiO_2 are not expected to react with HF. Based upon the thermal and chemical environment as well as the material properties, W, Mo, Al_2O_3, and ZrO_2 were selected for the basic thermal barrier materials.

The coatings were subjected to laboratory screening tests using a plasma torch to simulate the thermal environment only of the flox/propane engine. The final tests consisted of exposing coated, five-tube specimens to the exhaust stream of a flox/propane rocket engine. Specimens were water-cooled during these tests, thereby simulating a regeneratively-cooled chamber. The specimen was positioned in the exhaust stream in a manner that exhaust gas species, gas velocities, and temperatures at the specimen surface were similar to throat conditions. Severe regression was experienced on the graphite shield used to protect specimen water inlets. This graphite regression indicated a considerable oxidation attack, but it was not possible to determine the effect of this air entrainment upon coating performance.

The best coatings were obtained using:

- 3 to 5 mils (7.6 to 12.7×10^{-5}m) of nichrome for primer
- 10 mils (25.4×10^{-5}m) of 20% Ni-80% Al_2O_3 for thermal resistance

TABLE I. - COMPATIBILITY OF REFRACTORY METALS WITH FLOX/PROPANE EXHAUST GAS SPECIES

		Compatibility at 3000°F (1922°K) and 70 psia (482×10^3 N/m^2) that is based[1] on Free Energy Calculations			
Material	HF	CO	H	F	C_2F_2
W	NR	NR	NR	R	R
Mo	NR	R	NR	R	R
Ir	NR	NR	--	R	NR
Hf	R	R	--	R	R
Ta	NR	R	--	R	R
C	NR	--	R	R	--

(1) NR = Reaction not probable
R = Reaction probable

TABLE II. - COMPATIBILITY OF CERAMICS WITH FLOX/PROPANE EXHAUST GAS SPECIES

		Compatibility at 3000°F (1922°K) and 70 psia (482×10^3 N/m^2) that is based[1] on Free Energy Calculations			
Material	HF	CO	H	F	C_2F_2
Al_2O_3	NR	NR	R	R	R
ZrO_2	R	NR	R	R	R
HfO_2	R	NR	R	R	R
SiO_2	NR	NR	NR	R	R
ZrB_2	R	NR	R	R	R
TiB_2	R	NR	R	R	R

(1) NR = Reaction not probable
R = Reaction probable

- 14 mils (35.6×10^{-5}m) of 30% Mo-70% Al_2O_3 for thermal resistance
- 15 to 20 mils (38 to 50.8×10^{-5}m) of W, Mo, or ZrC/C for the flame barrier

The lowest regression rates, 0.4 mils/sec (1.016×10^{-5}m/sec), of coatings exposed to the flox/propane environments occurred with top coats of 100% Mo, W, or ZrC/C, but this is too high for practical use. It was concluded that this high regression rate was partially attributable to oxidation resulting from air entrainment as indicated by the severe regression observed on the graphite shield which was expected to have good compatibility with fluorinated exhaust gas. However, graphite regression would be expected to be severe in oxidation environments.

The high coating regression also resulted from the porosity in the coatings. Plasma-sprayed coatings are estimated to be 75% to 90% dense, which results in considerable porosity between the sprayed particles. In operation, the coatings are attacked at the particle boundaries and the particle is lifted into the exhaust stream. Therefore, the regression resistance of the pure metal coatings would be improved by increasing the density and purity of the coating to reduce mechanical forces and chemical degradation as observed in other nozzle materials (Ref. 1). Further, the regression resistance of carbide coatings would be improved by minimizing oxidation during spraying.

B. EVALUATION PROCEDURES

Studies to decrease regression of the thermal barriers in the fluorinated environment were conducted by increasing the density of the coating, decreasing oxides in carbide coatings, and evaluating silicate additions to the coatings. The coatings were prepared and evaluated using the procedures reported for the original program effort (Ref. 2).

1. Specimen Preparation

Two types of specimens were used in the evaluation of the thermal barrier; a disk coupon and a five-tube, internally-cooled specimen. The disk specimens were evaluated in the laboratory while the five-tube specimen was evaluated in the exhaust stream of a flox/propane combustor.

The disk and tube specimens were prepared by plasma torch spraying a candidate coating on a stainless-steel disk, 0.025-in. (6.4×10^{-4}m) thick x 3.25-in. (1.083 m) diameter. These disks were first grit-blasted on one surface using 24-mesh silicon carbide grit to produce a 250 to 300 rms micro-inch surface roughness. A 0.25-in. (6.4×10^{-4}m) wide ring at the perimeter of the disk was shielded from the grit blast to provide a sealing surface for O-rings when the disk is installed in a water-cooled holding fixture.

After being grit-blasted, the disks were plasma-spray coated using a 35 kw plasma torch, a powder feeder, and specimen-positioning fixture.

The plasma torch was mounted horizontally on a screw-driven traversing head to permit lateral travel across the specimen face at a programmed speed of 12 in./min (8.5×10^{-5}m/sec). A shield of argon gas was maintained around the spray cone and spray impingement area to exclude air from the test specimen hot surface.

The disk test specimen and five-tube specimen were held in a frame that was mechanically-oscillated vertically in front of the torch at a predetermined oscillation rate and amplitude; specimen surface speed was 300 in./min (0.002 m/sec). During deposition, cooling water was pumped through the specimen holder (disk specimen) or specimen tubes. The deposition rate of the plasma sprayed coatings was approximately 2 mils/pass (5.1×10^{-5}m/pass).

2. Laboratory Disk Tests

The equipment used for thermal shock testing of thermal barrier coatings on disk specimens as well as coatings on five-tube specimens largely was similar to that used for spraying. A specially-designed test bench was used for cycling specimens in the plasma torch flame under controlled heat flux conditions. The torch-generated heat flux was measured with a water-cooled calorimeter while the specimen flame surface temperature was measured continuously with a Pyro-650 recording pyrometer (Instrument Development Laboratories, Inc.), which was aligned, before each test, to view the center of the plasma flame impingement area on the specimen. The distance of the gun nozzle from the specimens or the calorimeter was adjusted to obtain the necessary heat flux at the specimen surface. A 150 psig (10.3×10^5 N/m^2) water system was used to cool the specimen, calorimeter, and torch.

Plasma gases were supplied to the torch through flowmeters. Nitrogen served as the plasma flame carrier gas with argon gas being introduced immediately downstream of the nozzle to provide an inert gas shield over the flame impingement area.

The condition of the coatings during flame exposure was visually observed to detect melting, cracking, or spalling. Following thermal shock testing, the coatings were subjected to further visual examination under 40X magnification.

3. Flox/Propane - Five-Tube Tests

The flox/propane test was designed to establish the compatibility of the thermal barrier coatings with the thermal and chemical environment of the exhaust stream of a flox/propane engine. The five-tube coated specimens were placed at the exit of the chamber at an angle of 22 degrees with the centerline of the chamber. The position of the specimen was established by the heat transfer and flow analyses described in the initial program report (Ref. 2).

The combustor consisted of a 17-element injector (P/N 709151-21) having an orifice pattern of nine triplets (F-O-F) and eight doublets (O-F).

Fuel orifices were 0.0177 in. (4.5×10^{-4}m) diameter and oxidizer orifices were 0.0295 in. (7.5×10^{-4}m) diameter. The injector face was fabricated from nickel.

A 0.5-in. (0.013 m) thick graphite liner extended the full length of the chamber, which was water-cooled, including the adapters used to hold the injector and nozzle. The water-cooled nozzle was fabricated from Nickel 200. Coolant flow was directed axially with water inlets located at the forward end and the outlets were rotated 90-degrees at the aft end. Chamber throat diameter was 1.135-in. (0.02885 m).

The five-tube, coated specimens were tested in the exhaust stream by placing them at the downstream edge of the nozzle at precisely the same position for each test. A graphite shield was used in all of the flox/propane tests to prevent gas from flowing along the sides of the coated specimen as well as to protect the water inlet. This shield was positioned directly in front of the specimen and impingement upon the coated specimen was accomplished through a window machined 0.5-in. (0.013 m) wide and 3.5-in. (0.089 m) long.

C. LABORATORY EVALUATION

The laboratory evaluations were concerned with increasing the density of the flame liner by:

- Adding ductile metals to the spray mixture to fill the pores around the tungsten particles.
- Alloying the liner to promote densification in the post-spray heating.
- Utilizing a new proprietary plasma procedure developed by Union Carbide.

Disk coupons were plasma-sprayed for use in these evaluations, which consisted of thermal stability tests in the plasma tester and metallographic examinations. These disk coupons were:

- Grit-blasted to a 250 micro-inch surface finish
- Primed with a 2 mil (5.1×10^{-5} m) layer of Nichrome
- Plasma-coated with a 3 mil (7.6×10^{-5} m) Al_2O_3 layer
- Top-coated with a 10 mil (25.4×10^{-5} m) layer of the flame barrier mixture

Following spraying, the specimens were plasma tested for 20 sec using a heat flux of 10 Btu/in.^{2}-sec (164×10^5 J/m^2 sec) which resulted in coating surface

temperatures ranging from 3000°F to 3500°F (1922°K to 2200°K). Then, the disk specimens were sectioned and examined metallographically.

1. Flame Liner Density Increase

The density of the metallic W and Mo plasma-sprayed flame liners previously evaluated in this program are estimated to range from 75% to 88% of theoretical density. These estimates are based upon tungsten coating data obtained in the Polaris Program wherein the conventional plasma-sprayed tungsten coatings ranged from 75% to 85% theoretical density. The spray coatings applied with the Union Carbide proprietary process ranged from 85% to 88% theoretical density. Coatings applied using both the conventional and proprietary processes were evaluated and described in the initial program report (Ref. 2). The higher density coating demonstrated superior regression resistance.

Further improvements in the proprietary plasma spraying process at Union Carbide resulted in tungsten deposits with densities of 95% of theoretical or greater. The use of this dense tungsten coating was the first selection to improve the regression rate of the coatings. Laboratory evaluations were not made of these dense coatings which were evaluated in the flox/propane tests.

A second technique evaluated for density improvement was the addition of ductile metals (i.e., NiAl, Ni, Nichrome, and copper) to the sprayed tungsten matrix for the purpose of filling pores and gaps around the W and Mo particles. The plasma torch disk samples were used in preliminary evaluations, the results of which are summarized on Table III. Metallographic examination of specimens F-1 through F-15 showed that melting had occurred during the plasma tests. In specimens F-1, F-3, and F-5, the W and NiAl alloyed resulting in melting points below the 3000°F (1922°K) surface temperature. In specimens F-11, F-13, and F-15, the copper melted out of the tungsten matrix. As a result of the W-Ni alloying observed and the significant loss of copper, these concepts were eliminated from further evaluation.

The density of the plasma-sprayed coatings also could be increased by heating after plasma spraying. Evidence of densificiation was observed in metallographic examination of a molybdenum liner by comparison of the fired and unfired part of the specimen (Ref. 2). This tendency for coatings to undergo densification was further explored as a means of density improvement. Attempts to densify the coatings were made by post-spray heating them in the plasma flame using an inert atmospheric shroud. The stainless steel substrate was water-cooled.

Tungsten powder that had been coated with approximately 0.2% Ni and 0.3% Cu was used to promote densification. The use of Ni and Cu to accelerate densification was based upon the work of McIntyre (Ref. 3). He reported sintering temperature as low as 2200°F in tungsten containing only 0.3% nickel and 0.2% copper by weight, compared to the normal sintering

TABLE III. - RESULTS OF LABORATORY TESTS OF DISK SPECIMENS

Spec. No.	Coating Composition, Wt %	Regression Rate, Increased Density Evaluation		Metallographic Examination Results of Plasma Heated Area
		mils/sec	m/sec	
F-1	10% NiAl - 90% W	0.3	0.76×10^{-5}	Regression due to melting and alloying of W and NiAl.
F-3	20% NiAl - 80% W	0.3	0.76×10^{-5}	Same as F-1.
F-5	50% NiAl - 50% W	0.1	0.25×10^{-5}	Heated area completely melted and alloyed.
F-7	10% Ni - 90% W	(Spalled during spraying)		
F-9	10% NiCr - 90% W	(Spalled during spraying)		
F-11	10% Cu - 90% W	0.3	0.76×10^{-5}	Cu infiltrated throughout specimens except heated area in which it melted out.
F-13	20% Cu - 80% W	0.2	0.5×10^{-5}	
F-15	50% Cu - 50% W	0.55	1.4×10^{-5}	Excessive amount of copper which melted out during heating.
F-41	Ni-Cu coated Tungsten	0.25	0.64×10^{-5}	Surface melted. NiCu content may be too high.
F-42	Ni-Cu coated Tungsten	0.25	0.64×10^{-5}	Same.
		Silicides Evaluation		
F-17	5% Si - 95% W	0.05	0.13×10^{-5}	Heated area porous indicating silica melted out during the test. F-23 more porous than F-17, F-19, or F-21.
F-19	10% Si - 90% W	0.0		
F-21	20% Si - 80% W	0.0		
F-23	40% Si - 60% W	0.0		
F-34	100% W Si_2	0.0		Three small melted areas about 1/16-in. (15.84×10^{-4} m) diameter
F-35	100% W Si_2	0.0		Melted areas not observed.

temperature of 3500°F to 4000°F (2200°K to 2480°K) for tungsten. In addition, the Ni-Cu coating could be expected to minimize oxidation of the tungsten powder during spraying. Disk specimens sprayed with the Ni-Cu coated tungsten powder were reheated for densification by placing them in the spray fixture and oscillating the plasma torch over the coated surface for 300 sec. The backside of the disk was water-cooled as is done in the spraying operation and the flame surface was shielded with argon gas to minimize oxidation. Examination of the coating after the post-spray heating revealed no indication of oxidation.

Metallographic examination of specimens F-41 and -42 (see Table III), which were plasma-sprayed with the coated tungsten powder, revealed a microstructure similar to uncoated tungsten powder. However, the coatings performed satisfactorily in the plasma evaluation. Also, the densification could occur during test firing (Ref. 2). Consequently, the coated tungsten powder was selected for evaluation in the flox/propane tests.

2. Silicide Coatings Evaluation

Silicide coatings were evaluated based upon the free energy of formation calculations reported in Reference 2. These calculations indicate SiO_2 is compatible with HF at 70 psia (482×10^3 N/m^2) and 3000°F (1922°K). However, both Si and SiO_2 react with F. The rate of the F-SiO_2 reaction could be low at the required conditions. This would permit silicon compounds to provide regression resistance even in the fluorinated exhaust. Also, the use of silicon has been successful in providing oxidation-resistant slurry and plasma coating. It would improve regression resistance by providing resistance to chemical attack in areas of low fluorine concentration.

Disk specimens were plasma-sprayed with both W-Si and W Si_2 powder mixtures and evaluated. The results of laboratory plasma tests of these coatings are shown on Table III. The regression resistance of the W-Si coatings in the oxidizing environment (specimens F-17 through F-23) was excellent. The microstructures in the heated area were porous indicating that free SiO_2 melted out of the tungsten during the test.

Excellent regression resistance was obtained in specimens F-34 and F-35 (deposited with W Si_2) similar to the regression resistance of the W-Si mixture. However, F-34 contained three, 1/16-in. (15.84×10^{-4} m) diameter melted areas which had a glassy appearance. Apparently, the coating reacted with the substrate. Melting was not observed in specimen F-35. Based upon these data, the W Si_2 coating was selected for evaluation in the flox/propane combustor tests.

3. Carbide Coatings Investigation

In the initial program (Ref. 2), one five-tube specimen was plasma-sprayed coated with ZrC/C hypereutectic and evaluated in the flox/propane test. A measured regression rate of 0.45 mils/sec (0.115×10^{-5} m/sec)

was obtained. The starting material for the carbide coating was ZrC/C eutectic with an excess of 30% vol. carbon. The as-sprayed deposit contained small amounts of ZrO_2. ZrC/C powder with additions of 50%, 70%, and 90% by volume carbon were plasma-sprayed on stainless steel disks for X-ray diffraction evaluation. ZrO_2 was detected in the coatings containing 50% and 70% excess carbon but not in the coating containing 90% excess carbon. Based upon these results, the ZrC/C with 90% excess carbon was selected for the flox/propane evaluation.

4. Plasma-Arc Deposition Parametric Study

The plasma arc deposition parameters required to yield good coatings (primarily high density) were evaluated by plasma depositing tungsten on stainless steel substrates under various parametric conditions. Evaluation of these coatings was conducted by means of visual and metallographic examinations as well as by measuring coating thicknesses.

The first series of plasma spray tests were made by varying the: hydrogen content of the primary gas; specimen shielding; torch-to-work distance; powder size; and shroud length. The power input was maintained relatively constant in these tests. Four passes, using W powder, were made on each of the stainless steel disks which had been primed with 2 mils (5.1×10^{-5} m) of Nichrome. The over-all deposit was measured for coating efficiency and the coatings were visually examined. The variables and deposit thickness are listed on Table IV. Coating thickness or efficiency increased as the hydrogen content in the primary gas become greater and the torch-to-work distance decreased. The hydrogen flow was limited to 15 cfh (1.2×10^{-6} m^3/sec) because of the nozzle size. Visual examination indicated that the use of a 3.5-in. (0.089 m) shroud did not appear advantageous. The addition of hydrogen to the shroud gas resulted in severe coating oxidation because of H_2 reaction with air which resulted in the formation of H_2O. The only significant improvement obtained was in the surface finish of the coating using fine powders. However, this use of fine powders significantly decreased the deposition rate because of the long torch-to-work distance and the difficulty experienced in penetrating the plasma with the fine powders. Fine powders offer an advantage over standard powders where the torch-to-work distance is short for obtaining high particle velocities which result in higher density coatings. These shorter torch-to-work distances are possible because complete melting of the fine powder is obtained with a reduced stay time in the plasma. As a result of the advantages offered by the fine powder sizes, additional studies of them were accomplished.

The following four tungsten powder sizes were used in the second series of plasma tests:

- 2.5 micron (2.5×10^{-6} m)
- 4.5 micron (4.5×10^{-6} m)
- 6.5 micron (6.5×10^{-6} m)
- Standard size, -74 + 20 micron (0.074 + 0.020 um)

TABLE IV. - PLASMA SPRAY EVALUATION

Spec. No.	W Powder Size, Microns	W Powder Size, μ meter	H_2 Flow Through Torch, cfh	H_2 Flow Through Torch, m^3/sec	Torch Distance, inches	Amps	Volts	Coating Thickness, inches	Coating Thickness, μ meter
			Variable - H_2 Content and Specimen Shielding						
F-60	-74 +20	-0.074 +0.020	10	7.9×10^{-7}	4	500	38	0.025	0.635
F-61	-74 +20	-0.074 +0.020	10	7.9×10^{-7}	4	500	38	0.022	0.558
F-62	-74 +20	-0.074 +0.020	15	12×10^{-7}	4	500	48	0.027	0.686
F-63	-74 +20	-0.074 +0.020	5	3.9×10^{-7}	5	500	30	0.015	0.381
			Variable - Torch-to-Work Distance and Powder Size						
F-64	-7	-0.007	10	7.9×16^{-7}	4	500	38	0.001	0.025
F-65	-7	-0.007	10	7.9×16^{-7}	3	500	38	0.003	0.076
F-66	-7	-0.007	10	7.9×16^{-7}	2	500	38	0.006	0.1525
F-67	-74 +20	-0.074 +0.020	10	7.9×16^{-7}	3	500	38	0.029	0.736
F-68	-74 +20	-0.074 +0.020	10	7.9×16^{-7}	2	500	38	0.030	0.761
					(Deposit blistered.)				
			Variable - Shroud and Shielding Gas						
F-69	-74 +20	-0.074 +0.020	10	7.9×16^{-7}	4	500	38	0.015	0.381
F-70	-74 +20	-0.074 +0.020	10	7.9×16^{-7}	4	500	39	-	-
					(Poor deposit--oxidized.)				
			Variable - Torch-to-Work Distance						
F-73	-74 +20	-0.074 +0.020	0		4	650	30	0.015	0.381
F-74	-74 +20	-0.074 +0.020	0		3	650	30	0.016	0.446
F-75	-74 +20	-0.074 +0.020	0		2	650	30	0.020	0.508
F-76	-7	-0.007	0		3	650	30	0.003	0.076
F-77	-7	-0.007	-		2	650	30	0.005	0.127

The 2.5 micron (2.5×10^{-6} m) size powder was eliminated from further study because it could not be readily fed with the existing powder feed system, which proved adequate for feeding the remaining powder sizes.

The torch-to-work distance was varied from 0.25-in. (0.0064 m) to 3-in. (0.076 m). To prevent overheating of the substrate, power settings of less than 350 amp were required with a torch-to-work distance of less than 1-in. (1.0254 m). For longer torch-to-work distances, power settings of 400 to 500 amp were used.

Significant increases in density were achieved by decreasing powder size, torch-to-work distances, and amperage. The highest density coatings were obtained with the 4.5 micron (4.5×10^{-6} m) powder size, a torch-to-work distance of 0.5-in. (0.0127 m), and a power setting of 100 amp. Photomicrographs of the conventional tungsten coating compared to the new tungsten coating are shown on Figure No. 1. The deposit made with the new technique contained significantly less porosity (black areas) than the deposit made with the conventional technique.

Changes in torch-to-work distance and powder size resulted in the major improvement in density. However, density increased with decreased torch distance and amperage regardless of powder size. Increasing torch distance resulted in a decrease in deposition efficiency and at distances of 2.5 in. (0.0635 m) or greater, coatings were not obtained with the fine powders 4.5 micron (4.5×10^{-6} μm).

The porosity observed in the deposits was concentrated in the outer layer of the bead and resulted from the oxidation of the deposited tungsten. With increases in amperage, porosity became greater as a result of overheating because the surface speed of the substrate was maintained constant.

A third series of plasma tests were conducted to investigate the effects of substrate speed and torch travel speed upon the observed porosity. In these tests, the stainless steel disk substrates were attached to the surface of a 6-in. (1.152 m) diameter pipe held in the chuck of a lathe. Coatings were deposited without cooling on the backside of the disk. The variables investigated were torch traverse speed of 4 ipm to 20 ipm (2.8×10^{-5} m/sec to 14×10^{-5} m/sec) chuck speed of 100 ipm to 1600 ipm (7.1×10^{-4} - 11.4×10^{-3} m/sec), and torch-to-work distance 1/4-in. to 1 in. (0.0064 to 0.025 m). Tungsten powder size was held constant at 4.5 microns (4.5×10^{-6} m) along with amperage at 100 amp. The torch gas flow was held constant at 100 cfh (7.9×10^{-6} m^3/sec) for both the argon and hydrogen.

Both deposition rate and substrate temperature increased with decreased torch speed. For example, torch speeds of 12 ipm (85.2×10^{-6} m/sec) resulted in deposition rates of 0.2 mil (0.5×10^{-5}) pass compared to 1 mil (2.54×10^{-5} m) pass for torch speeds of 4 ipm (2.8×10^{-5} m/sec). The temperature of the stainless steel substrate and tungsten coating increased with torch speed as evidenced by the color of the specimen and spalling of

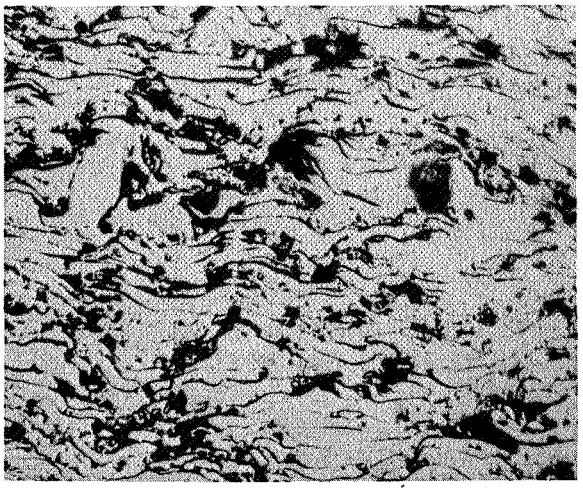

250X

Conventional Technique

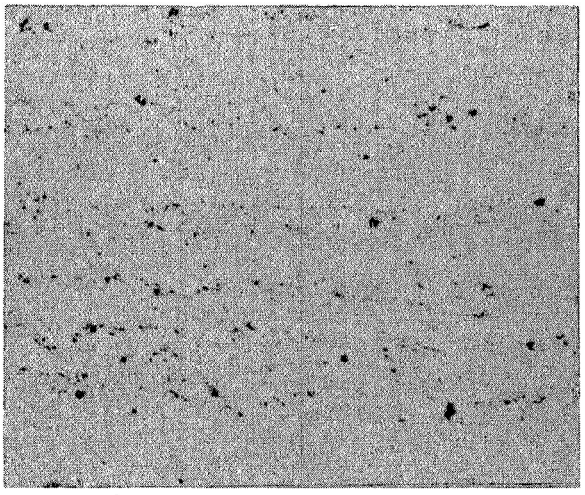

250X

New Technique

Figure 1. Comparison of Density of As-Deposited Plasma-Sprayed Tungsten Made with Two Different Spray Techniques

the coating. Generally, the coating spalled at torch speeds of less than 6 ipm (42.6 x 10^{-6} m). The back of the stainless steel disk had a gold color at 4 ipm (2.8 x 16^{-5} m/sec) and no discoloration at 12 ipm (85.2 x 10^{-6} m/sec). The tungsten coating was dark blue at 4 ipm (2.8 x 10^{-5} m/sec) compared to light blue at 12 ipm (85.2 x 10^{-6} m/sec).

The density of the coating appeared best with a torch travel speed of 10 ipm (17.1 x 10^{-5} m/sec), a chuck speed of 800 ipm (56.8 x 10^{-4} m/sec), and a torch-to-work distance of 0.25-in. (0.0064 m). The density of these coatings (see Figure No. 2) was higher than the standard coating but not as dense as the single bead deposits shown on Figure No. 1. Also, the density of the coating was less than that obtained with the commercial coatings made with Union Carbide's proprietary process.

In summary, it was determined that the density of the plasma-sprayed coatings could be increased significantly by decreasing the torch-to-work distance from 4.0-in. (0.161 m) to 1/4-in. (0.064 m), decreasing powder size from -74 + 20 to 4.5 microns (-0.074 + 0.020 μm to 4.5 x 10^{-3} μm) and by decreasing amperage from 500 to 100. The density of single bead deposits was higher than the standard coating. This difference in density is attributed to an overspray consisting of unmelted particles along the edges of the bead. In the single bead deposits, the overspray does not significantly affect the density of the coating, but in coating the entire surface, this overspray significantly affects the coating density. The overspray could be minimized by using a smaller diameter nozzle, because the use of the low amperage in this study resulted in a relatively small diameter plasma stream as compared to that obtained with the 500 amp operation. The nozzles used in this parametric study were designed for 500 amp service. Using a smaller diameter nozzle designed for 100 amp service would compensate for the difference in plasma size and allow the plasma stream to flow fully. Then, the powder would be forced into the gas stream in the small diameter nozzle which would provide uniform powder melting and deposition. Studies were not made with small diameter nozzles, but their use would be recommended for future studies.

D. FLOX/PROPANE EVALUATION

The flox/propane tests were conducted to evaluate the regression resistance of the improved flame liner in a flox/propane exhaust environment. Before starting the tests, the flox/propane combustor was checked out in a 5 sec duration test firing. All systems were satisfactory and the evaluation tests were made with the five-tube specimens placed at an angle of 22 degrees with the exhaust stream. All test durations were 15 sec.

Each of the five-tube specimens had the same undercoat applied. It consisted of:

- 3 mils (7.6 x 10^{-5} m)primer coat of NiCr
- 10 mils (25.4 x 10^{-5} m) of 20% Ni-80% Al_2O_3
- 14 mils (35.6 x 10^{-5}) of 30% Mo-70% Al_2O_3

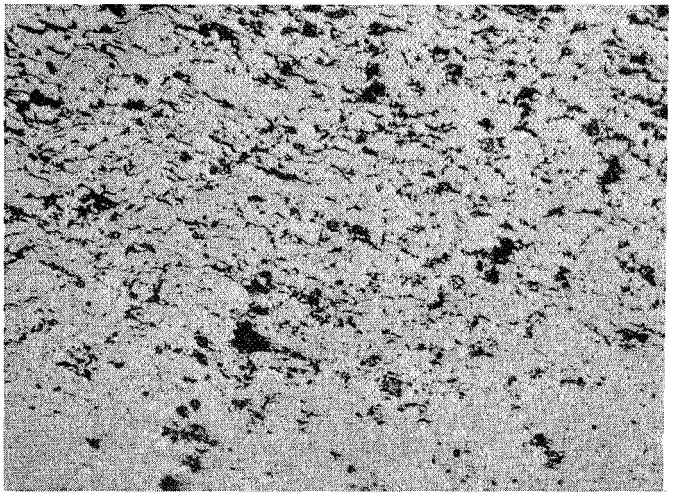

250X

Figure 2. Density of Plasma-Sprayed Tungsten with 4.5 Micron (4.5×10^{-3} m) Powder, 800 ipm (56.8×10^{-4} m/sec) Chuck Speed, 10 ipm (7.1×10^{-5} m/sec) Torch Speed and Torch to Work Distance of 1/4-in. (0.0064m)

These undercoats provided a thermal resistance of 1200 $in.^2$-sec-°F/Btu (4.1×10^{-4} m^2 sec °K/J). After each test, the specimen was visually examined, measured, and sectioned for metallographic examinations.

The data for these test firings and regression rate performance are shown on Table V. Cracking was observed in the coating. Generally, these were longitudinal cracks along the valleys between the tubes. Transverse cracks were observed at the edge of the window area provided by the graphite shield. The ensuing discussions provide specific information regarding each coated specimen.

1. Specimens T-31 and T-35

The flame liner on specimens T-31 and T-35 consisted of 95% dense tungsten as plasma-sprayed by Union Carbide using the improved technique of their proprietary process. There was no regression on the dense tungsten flame liner of specimen T-31 after a 15 sec test and 0.1 mil/sec (0.25×10^{-5} m/sec) for specimen T-35 after a 30 sec test. Cracks were observed in the flame liner in the valley between the tubes in both specimens. These cracks were similar to those observed in all the previous tests. Also, transverse cracks were observed in specimen T-35. The as-fired condition of T-31 is shown on Figure No. 3. Cross-sections of the tube specimen showing the tube, undercoat, and flame liner are illustrated on Figure No. 4.

The excellent regression resistance observed in this test is attributed to the high density of the flame liner. In previously reported tests (Ref. 2), tungsten flame liners with densities of 87%, tested under the same conditions, had regression rates of 0.4 mils/sec (1.02×10^{-5} m/sec). The density of the tungsten flame liner in the latest test was 95%. This difference in density of the flame liners was apparent as shown on Figure No. 5. Based on this test, the 95% dense tungsten flame liner was selected for final evaluation in the flox/methane tester.

2. Specimen T-29

Specimen T-29 was similar to the previous specimen except that the flame liner consisted of 100% Mo with a density of approximately 90%. The flame liner also was plasma-sprayed by Union Carbide using their proprietary process. The regression rate after a 15 sec exposure to the exhaust gas was 0.4 mils/sec (1×10^{-5} m/sec). This was the same as that obtained from the Mo flame liners previously evaluated (Ref. 2).

3. Specimen T-30

The flame liner of specimen T-30 consisted of a commercial tungsten carbide coating normally used for hard facing. This tungsten carbide contains 8% Co to promote bonding. Regression of the coating from exposure to exhaust stream was 2 mils/sec (5.1×10^{-5} m/sec). This was considered too severe and tungsten carbide was eliminated from further consideration in the program.

TABLE V

RESULTS OF FLOX/PROPANE FIVE-TUBE SPECIMEN EVALUATION

Specimen	Firing Duration sec	Oxidizer/Fuel Mixture Ratio	Chamber Pressure psia	Chamber Pressure N/m^2	Flame Liner Composition	Regression Rate mils/sec	Regression Rate m/sec
T-31	15	4.3	89	630×10^3	100% W (95 Dense)	nil	
T-29	15	4.8	97.5	672×10^3	100% Mo	0.4	1.0×10^{-5}
T-30	15	5.2	90	620×10^3	Commercial WC bonded with Co	Coating Completely Eroded	
T-38	15	4.6	88	606×10^3	10% Zr C/C 90% C by Vol	0.5	1.3×10^{-5}
T-39	15	4.4	97	668×10^3	100% WSi_2	0.3	0.76×10^{-5}
T-40	15	4.5	94	648×10^3	100% Ni-Cu Coated W	0.3	0.76×10^{-5}
T-35	30	4.5	100	689×10^3	100% W (95% Dense)	0.1	0.25×10^{-5}

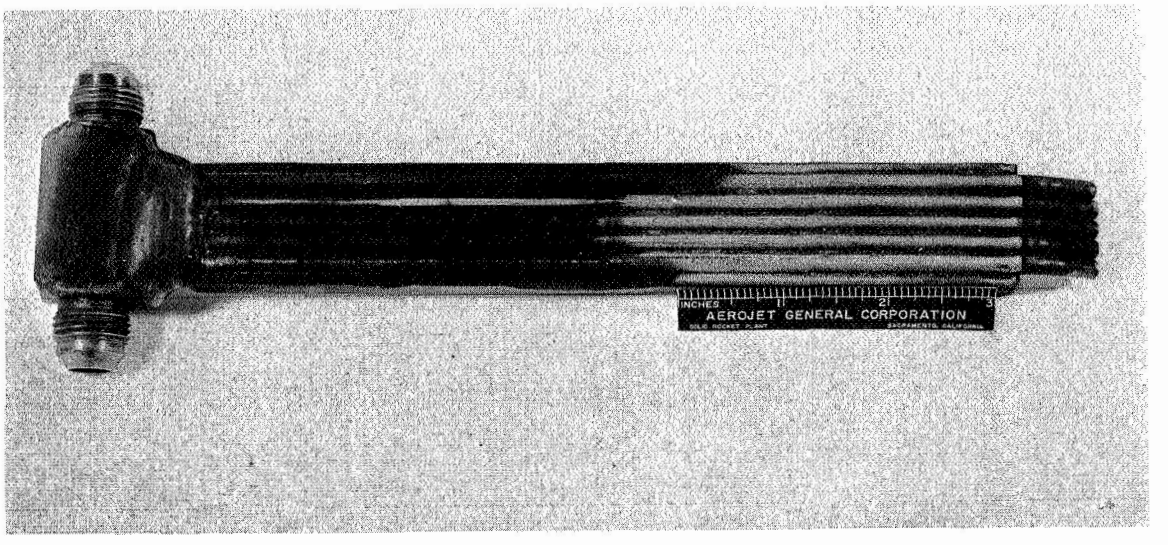

Figure 3. Tungsten Topcoated Specimen after 15 sec Flox/Propane Test Firing (Specimen No. T-31)

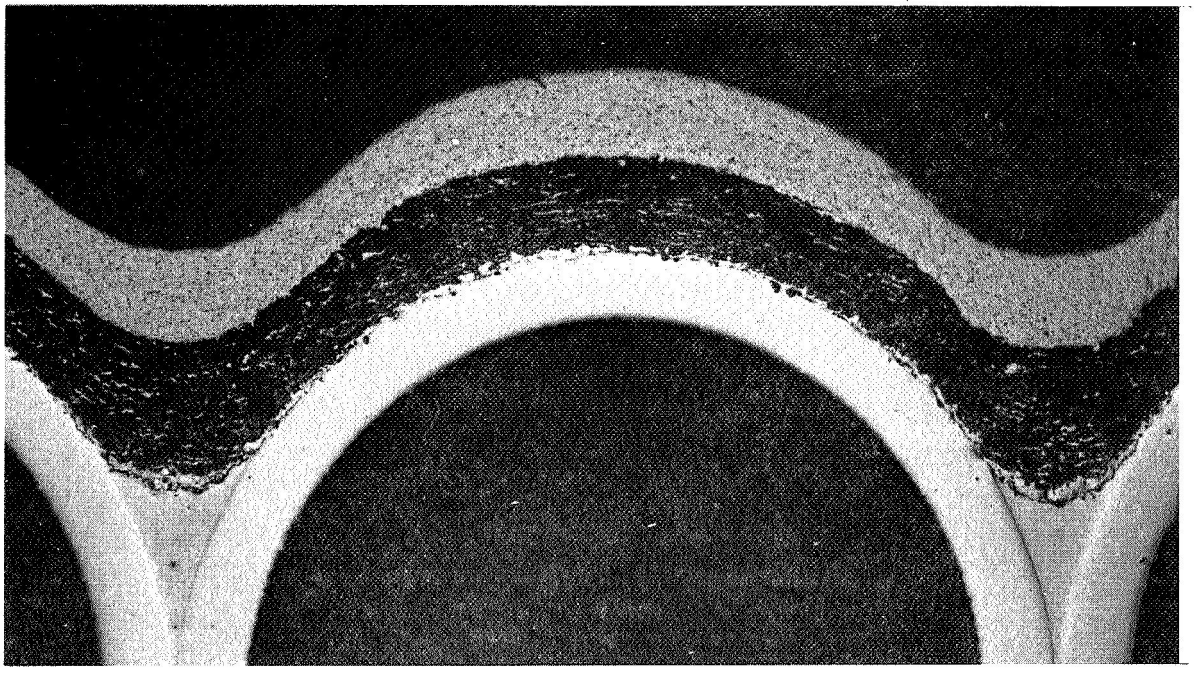

24X

Figure 4. Pre-Fired Coated Specimen Consisting of Ni-Al_2O_3 and MO-Al_2O_3 Undercoats and a Union Carbide W-Deposited Topcoat

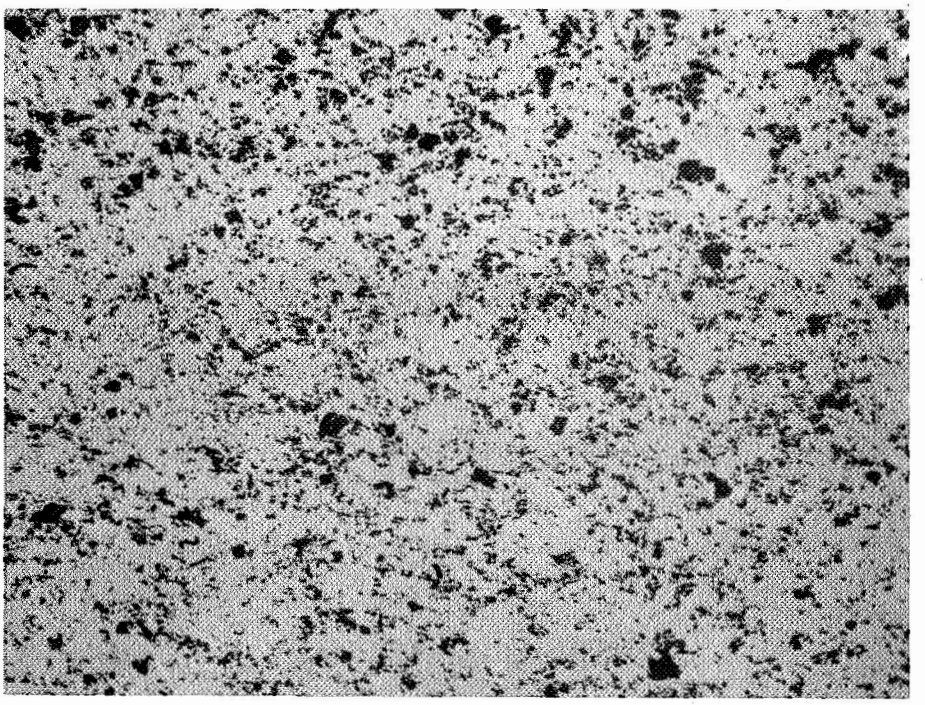

Mag: 250X

Old Technique (87% Dense)

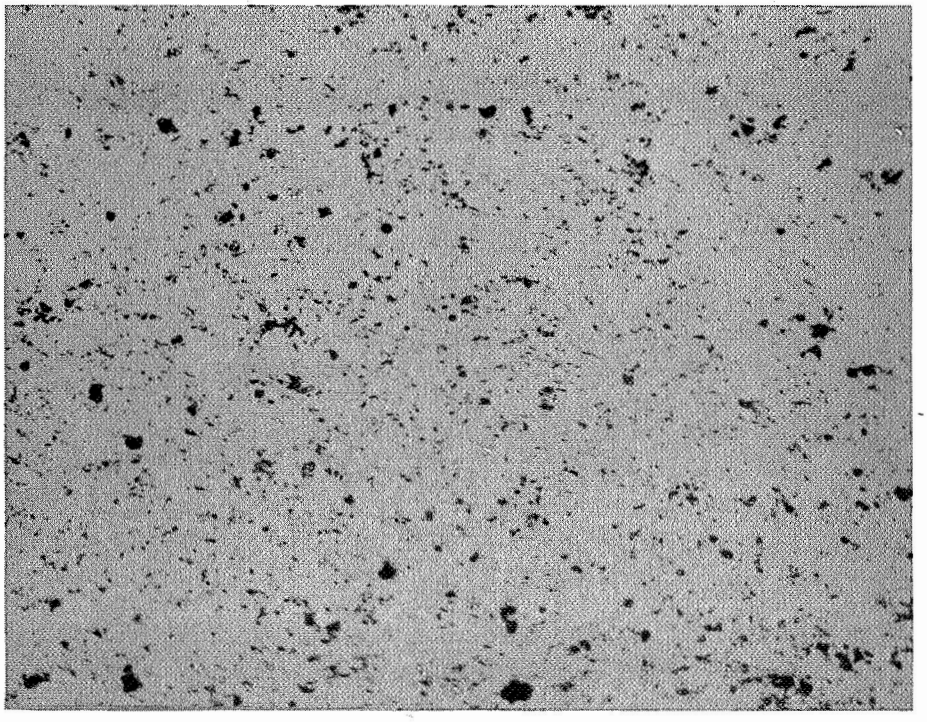

Mag: 250X

New Technique (95% Dense)

Figure 5. Comparison of the Density of Tungsten Plasma-Sprayed by Union Carbide using Two Techniques

4. Specimen T-38

This specimen consisted of a flame liner of plasma-sprayed hypereutectic ZrC/C mixed with 90% by volume excess carbon. The hypereutectic powder contained approximately 30% vol excess carbon in the form of graphite flakes. In previous tests (Ref. 2) with the ZrC/C powder, ZrO_2 was detected in the as-deposited flame liner. Excess carbon was mixed with the ZrC/C in the subject program to minimize the ZrO_2 formation.

However, the regression rate of the ZrC/C flame liner was 0.5 mils/sec (1.3×10^{-5} m/sec). This was similar to the regression rate of the previously tested (Ref. 2) ZrC/C liner without the excess carbon.

5. Specimen T-39

The flame liner consisted of plasma-sprayed WSi_2. The silicide coating, which had excellent regression resistance in oxidizing atmospheres in the laboratory evaluation, is compatible with HF based upon free energy of formation calculations. However, both Si and SiO_2 react with F. Regression rate after a 15 sec exposure to the exhaust was 0.3 mils/sec (0.76×10^{-5} m/sec) for the forward 2-in. (0.05m) of exposure. The coatings on the last 1-in. (0.025 m) of the specimens were melted and the flame liner was completely eroded. The results of these tests revealed that the use of the silicide was not beneficial in minimizing regression and, therefore, it was eliminated from further evaluations.

6. Specimen T-40

The flame liner on this specimen was plasma-sprayed with tungsten powder that had been coated with 0.2% Ni and 0.3% Cu. The coating on the tungsten was used to promote densification and to minimize oxidation during the spraying. The regression rate of this liner after exposure to the exhaust stream was 0.3 mils/sec (0.76×10^{-5} m/sec), comparable to an uncoated tungsten powder flame liner.

Metallographic examination revealed that densification occurred during the test firing in the flame liner made from the Ni-Cu coated tungsten. The pre-fired and post-fired structures are shown on Figure No. 6. Densification in the structures was not observed in the tungsten liners made without the coated powders indicating the Ni-Cu promoted densification. However, this densification was inadequate to significantly increase regression resistance.

In summary, the 95% dense tungsten flame liner provided the best regression in the flox/propane tests of any of the coatings evaluated. The use of plasma spray molybdenum, carbides, or silicide did not provide the regression resistance required for coatings. Based upon this evaluation, the 95% dense tungsten flame liner was selected for evaluation in the flox/methane tester.

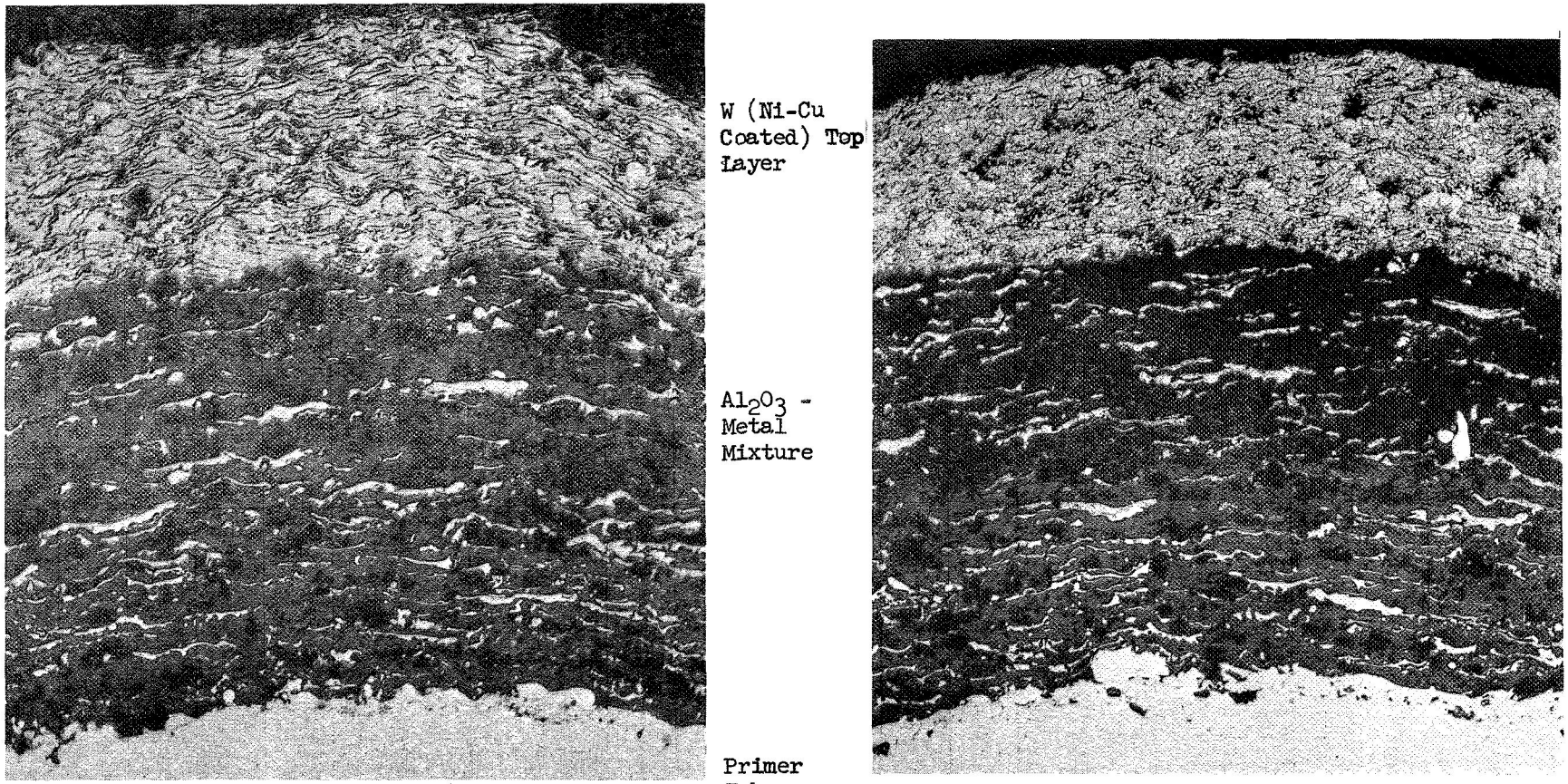

Figure 6. Comparison of Pre-Fired and Post-Fired Coatings Consisting of a Top Layer Plasma Sprayed with Tungsten Powder Coated with Ni-Cu (Specimen T-40)

IV. DEVELOPMENT OF A THRUST CHAMBER SIMULATOR AND INJECTOR

A rectangular chamber and injector were designed to subject the plasma-sprayed coatings to Flox/methane combustion environments that were similar to those existing in an actual engine. Coated panels actually formed two of the side walls of the chamber. These panels could be readily replaced to facilitate repeated testing with minimum hardware requirements. The other two sides of the rectangular cross-section chamber were nonremovable, uncoated, water-cooled, copper panels. The injector design evolved upon the basis of attaining good performance, minimum oxidizer streaking, and providing adequate face cooling.

The thrust chamber simulator design conditions were:

Propellants	82.6% liquid flox/gaseous methane
Chamber Pressure	500 psia (345×10^4 N/m^2)
Mixture Ratio	5.25
Thrust	1000 lb (454 Kg)

The discussion which follows covers the details of both the injector and thrust chamber designs as well as pertinent testing results.

A. INJECTOR

Three injectors were fabricated and tested in this program. They were designated 36-1 injectors (the solid face, 36-element, impinging unit shown on Figure No. 7), 20-1 (the N-155 Rigimesh face, 20-element, impinging unit on Figure No. 8); and the 20-2 (the modification of the 20-1 design with a Nickel-200 Rigimesh face shown on Figure No. 9).

The 36-element and 20-element injectors were designed concurrently so that the injector body could be finished in either configuration. The body was fabricated from nickel 200 because this material had been successfully used in previous Aerojet programs with fluorine and flox oxidizers. The two pattern designs were intended to be complementary. The 36-element design was biased in favor of performance while the other design was biased to assure adequate face cooling capability, but with a slight reduction in performance.

Early consideration was given to the use of coaxial elements because this element type had been demonstrated with gaseous flox/gaseous methane in other contractual efforts. However, coaxial elements were rejected primarily as the result of Aerojet's success with triplet elements in Phase I of this contract and in its fluorine/amine programs wherein chamber pressures reached 500 psia (345×10^4 N/m^2).

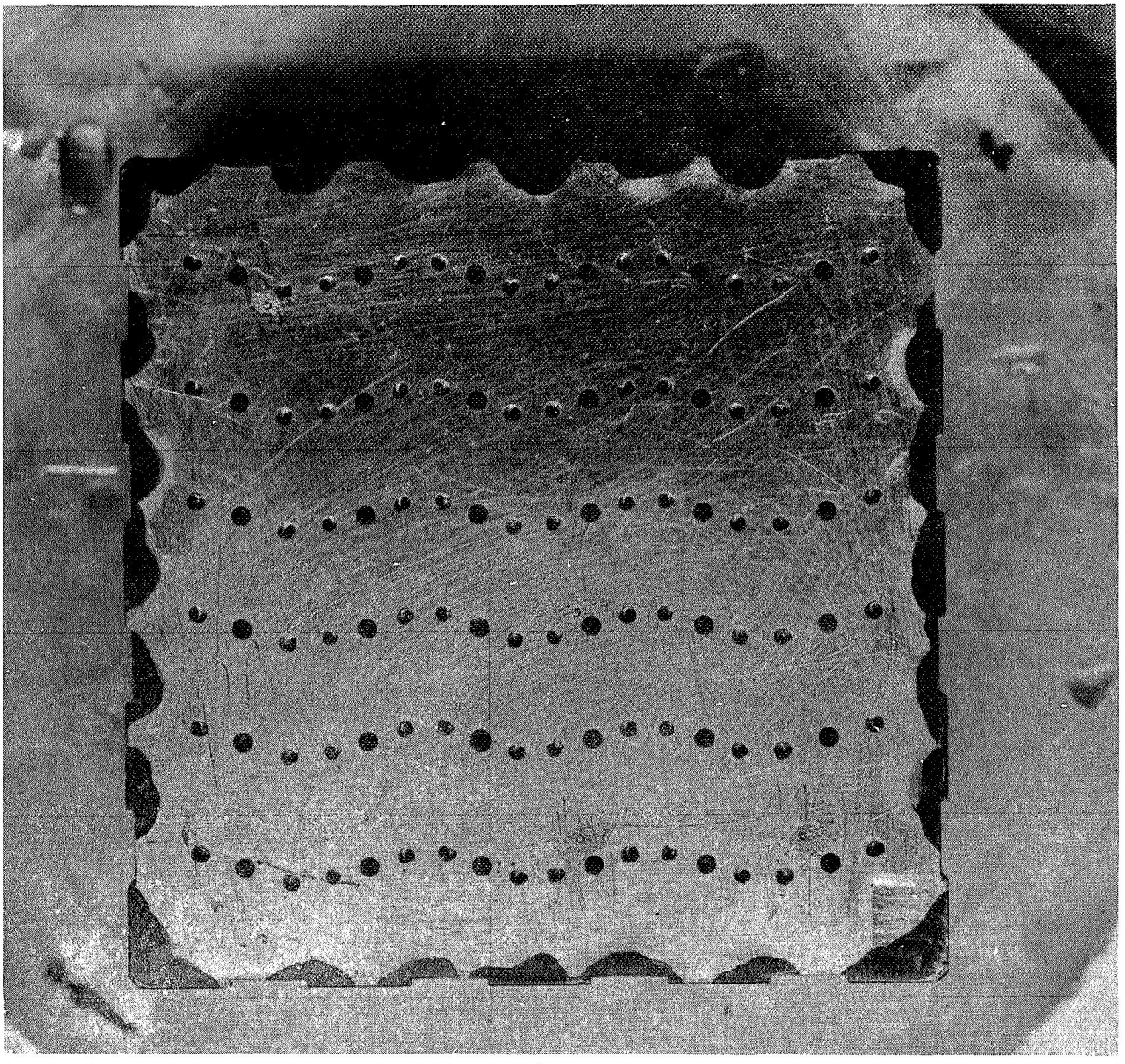

Figure 7. Orifice Pattern for the 36-Element Injector (36-1)

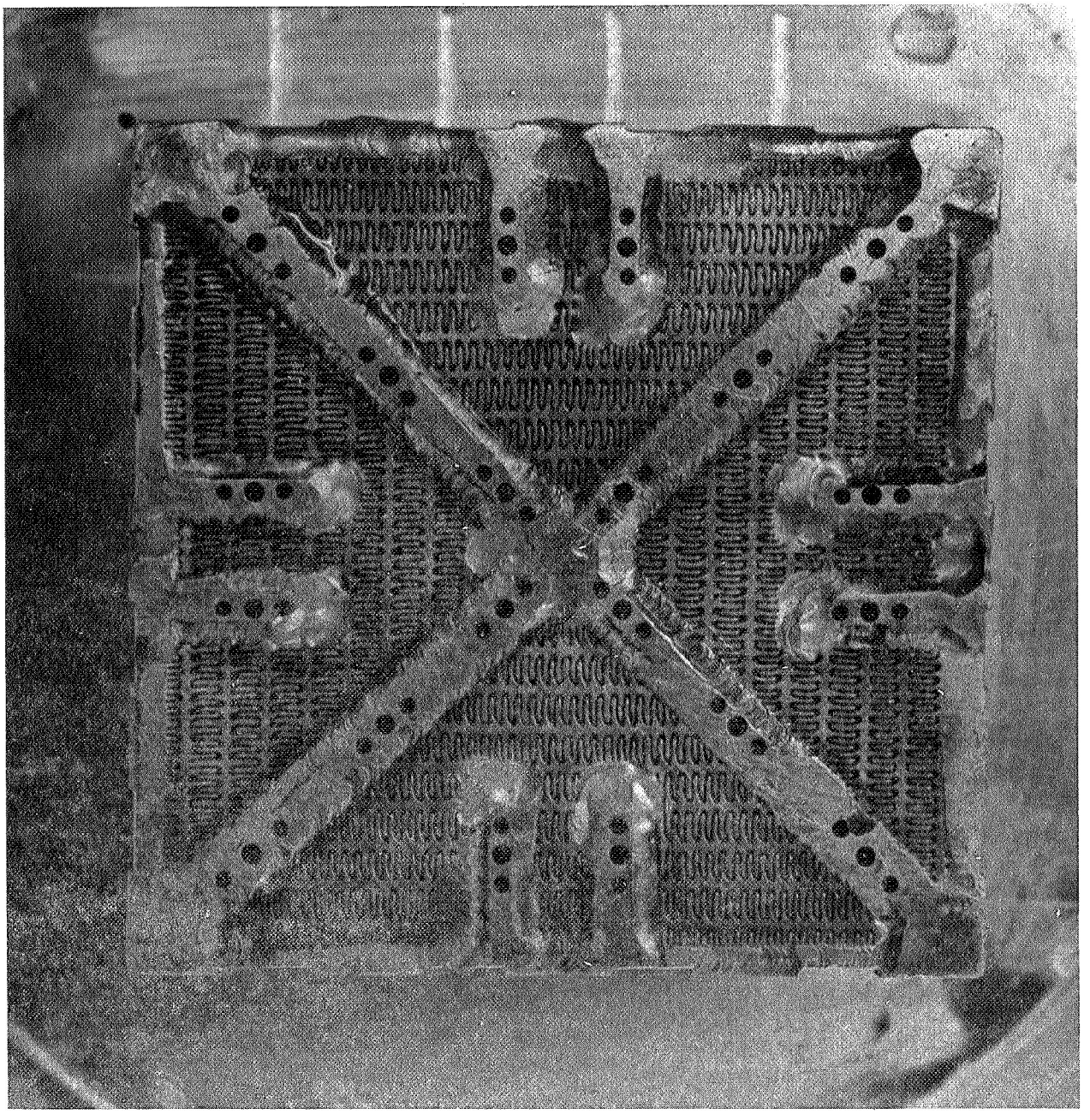

Figure 8. Orifice Pattern for the 20-Element Injector (20-1)

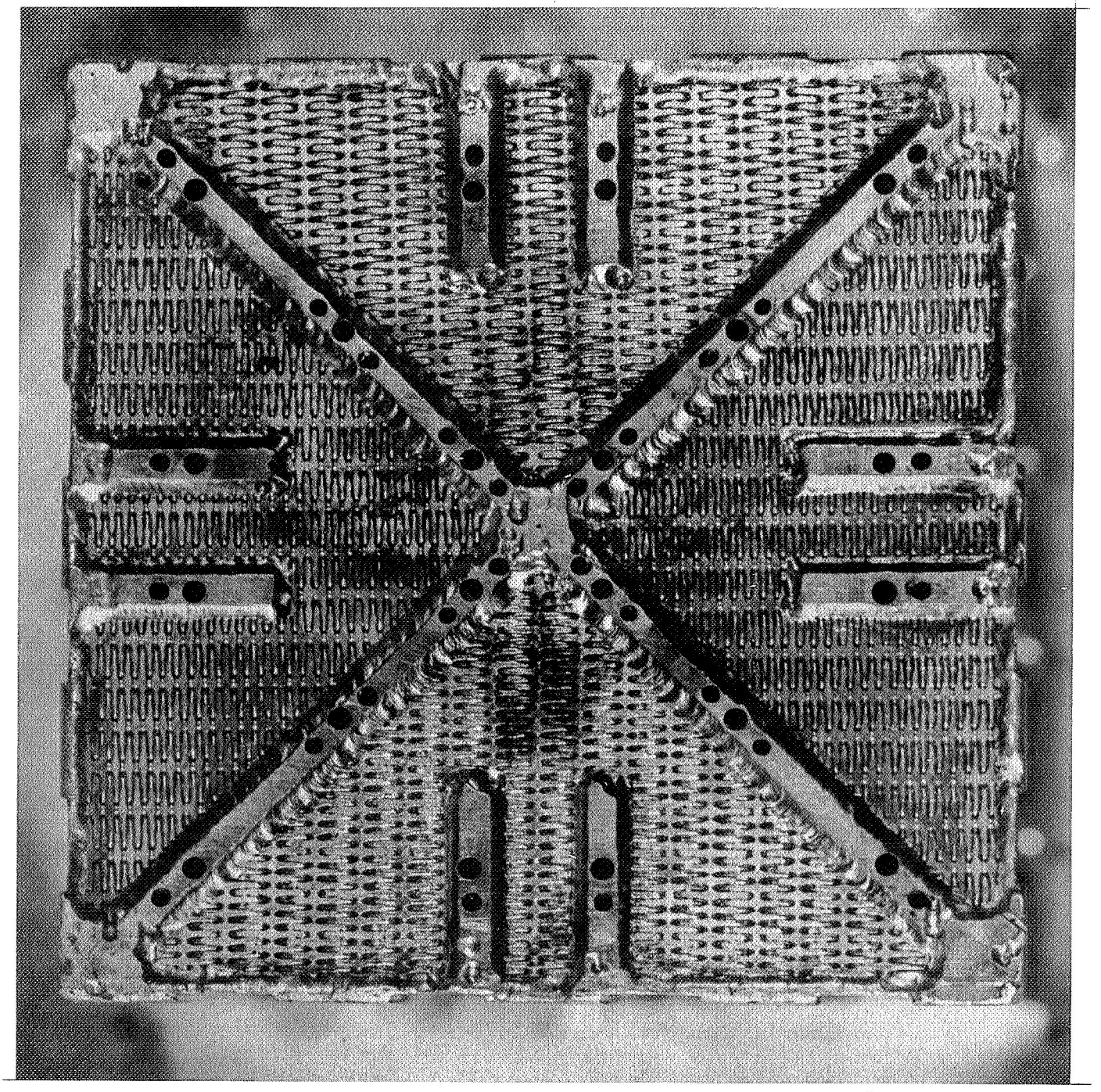

Figure 9. Orifice Pattern for the Injector Consisting of 12 Doublets and 8 Triplets (20-2)

1. 36-1 Injector

a. Design

The 36-1 injector assembly had a 2.0-in. (0.051 m) square face, which piloted into the thrust chamber for a distance of 1.68-in. (0.043 m) so as to locate the multiple injector-to-side plate seals away from the combustion zone. This resulted in the propellant manifolds being contained within the 2.0 in. (0.051 m) square cross-section. Oxidizer was fed to the orifices from a grid of 0.093 in. dia (0.00236 m) holes drilled parallel to the injector face (the Aerojet cross-drilled concept). The distance from the face surface to the hole was 0.045-in. (0.00115 m). The seven holes in the x and y planes were fed from a peripheral oxidizer manifold. Fuel was flooded across the back surface of the injector. A showerhead fuel orifice was located in each small square bounded by the cross-drilled oxidizer manifolds. The oxidizer orifices were drilled at an angle of 53 degrees to the face resulting in 36 O-F-O type elements. These elements were positioned so that the sprays would overlap in a complementary fashion. Fuel orifices were 0.046-in. diameter (0.00117 m) and oxidizer holes were 0.026-in. diameter (0.00066 m).

b. Pattern Analysis

The pattern for this configuration was designed to provide maximum performance and propellant mixing. Use of a solid face minimized geometric constraints on the location and orientation of elements, which permitted the 36 O-F-O elements to be designed for an even mass distribution by spacing them equally across the face. Propellant mixing was enhanced by orienting adjacent elements so that oxidizer-rich portions of one spray fan overlapped fuel-rich portions of the adjacent spray fan. The derived pattern is shown on Figure No. 7. It was recognized that the solid face required for this pattern imposed some design risk because the capability of the pattern to adequately transmit the resultant heat flux away from the injector face was not known. Some face erosion would occur unless the dense pattern spacing would provide reduced heat loads.

c. Test Results

The test results were generally as expected for the combustion performance; however, incipient melting of the face was apparent in a few local spots where adjacent spray fans overlapped between elements. The performance data for the three tests conducted with this unit are included on Table VI. Both pressure-based and thrust-based c* efficiencies are shown. The pressure-based data usually are not as accurate in determining combustion efficiency because only one upstream pressure tap was used to determine the effective pressure at the throat. Also, these data require an accurate thermodynamic throat area value, which normally is not available. The thrust-based measurements circumvent these difficulties because the effective integrated pressure or thrust is directly measured. For this reason, thrust-based measurements were used wherever available. The 36-1 injector had a thrust-based c* of nearly 96% at an average mixture ratio of 5.1. While these values were within the requirements limits, work with this injector was discontinued because face erosion precluded the necessary long durations.

2. 20-1 Injector

a. Design

This injector used the same body design as the 36-element unit. It was configured to assure adequate face cooling by adding a Rigimesh face plate thereby allowing the face to be cooled by the mass addition of gaseous fuel. Nickel 200 was selected for the Rigimesh face plate because of its proven compatibility with the oxidizer and HF combustion products.

Analysis of the injector showed that the more desirable 36-element pattern did not allow sufficient space for the Rigimesh to be located between the discrete lands containing the orifices. Therefore, it was necessary to reduce the number of elements to 20 O-F-O triplets as on the previous unit. Orifice sizes were 0.035 in. (0.00089 m) and 0.046-in. (0.00117 m) for the oxidizer and fuel, respectively. This selection of 20 elements was based upon the need to provide sufficient space between elements to allow for incorporation of the Rigimesh plus some allowance for welding to the orifice lands. Non-welded material was incapable of resisting the pressure loading on the Rigimesh.

Delays were experienced in fabricating this injector because the manufacturer of Rigimesh encountered difficulties in providing material with sufficient porosity. Consequently, Rigimesh material made from N-155 was substituted for the more optimal Nickel 200 material. The N-155 is an iron-chromium-nickel-cobalt alloy containing approximately 20% nickel and is less compatible with the propellants and it has a much lower thermal conductivity than pure nickel.

b. Pattern Analysis

This pattern was designed concurrently with the 36-1, but with a different emphasis. The Rigimesh injector face, used for face cooling, limited the application of the compatibility design criteria which called for equally-spaced elements with complete freedom of orientation to enhance inter-element mixing. To design a practical Rigimesh face for the 2.0-in. (0.051 m) square injector, it was necessary to restrict the element location to the basic pattern shown on Figure No. 8. This resulted in a coarser pattern without a favorable element-to-element interaction. Actually, subsequent cold flow tests indicated that the "twin" elements located at the wall (see Figure No. 8) resulted in an adverse concentration at the chamber wall. Although a propensity for streaking was predicted for this design, the exact consequences of compromising the compatibility design criteria were unknown prior to test demonstration.

c. Test Results

The test results indicated that the 20-1 injector achieved an average performance of nearly 95% of theoretical c* based upon thrust measurements and an average mixture ratio of 4.6 (see Table VI). Post-test examination of the injector face revealed local hot spots in the Rigimesh.

TABLE VI. - RESULTS OF THE FLOX/METHANE TESTS

Test No.	Firing Duration Sec.	Injector, No. of Element	Oxidizer Fuel Mixture Ratio	Chamber Pressure psia	Chamber Pressure N/m^2	Efficiency % c* Thrust Based	Efficiency % c* Pc Based	Chamber	Remarks
001	1.2	36	5.8	458	316×10^4	94.8	96.8	Copper heat sink	Check out test using heat sink chamber.
002	1.36	36	4.6	465	320×10^4	97.3	100	Copper heat sink	Check out test using heat sink chamber.
003	1.12	36	4.8	511	352×10^4	94.7	97.8	Copper heat sink	Check out test using heat sink chamber.
004	0.98	20-1	5.8	462	318×10^4	91.7	96.0	Copper heat sink	Rigimesh eroded in three places and heat marked in 4 others.
005	1.5	20-1	4.2	490	338×10^4	94.8	101.2	Copper heat sink	Eight bleed holes added through rigimesh. No erosion but three heat marks.
006	2.5	20-1	4.2	530	365×10^4	96.2	101.9	Copper heat sink	Nine bleed holes added through rigimesh.
007	4.0	20-1	4.1	514	354×10^4	92.8	98.8	Copper heat sink	No erosion on injector face.
008	5.94	20-1	3.4	341	235×10^4	N/A	N/A	Water-cooled	Oxidizer streaks.
009	2.5	20-1	4.0	410	282×10^4	N/A	N/A	Water-cooled	Twenty bleed holes added to rigimesh face to minimize streaking. Injector eroded in center of face.
010	2.0	20-2	3.9	408	281×10^4	N/A	88.3	Copper heat sink	No evidence of face deterioration.
011	2.0	20-2	4.4	408	281×10^4	N/A	96	Copper heat sink	No evidence of face deterioration.
012	8.0	20-2	5.8	470	324×10^4	N/A	85	Water-cooled and Mixer section	No erosion on injector face but oxidizer streaks.
013	15.0	20-2	4.6	431	297×10^4	N/A	92	Water-cooled and Mixer section	No erosion on injector face but oxidizer streaks.
014	15.0	20-2	5.0	385	265×10^4	N/A	83	Water-cooled No mixer	No erosion on injector face but oxidizer streaks on chamber side walls and specimens.
015	30.0	20-2	4.0	336	231×10^4	N/A	85	Water-cooled No mixer	No erosion on injector face but oxidizer streaks on chamber side walls and specimens.

Selective drilling of small holes at these hot spots was accomplished in an effort to prevent further damage. However, subsequent tests demonstrated this to be an inadequate solution for long duration testing. In addition, the chamber walls showed signs of oxidizer streaking near the injector face and at the throat location. This testing conclusively demonstrated that additional injector modification was necessary before any valid material sample testing could be conducted.

3. 20-2 Injector

a. Design

A thrust chamber modification study was undertaken when tests indicated the 20-1 injector streaking characteristic and face erosion tendencies. This study had three primary purposes. First, candidate injector pattern changes had to be made to decrease the flox concentration at the chamber wall. Next, simulated propellant flow distribution tests were required to select the best configuration. Finally, a water-cooled, combustion gas mixing chamber was designed to insert between the injector and test material specimens.

The injector was a redesign of the 20 element unit. It was intended to provide improved durability and to reduce the injector-induced oxidizer streaking. Durability was improved by using Nickel 200 Rigimesh which became available following the testing of injector 20-1. However, significant compatibility improvements were constrained by the desire to use an existing injector body which prevented any major relocation of injection elements.

b. Pattern Analysis

The types of injector pattern modifications were limited by the basic injector geometry because the injector body had already been fabricated and only slight orifice changes could be accommodated. In view of these limitations, a cold flow analysis was conducted to determine the flox propellant distribution.

The cold flow analysis was conducted using the flow collection device shown on Figure No. 10. Water was used for the flox simulant and distribution was measured by means of the bottles shown on Figure No. 10. Gaseous nitrogen was used to simulate the effect of gaseous methane and its distribution was not measured. However, its effect upon the liquid propellant distribution was measured.

Five configurations which were obtained by selectively plugging oxidizer holes of injector 20-1 were analyzed. These cold flow tests resulted in the selection of injector 20-2 (Figure No. 9) as the most effective modification for minimizing oxidizer concentration at the wall. Figures No. 11 and No. 12 are plots of the flox flow distribution for the 20-1 and 20-2 injectors, respectively. They illustrate the effectiveness of this modification. However, it was also recognized that streaking may be influenced by dynamic combustion effects on the ultimate chemical species distributions.

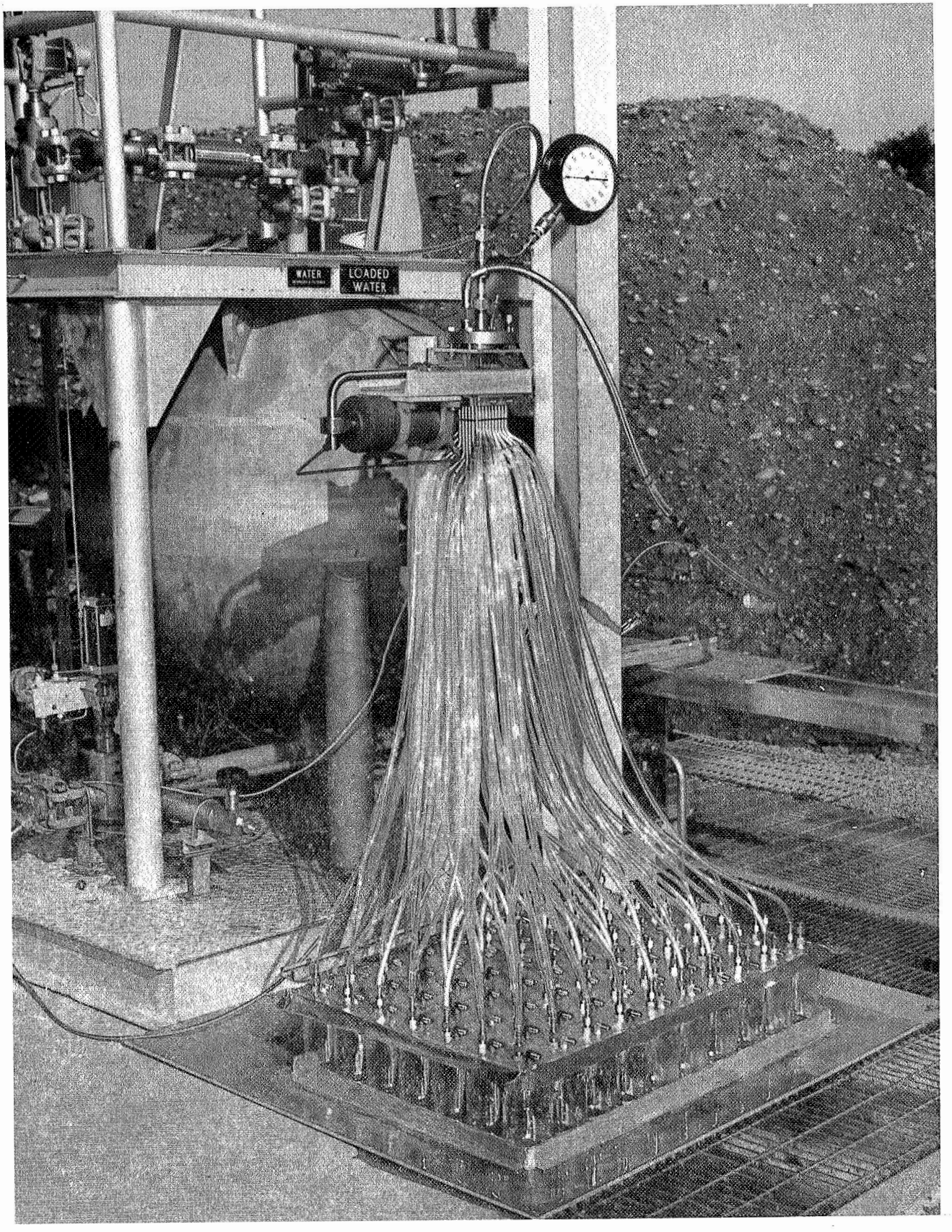

Figure 10. Gas-Liquid Flow Device

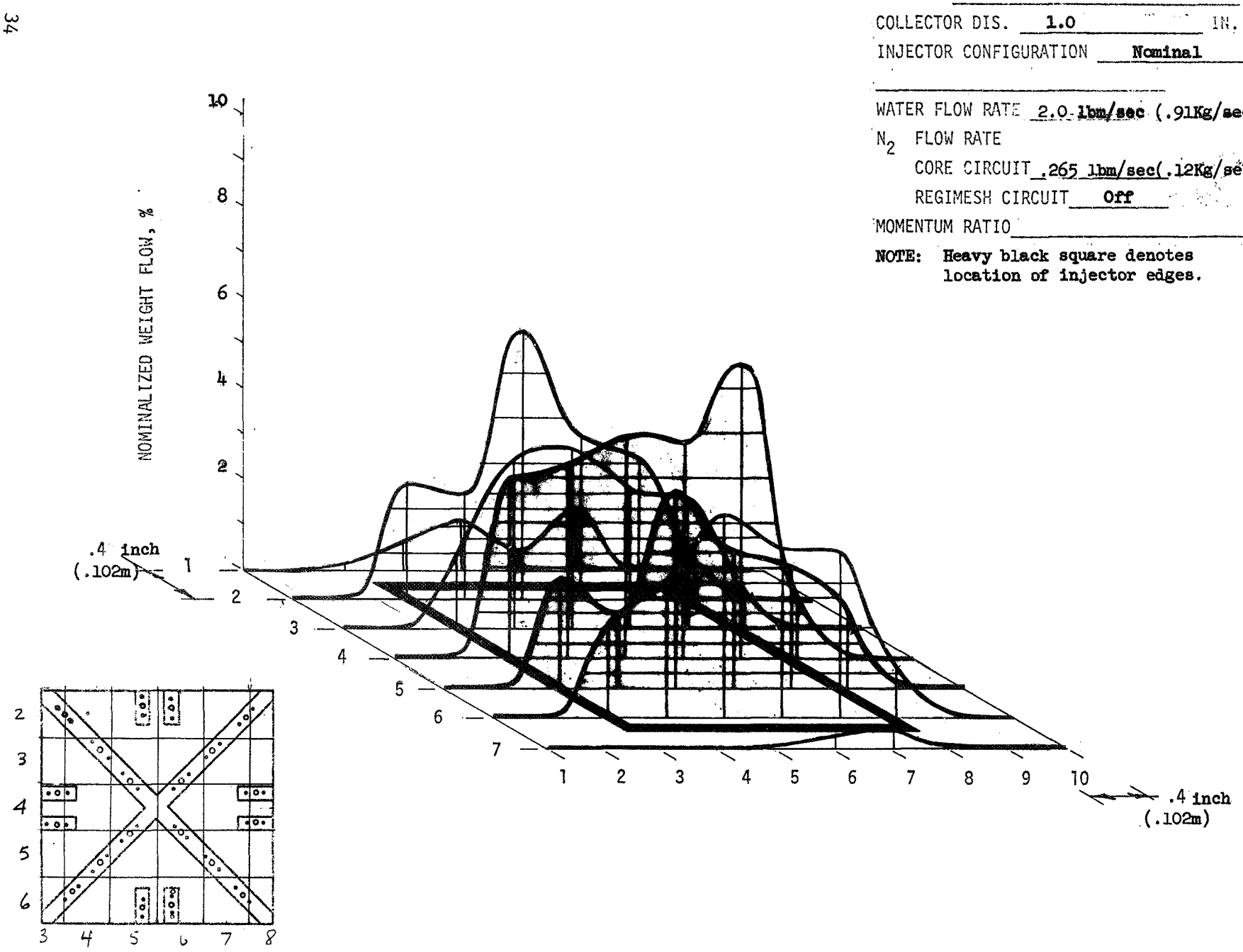

Figure 11. Injector 20-1 Simulated Flox Distribution, MOD O-A

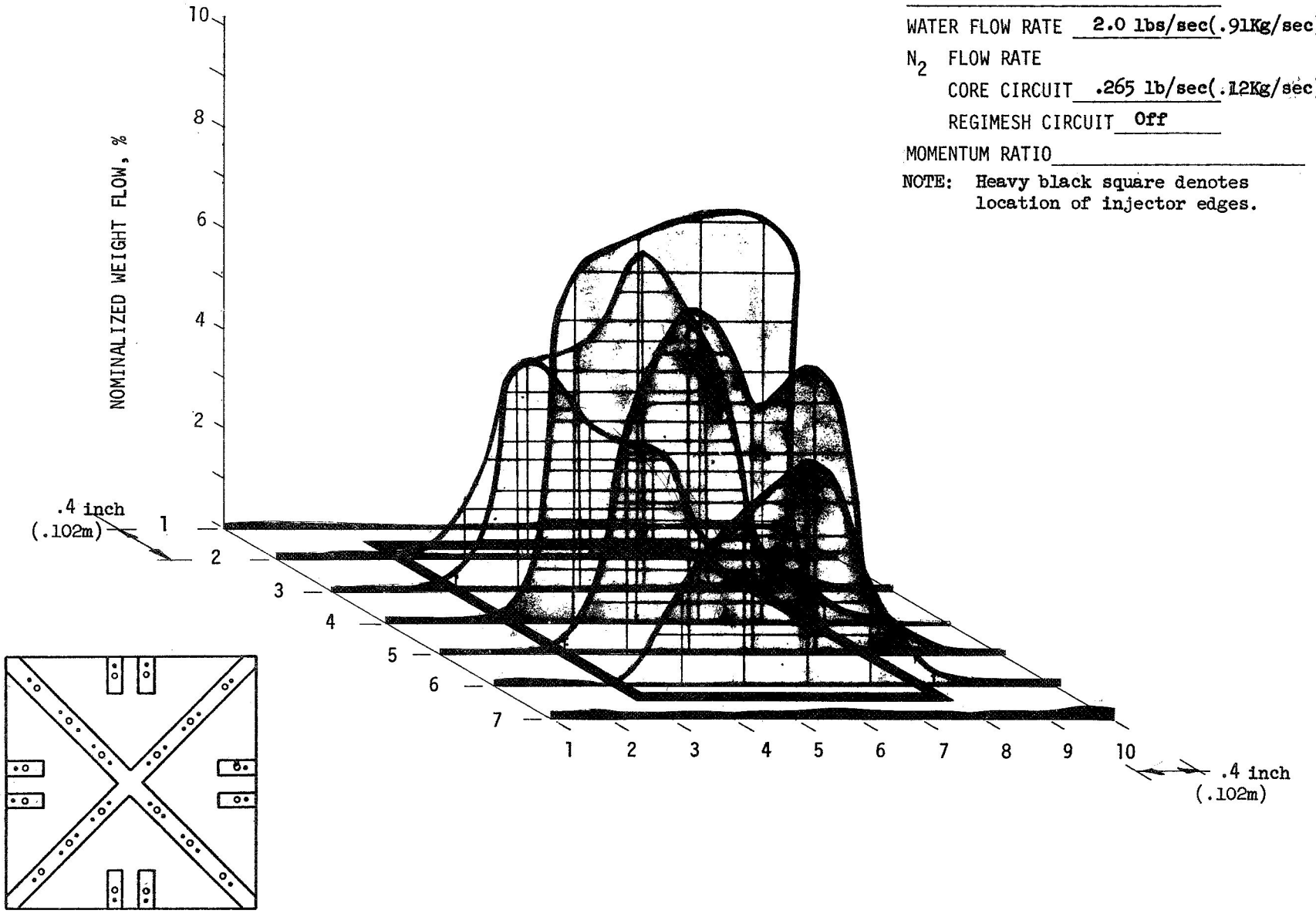

Figure 12. Injector 20-1 Simulated Flox Distribution, MOD 1A

Therefore, it was decided to enhance the mixing achieved by the injector modifications with the addition of a mixing section between the injector and the thrust chamber.

c. Test Results

Hot-fire testing demonstrated that the 20-2 injector, in conjunction with the subsequently discussed mixing chamber, was completely effective as a uniform combustion source for use in evaluating material samples. The mixer was used successfully in two firing tests for an accumulated duration of 23 sec. Its coolant capability was demonstrated by the absence of damage or localized erosion. The effectiveness of the unit in promoting mixing of the combustion products was shown by the absence of streaks in the downstream chamber. The mixer section was not used in tests 014 and 015 because of a leak in the braze joint.

Although thrust measurements were not made for tests 010 through 015, the chamber pressure data indicated a lowering of performance caused by the injector modification. The performance data shown in Table VI for the 20-2 injector is suspect because of large variations in c* efficiency with seemingly small changes in operating conditions. A cursory analysis of the flox flow data showed large variations in K_w factors (pressure drop) which could only be explained by flow measurement errors or injector plugging. Post-test analysis revealed that streaking still occurred at the throat location and subsequent testing with this injector would require that the mixer be incorporated as an integral part of the configuration.

B. THRUST CHAMBER

The thrust chamber design selected was a rectangular configuration with the test specimens forming the convergent-divergent contour. Both the thrust chamber and test specimens were water cooled by separate manifolds. The tester geometry is shown on Figures No. 13 through No. 16. It contains two copper (OFHC) opposing side panels which form a permanent part of the test rig. The remaining two opposing sides of the rectangular-shaped chamber are cooled by replaceable test panels upon which the thermal barrier composites to be evaluated were applied.

The test specimens are held in place by a backing fixture bolted to the chamber panels. Seals between the test specimen and the primary chamber hardware are provided by Durabla sheet. The specimen backing fixture is machined to match the backside of the test specimen to provide a uniform distribution of sealing force as well as for structural support.

In addition to the thrust chamber, an adapter section was designed and fabricated to fit between the injector and chamber section. This adapter, which served to mix the exhaust gases to minimize streaking in the chamber sections, was water-cooled because of the duration requirements. The unit protruded into the chamber almost 2.0-in. (0.051 m) so as to avoid exposing the

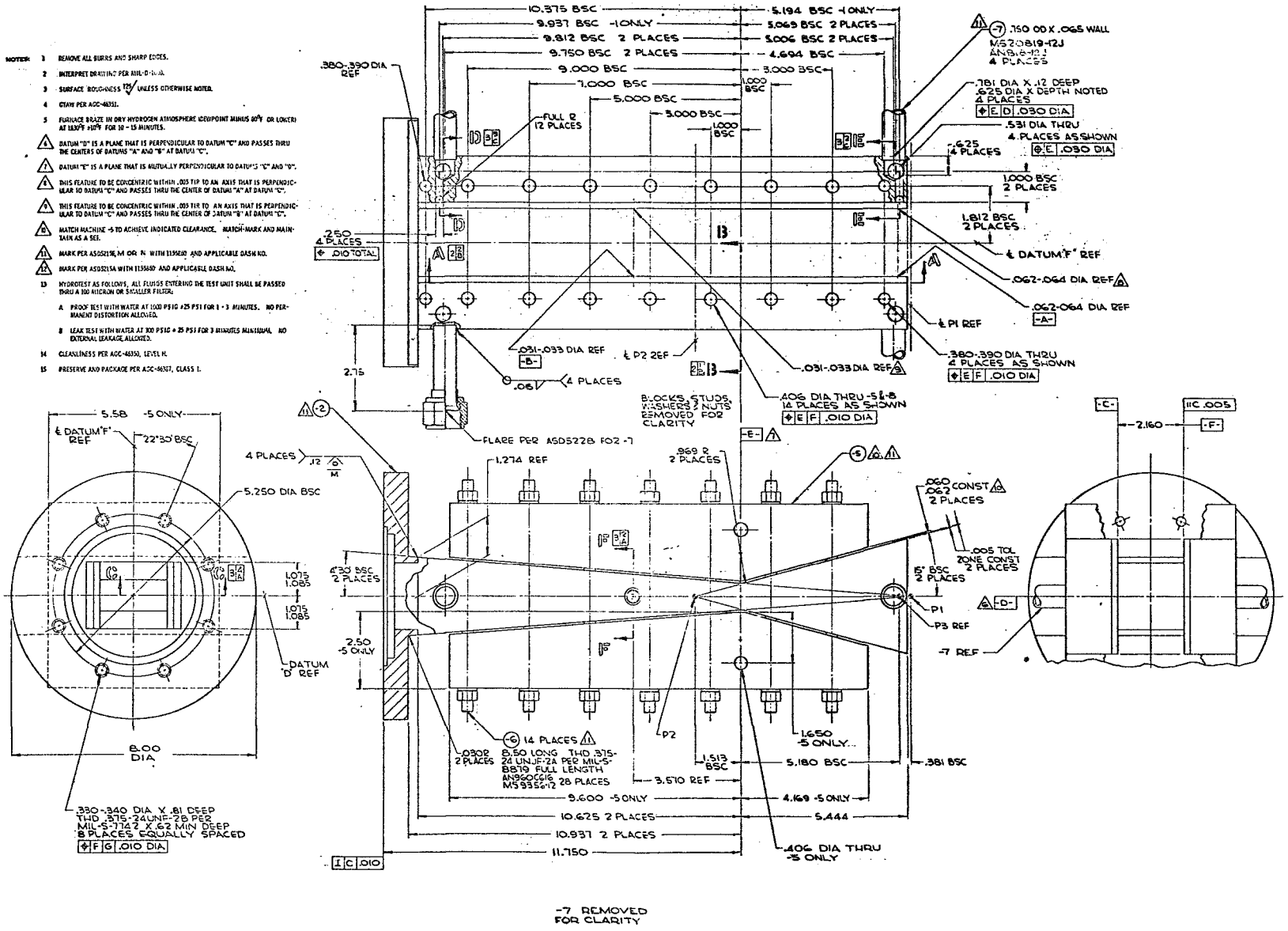

Figure 13. Thrust Chamber Assembly

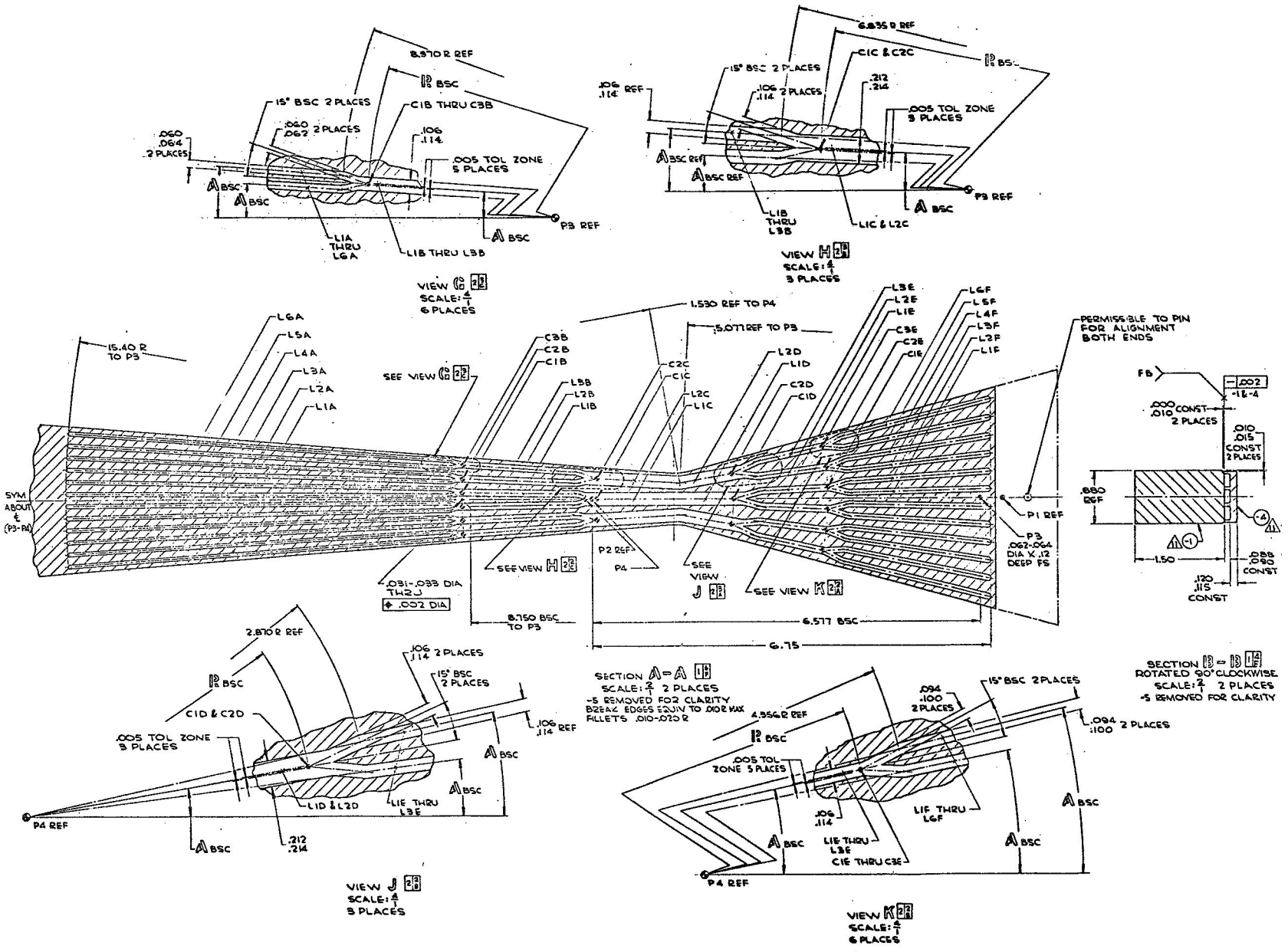

Figure 14. Side Panel Configuration

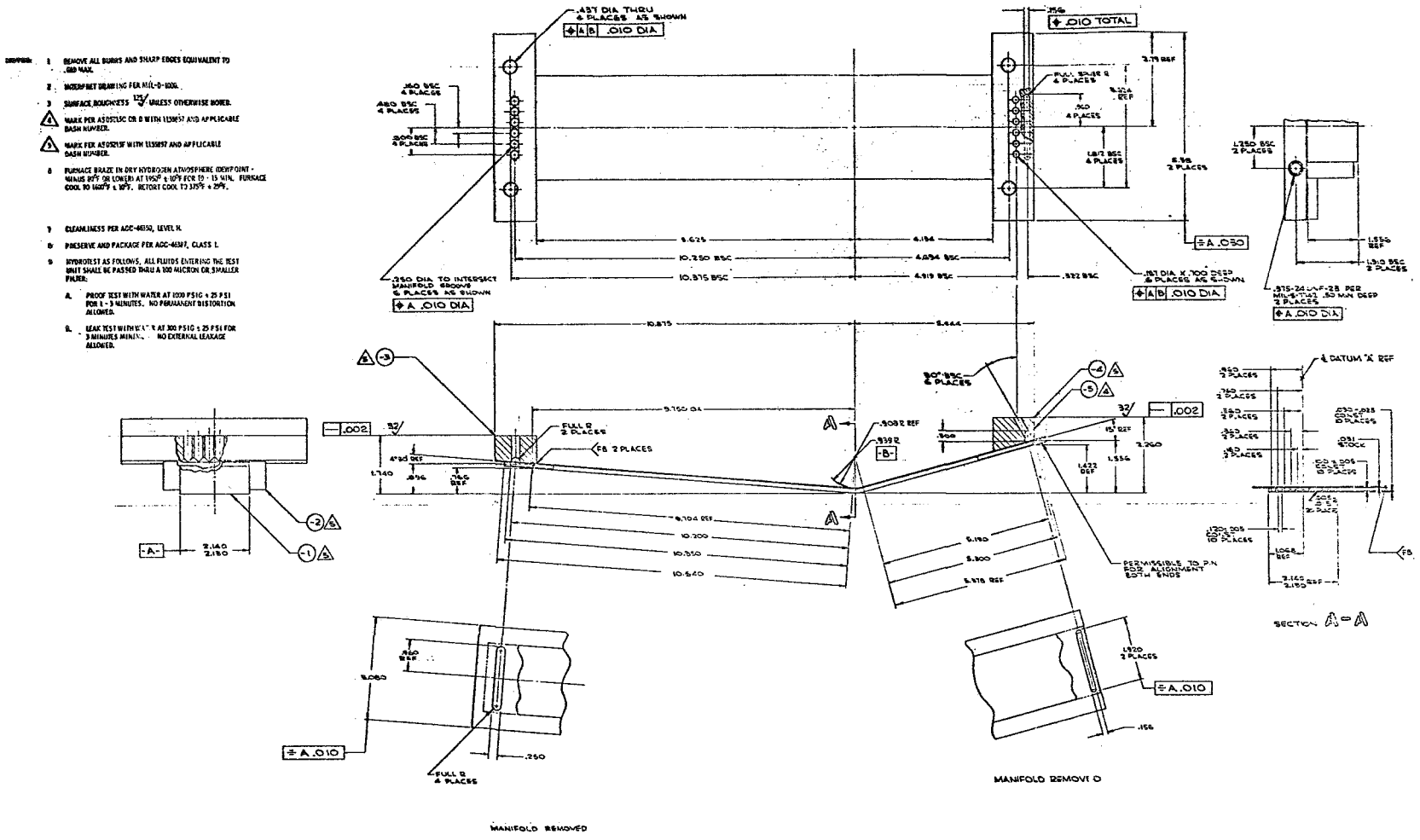

Figure 15. Test Panel Configuration (Flat Ni Plate)

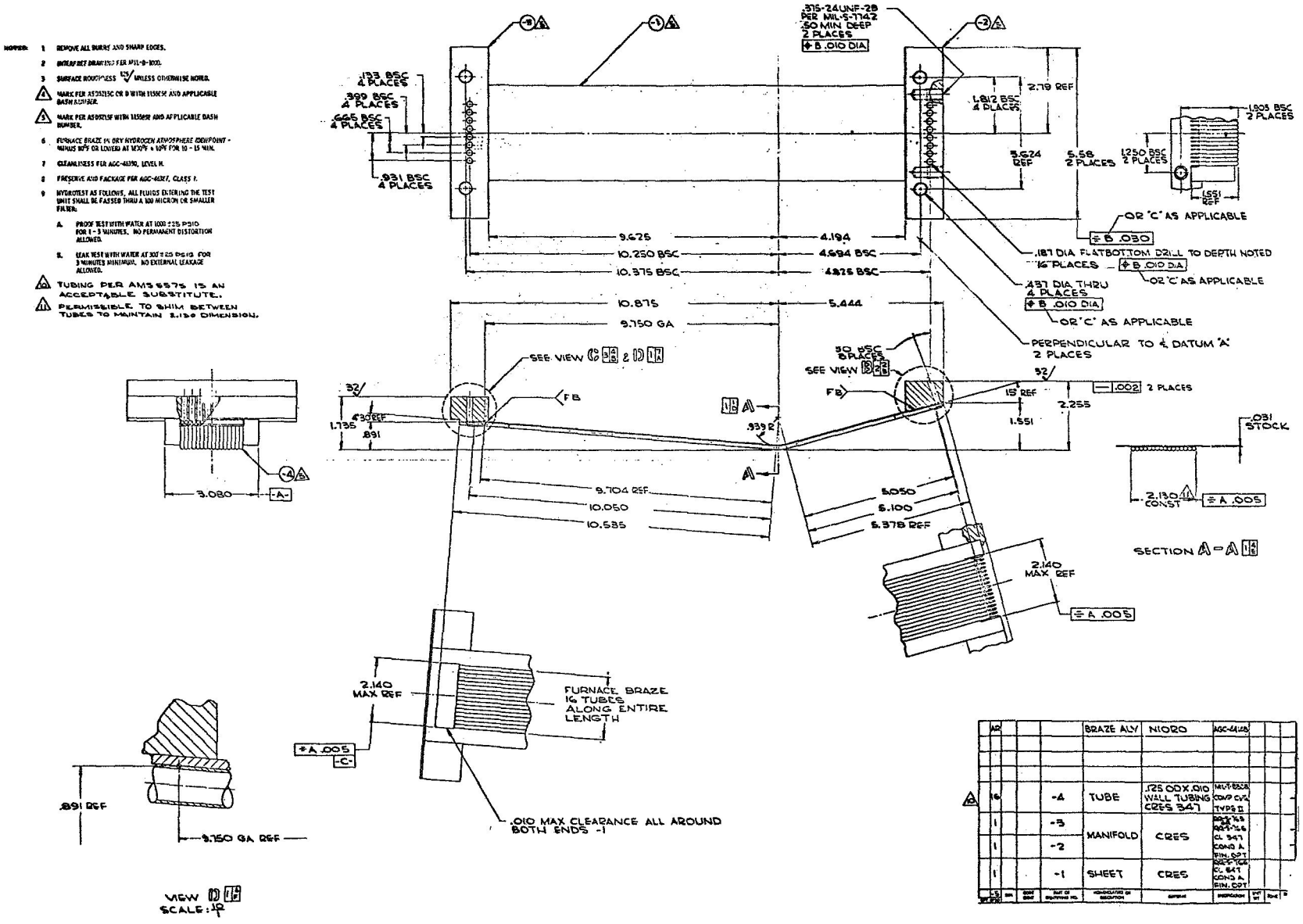

Figure 16. Test Panel Configuration (Tube Type)

chamber seals to the combustion products while accepting injector entry for a similar distance. Consequently, the mixer consisted of a circular member, which accepted the injector, and then converged to a smaller circular section, which fit into the square test chamber (see Figure No. 17).

Starting at the injector face, the mixer consisted of a 3.0-in. (0.076 m) diameter by 2.5-in. (0.064 m) long cylinder which discharged into a 1.25-in. (0.032 m) long cone that converged from a diameter of 3.0-in. (0.076 m) to 1.60-in. (0.041 m). The conical section matched a 2.0-in. (0.051 m) long by 1.60-in. (0.041 m) diameter cylinder, which discharged into the 2.0-in. (0.051 m) square thrust chamber. Adding this mixing assembly had a twofold effect. First, it increased the distance from the injector face to the throat by 5.75-in. (0.146 m). Secondly, it provided a significant discontinuity along the chamber wall.

The assembly was made from 347 stainless steel and oxygen-free, high conductivity (OFHC) copper. All flame surfaces were copper and the copper-to-steel joints were brazed. The coolant passages were a combination of milled slots and drilled passages. Provisions were made for the introduction of either water or fuel film cooling from the downstream edge of the part.

1. Method of Heat Transfer Analysis

The Heat Transfer Analysis is discussed in three sections; the prediction of gas-side boundary conditions, the coolant-side burnout, and heat conduction within the chamber wall.

a. Gas-Side Boundary Conditions

Gas-side boundary conditions include convective and radiative heat loads. Convective heat fluxes were calculated using enthalpies for thermal driving potential assuming that chemical reactions in the boundary layer are rapid enough to provide equilibrium conditions. Figure No. 18 is a temperature enthalpy plot for the products of combustion at the stagnation and throat static chamber pressures. Local chamber heat fluxes were calculated from the following equation

$$Q/A = h_{gi} \left(i_{stagnation} - i_{wall}\right) \qquad \text{Eq. (1)}$$

in which, h_{gi} is the local heat transfer coefficient. The stagnation enthalpy was selected because it is a reasonable, slightly conservative approximation to the actual recovery enthalpy and simplifies the calculation time required.

Heat transfer coefficients were calculated using the following Stanton number relation:

$$St_i = \frac{h_{gi}}{\frac{\dot{W}}{A}} = C_g \, Re^{-0.2} Pr^{-0.66} (Z) \qquad \text{Eq. (2)}$$

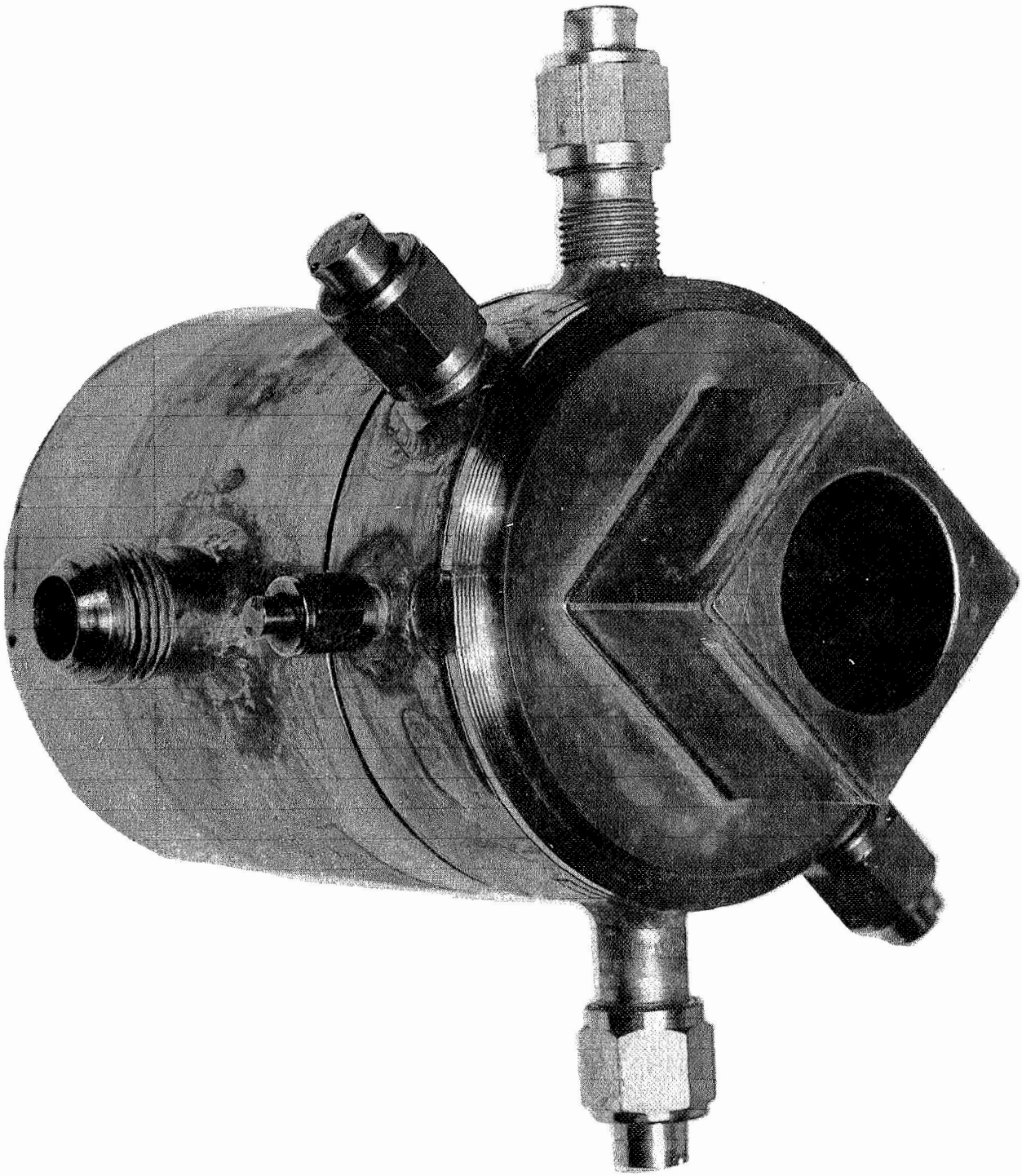

Figure 17. Adapter Used to Mix Exhaust Gases

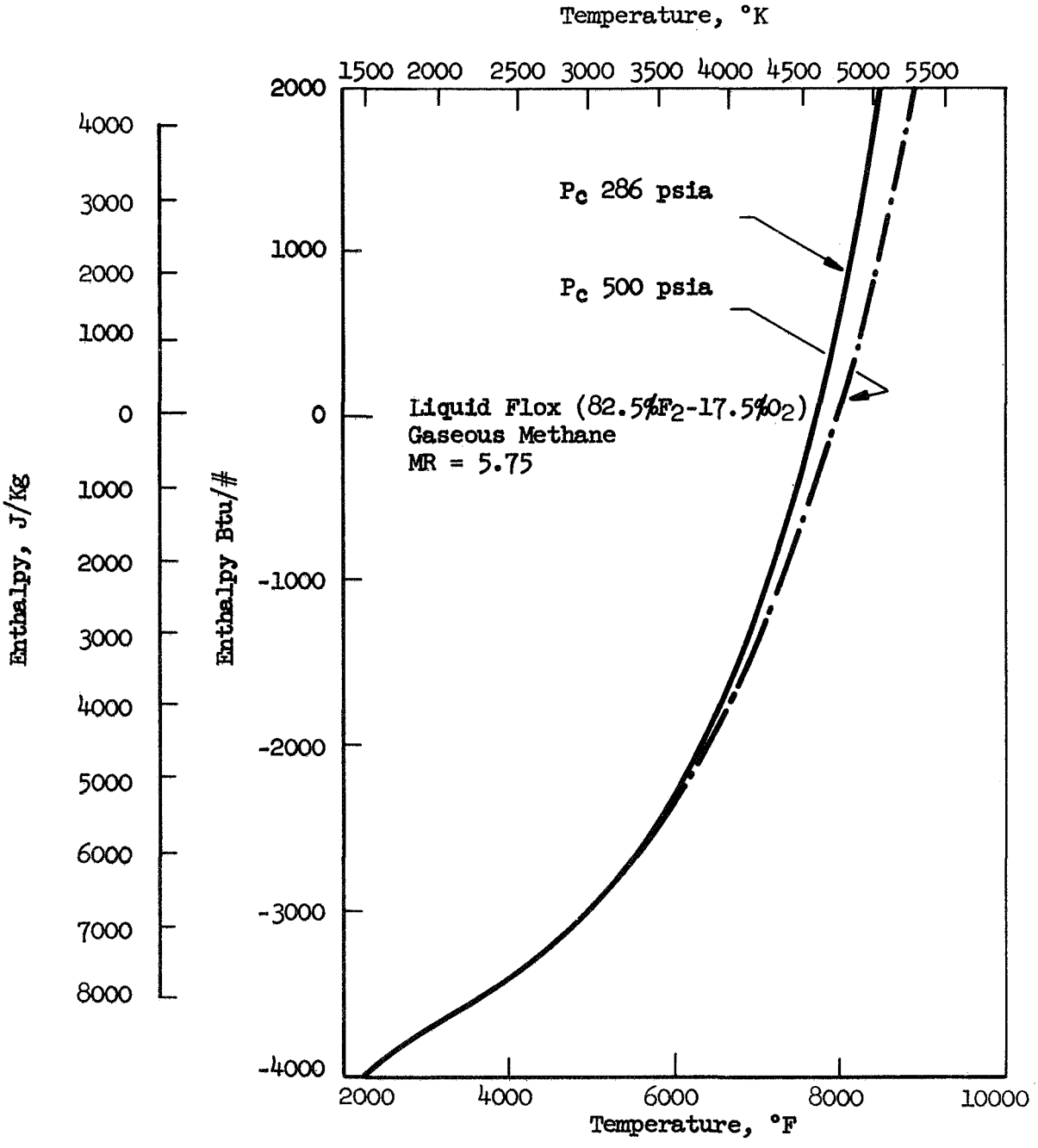

Figure 18. Temperature-Enthalpy Flox/Methane Combustion Products

In this equation, h_{gi} is the heat transfer coefficient, $\dot{W}$ is the total propellant flow rate, 3.27 lb/sec (1.484/(kg/sec), and A is the local cross-sectional area of the duct. The hydraulic diameter in the Reynolds Number (Re) is taken as the usual 4A/P, where P is the periphery of the duct. A correction for film temperature properties is used in a factor

$$Z = \left(\frac{T_{FS}}{T_{Am}}\right)^{0.8} \cdot \left(\frac{\mu\ Am}{\mu\ FS}\right)^{0.2}$$

where T_{FS} = freestream temperature, $T_{Am} = \frac{T_{stag} + T_{wall}}{2}$ and μ is the gas viscosity evaluated at the designated reference temperatures. Values of Z are approximately 1.35 for a 1500°F (1080°K) wall and 1.2 for a 3500°F (2200°K) wall. The thermal properties used in the analysis are shown on Figure No. 19.

Two sets of heat transfer coefficients were calculated. One was a best estimate calculation to be used in conjunction with best estimate combustion conditions. It was applied in selecting coating thickness and for predicting coating surface temperatures. The other set was a conservative estimate used for designing a test fixture and calculating minimum water flow rates and velocities. Both sets of heat transfer coefficients were obtained through appropriate selection of empirical C_g values in Equation (2). The specific values used are shown on Figure No. 20 and were based upon Aerojet's design and testing experience. High design values were selected for the chamber region because of the many unknowns associated with the combustion process. Lower factors of safety were applied in the throat and beyond where experience has shown the combustion effects to be greatly diminished. Detailed predictions of the radiation heat flux were not made because experience has shown these to be small when compared to the convective loads. It was estimated that there was sufficient margin in the convective design loads to accommodate cold-wall radiation from both coated test panels and HF in the combustion products. Maximum radiation loads to the cold side panels were estimated to be 0.5 Btu/sec-in.^{2} (82 x 10^4)/m^2 sec) from 3540°F (2220°K) coated panels and 0.8 Btu/sec-in.^{2} (131 x 10^4)/m^2 sec) from the 7340°F (4450°K) combustion products.

The predicted maximum gas-side flux for an uncoated wall based upon 100% c* and best estimate flux (95% c*) are shown on Figure No. 20. The best estimate flux to a coated wall with a 3500°F (2200°K) surface temperature also is shown. As can be noted, there is a considerable margin of safety built into the maximum flux predictions.

b. Coolant-Side Analysis

The usual approach to calculation of the coolant-side convective coefficients is to first iterate the coolant-side wall temperature assuming that a conventional duct flow equation applies

$$h_{S_L} = 0.023 \frac{K}{D} Re^{0.8} Pr^{0.4} \qquad \text{Eq. (3)}$$

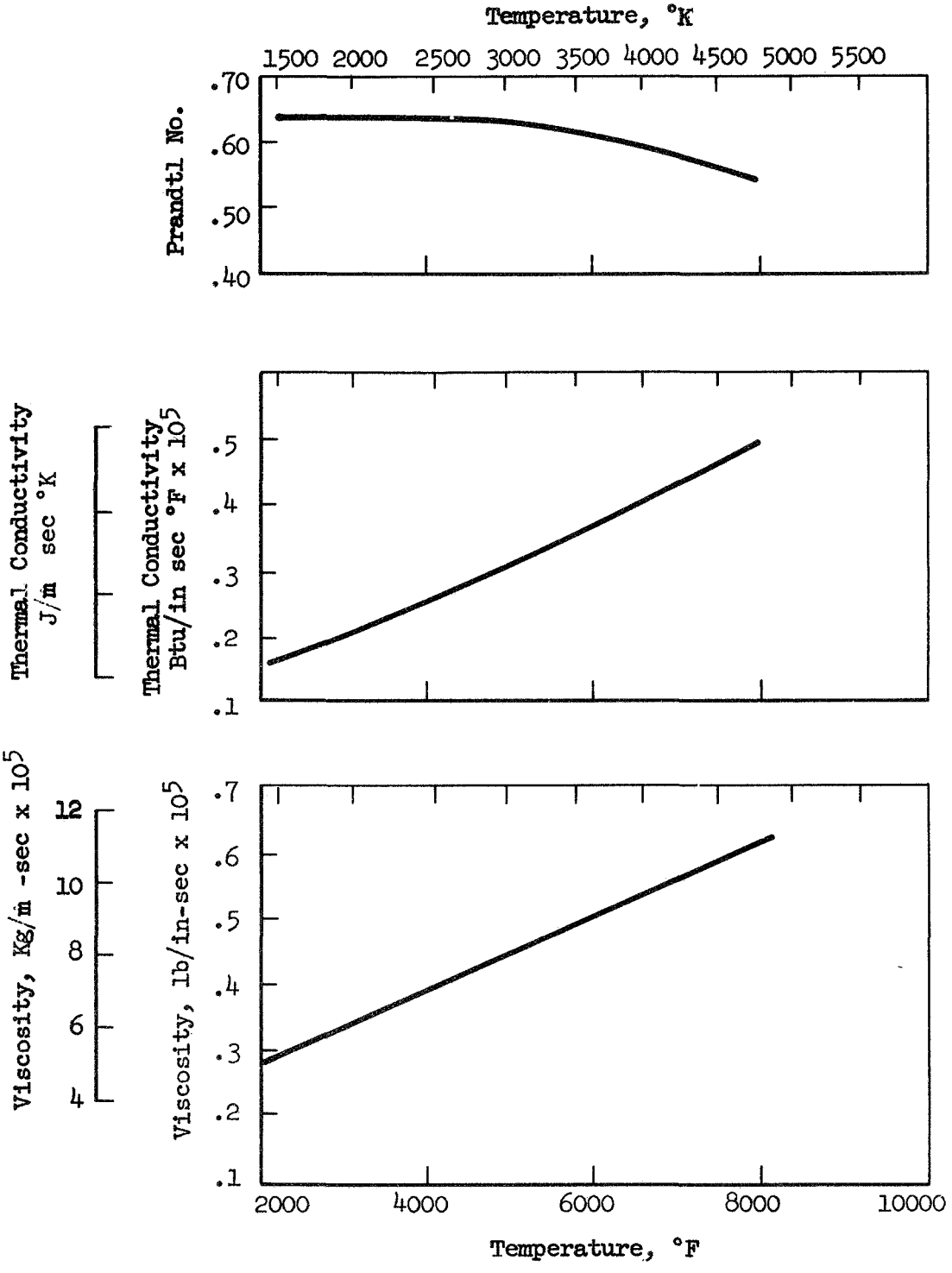

Figure 19. Properties of Combustion Products of Flox/Methane for MR = 5.75

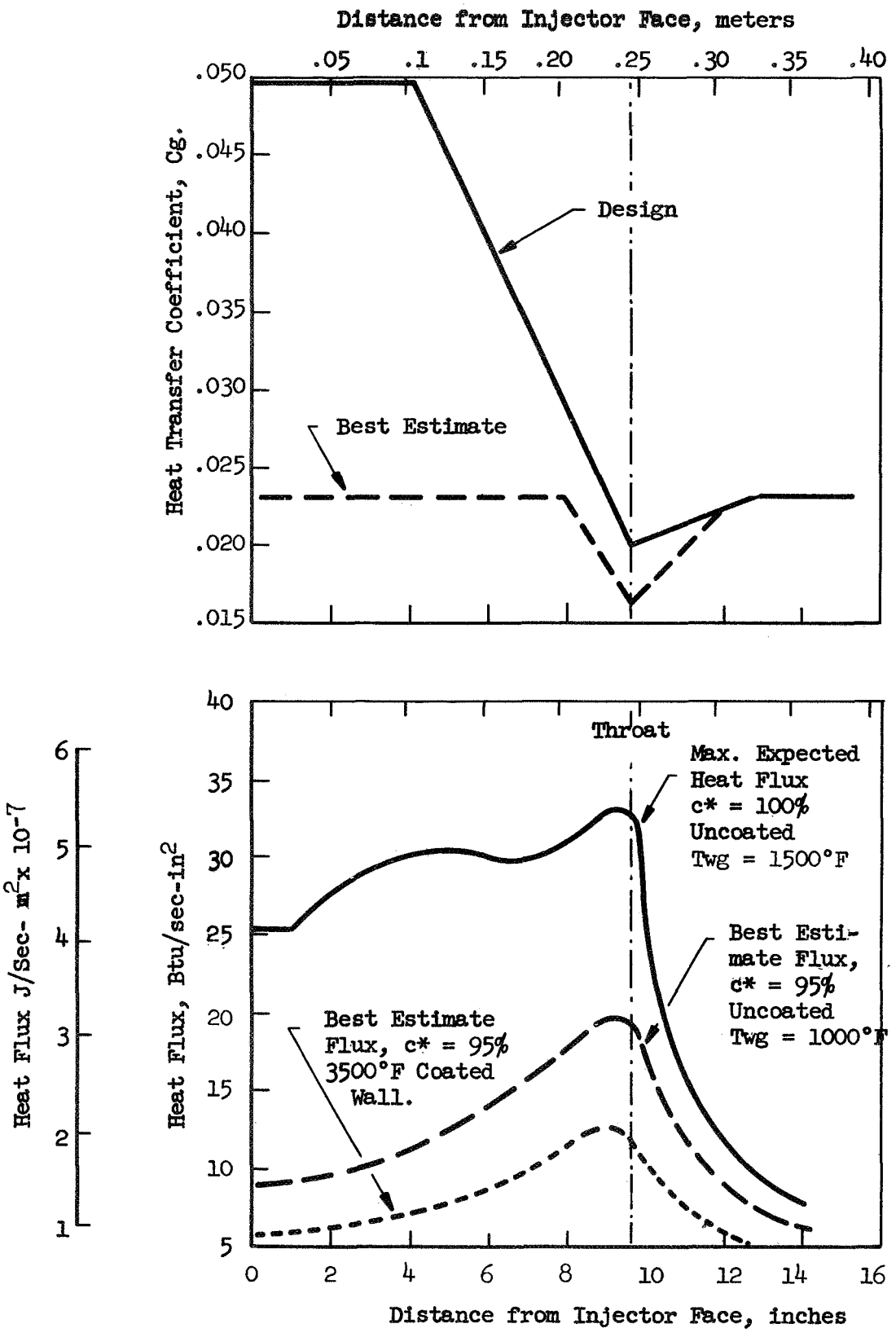

Figure 20. Tester Thermal Design Parameters and Heat Flux Profiles

The liquid-side wall temperature then was calculated to determine if it was above the saturation temperature of the water at the local static pressure. If the wall temperature was found to exceed the saturation temperature, the wall was assumed to be at the saturation temperature plus some super heat value which could be expressed as an exponential function and a new heat flux was calculated. This latter flux then was compared to the flux that would result in incipient film boiling and subsequent burnout. However, several simplifying assumptions were made to expedite the design point analysis. Conservatism appeared to be of greater importance than detail. Because the heat fluxes were relatively high, it was assumed that boiling was occurring and that liquid side wall temperature was equal to the local saturation temperature +50°F (283°K). Heat fluxes then were calculated and compared to the burnout flux which was calculated from the following equation

$$Q/A_{Bo} = 2.0 + \left(\frac{V\Delta T_{sub}}{1000} \right)^{0.95} \qquad \text{Eq. (4)}$$

in which, V is the velocity in ft/sec and ΔT_{sub} was the difference between the saturation temperature at the local coolant static pressure and the local bulk temperature. Equation (4) was derived empirically by Aerojet as a design limit value for water flowing at subcritical pressures and temperatures.

c. Wall Conduction and Geometry Effects

Heat conduction within the chamber wall was based upon one-dimensional flow within the copper and nickel walls and one-dimensional radial flow within the tubes. Heat flux at the coolant side was corrected by the ratio of the local coolant-side to gas-side surface area. In the copper side plates, this varies with axial position and only the three sides of the rectangular coolant channel bounded by the copper were considered as effective coolant surfaces. The surface formed by the steel backplate was assumed to be adiabatic. If the correction for the Ni plate was made on the same basis as for the copper, the correction factor would be 1.6. However, because of the lower conductivity of the Ni, much of the coolant channel side surface could be of low cooling effectiveness. Therefore, the surface correction was assumed to be 1.0.

The heat transfer rates used to calculate coolant bulk temperature rise were based upon the design heat flux using the flat surface area of the Ni and Cu wall. In the case of the tubes, however, additional heating surface in the form of the rounded tube crown would be exposed to the hot gas. The effective extra surface attributable to this curvature was estimated to increase the heat load by a factor of 1.28. Therefore, the tubular design had higher total flow rates and velocities than the flat surface design.

2. Results of Heat Transfer Analysis

Figures No. 21 through No. 27 summarize the results of the thermal analysis of the copper side plates, the flat nickel, and CRES 347 tubular test panels. Figures No. 21 through No. 24 provide the following information for each respective component plotted as a function of axial distance from the injector:

- The maximum expected gas-side heat flux without coating for 100% c* (design point).
- The maximum heat flux to the coolant (the gas-side flux corrected for appropriate two-dimensional or radial heat conduction effects).
- The maximum heat flux that can be sustained without initiating local film boiling (the burnout heat flux).
- Coolant velocity and flow rate.
- Coolant static pressure.
- Maximum coolant bulk temperature.

Heat fluxes also are provided for comparison in instances of non-conservative design. These include a best estimate flux, both with and without the thermal coating.

Figures No. 25, No. 26, and No. 27 provide predicted gas-side, liquid-side, and coolant bulk temperatures for each of the components based upon the design point heat flux. These are summarized as follows for the throat station which is the point of maximum heat flux and gas-side wall temperature:

	Wall Thickness, in.	Temperature, °F		
		Gas-Side	Coolant-Side	Bulk
Copper-Side Panel	0.120 (0.003 m)	1380 (1024°K)	525 (547°K)	185 (558°K)
Ni Test Panel	0.030 (0.0008 m)	1940 (1335°K)	520 (544°K)	170 (350°K)
CRES 347 Tubular Panel	0.010 (0.0003 m)	730 (660°K)	520 (544°K)	170 (350°K)

There are three considerations of note regarding the above temperatures. The predicted wall temperatures are probably much higher than can be expected in normal operation because the combustion temperatures and heat transfer coefficients will be lower than the design point values (see Section IV,B,1). Some carbon probably will deposit upon the wall. Finally, the test panels will be protected by a thermal barrier. As an example, at 95%

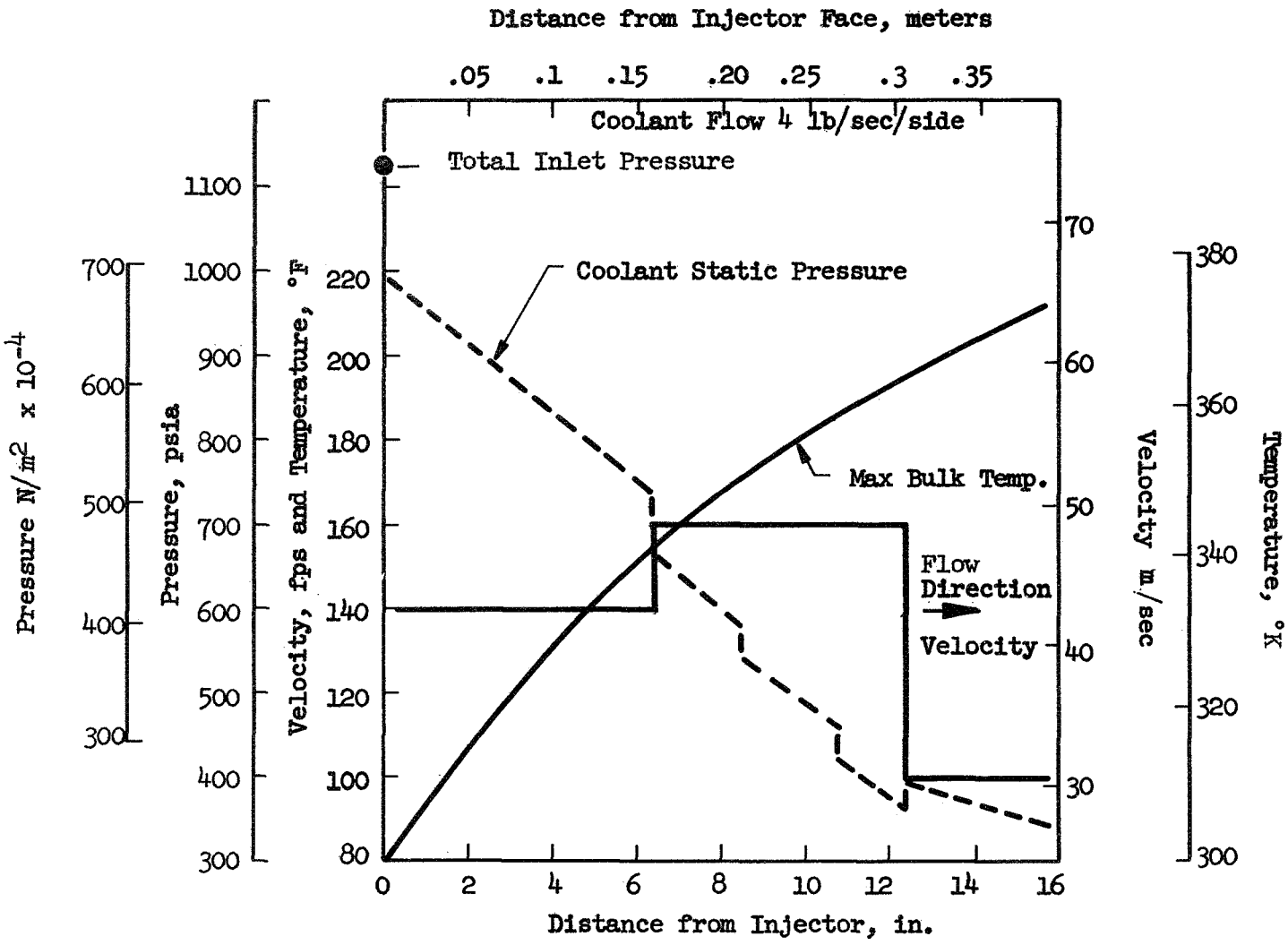

Figure 21. Copper Side Panel Coolant State Profiles

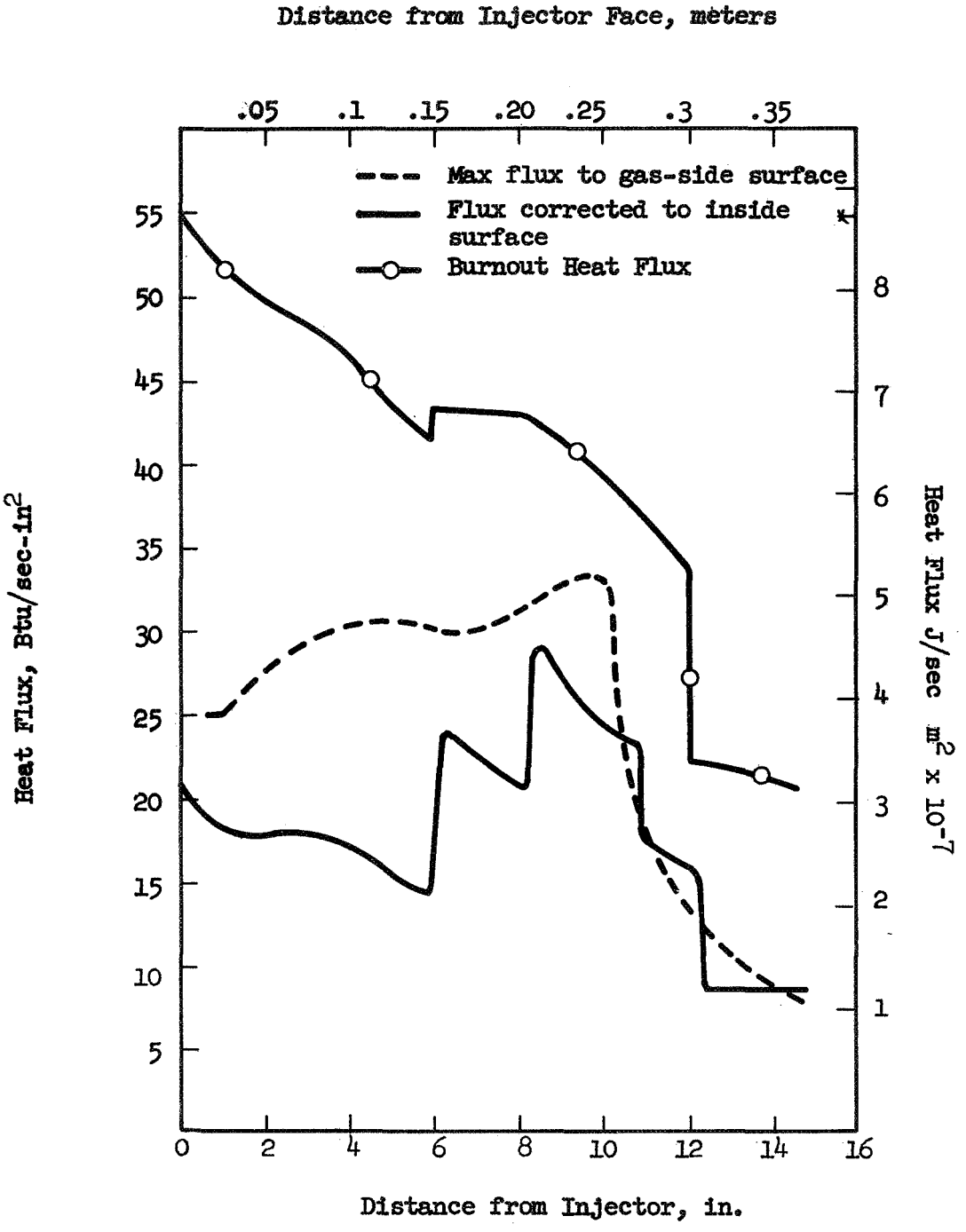

Figure 22. Copper Side Panel Design Point Heat Flux

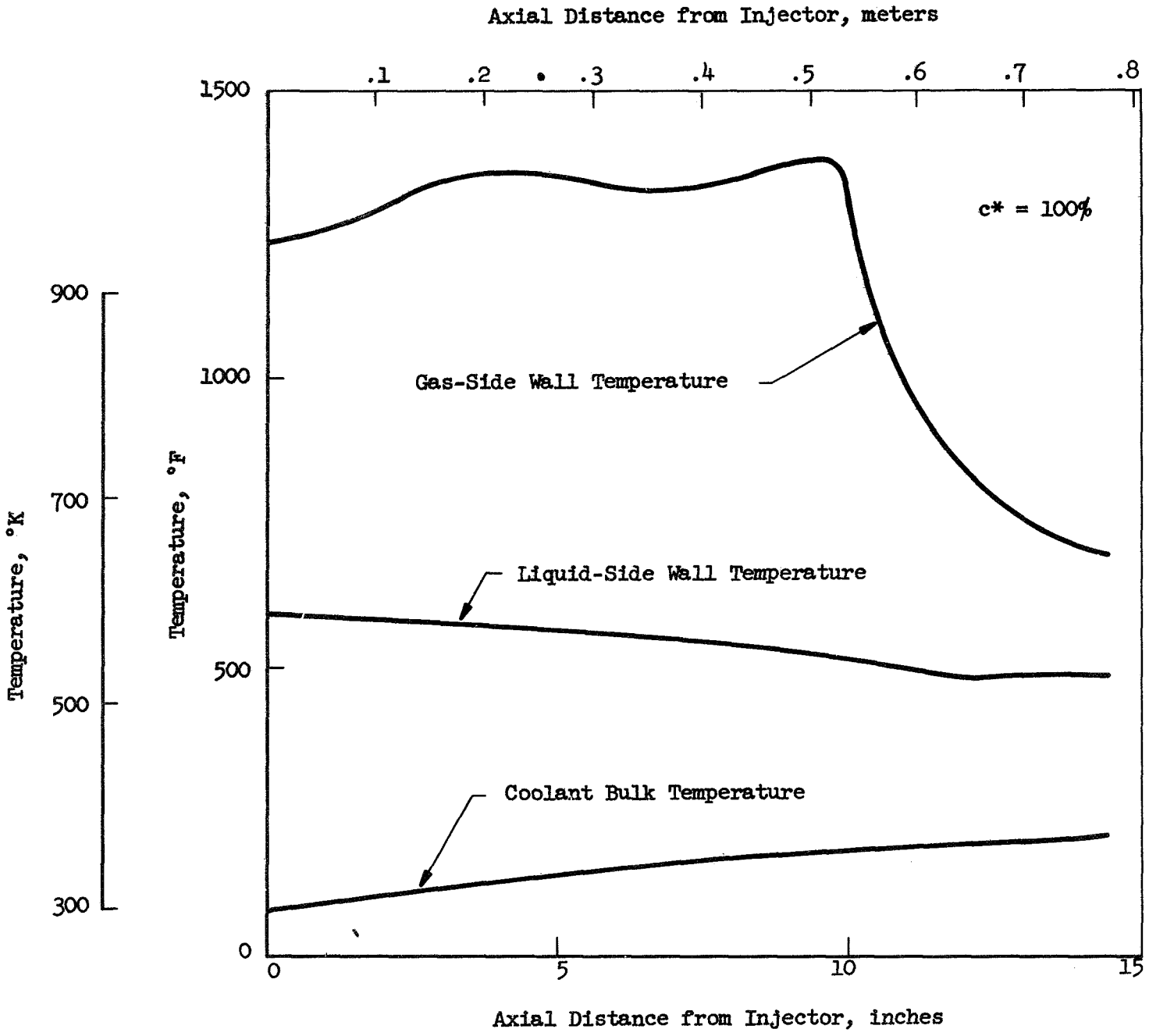

Figure 23. Copper Side Panel Design Point Temperature Profiles

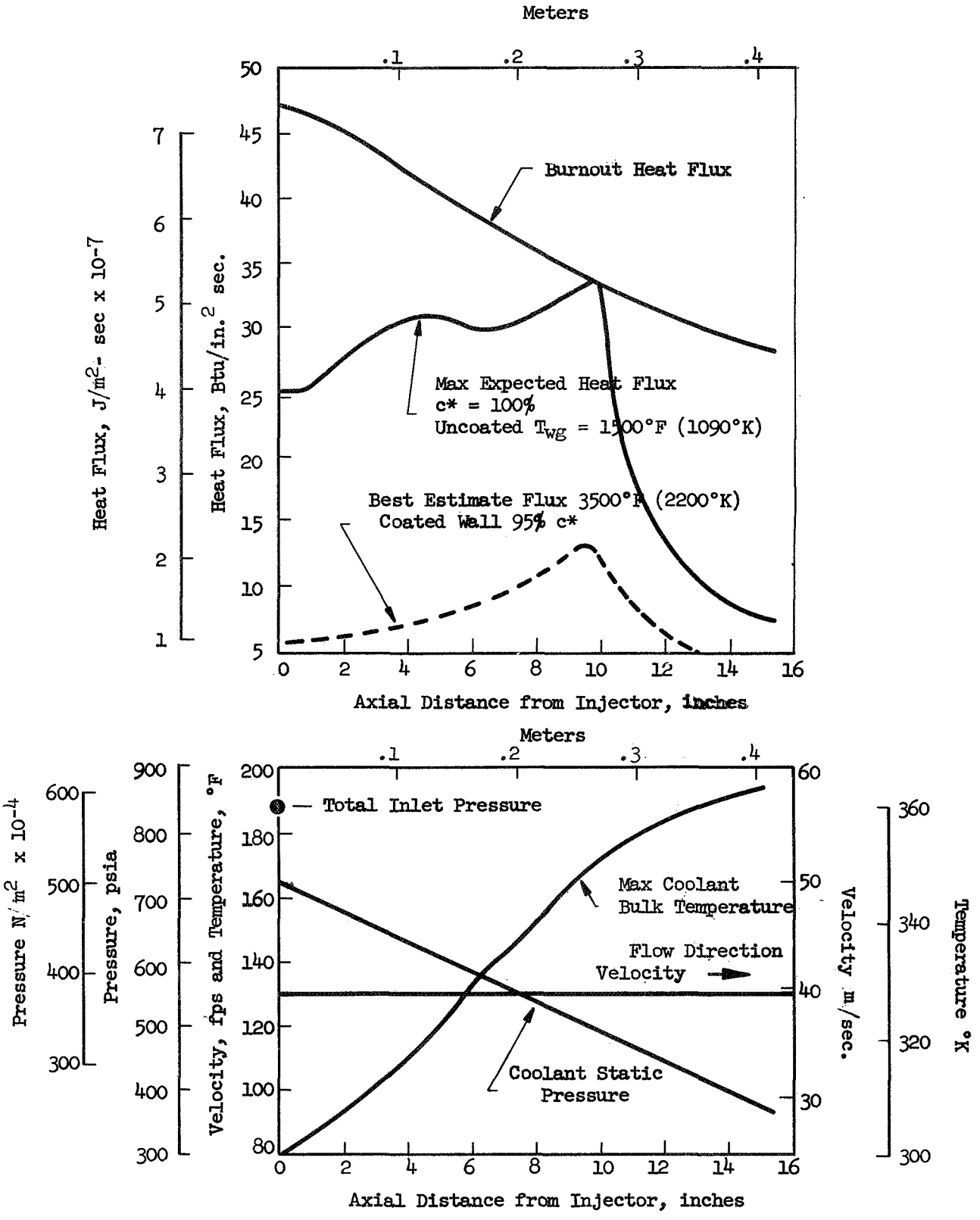

Figure 24. Ni 200 Test Panel Design Point Heat Flux and Coolant State Profiles

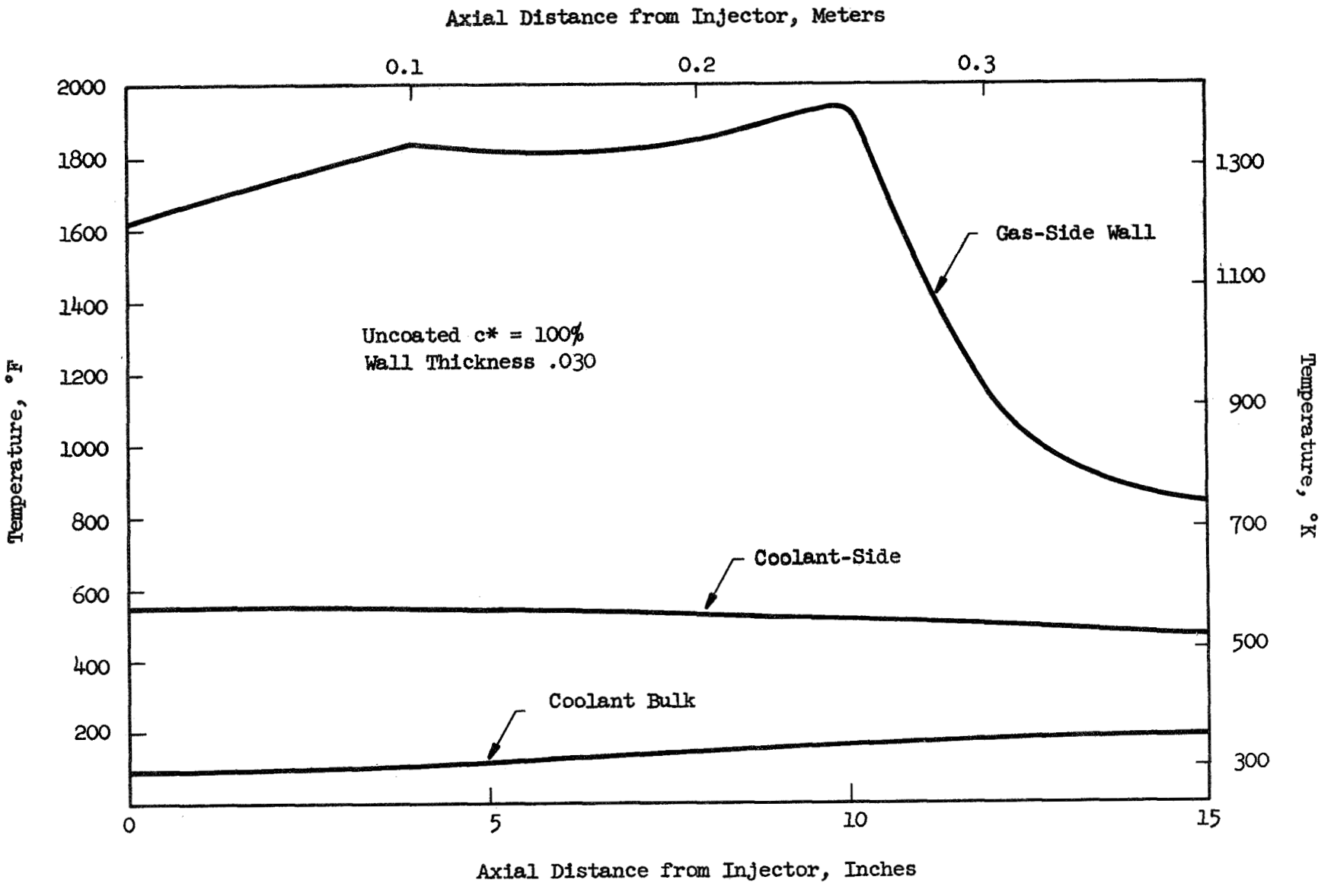

Figure 25. Ni 200 Test Panel Design Point Temperature Profiles

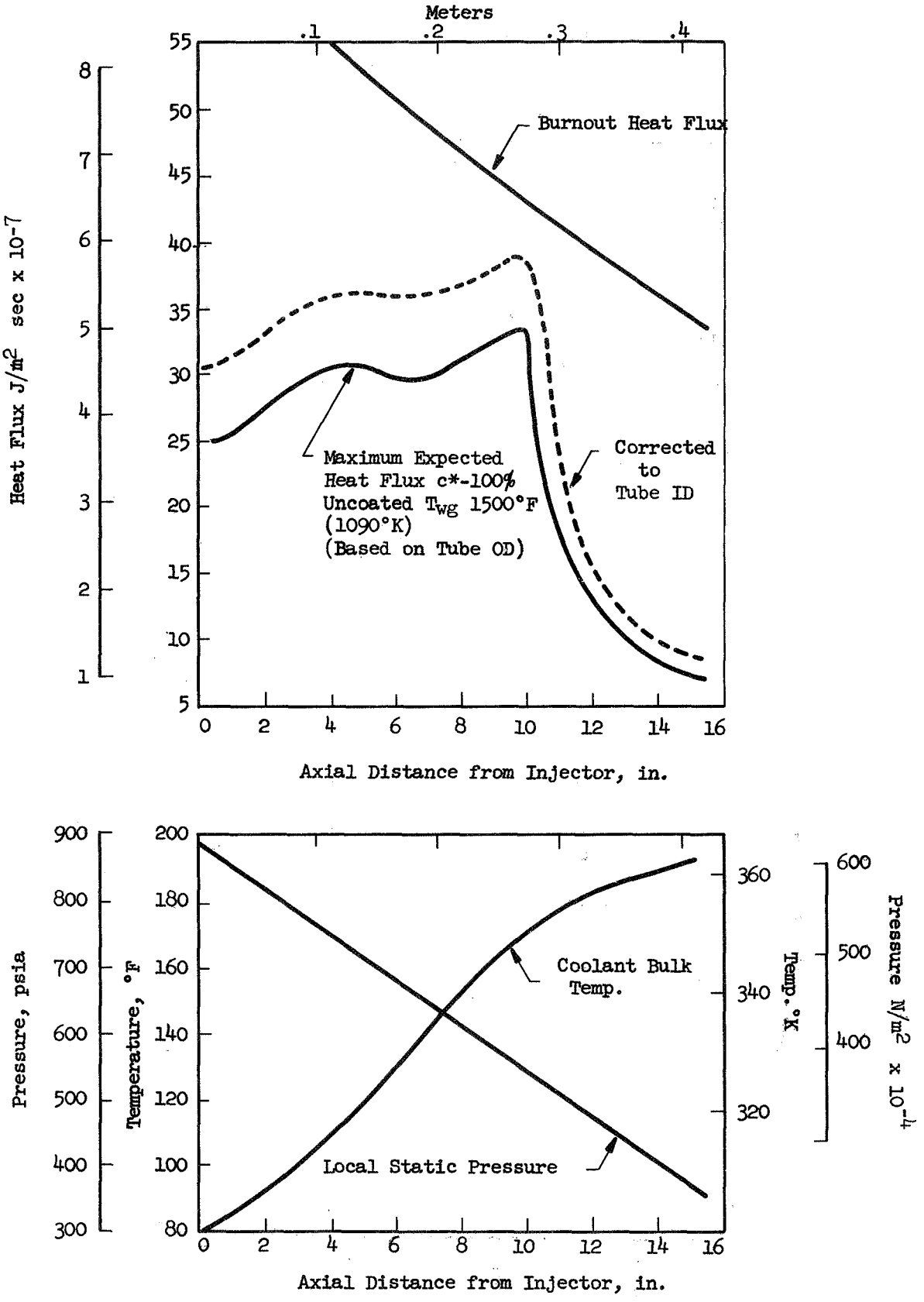

Figure 26. CRES 347 Tubular Test Panel Design Point Heat Flux and Coolant State Profiles

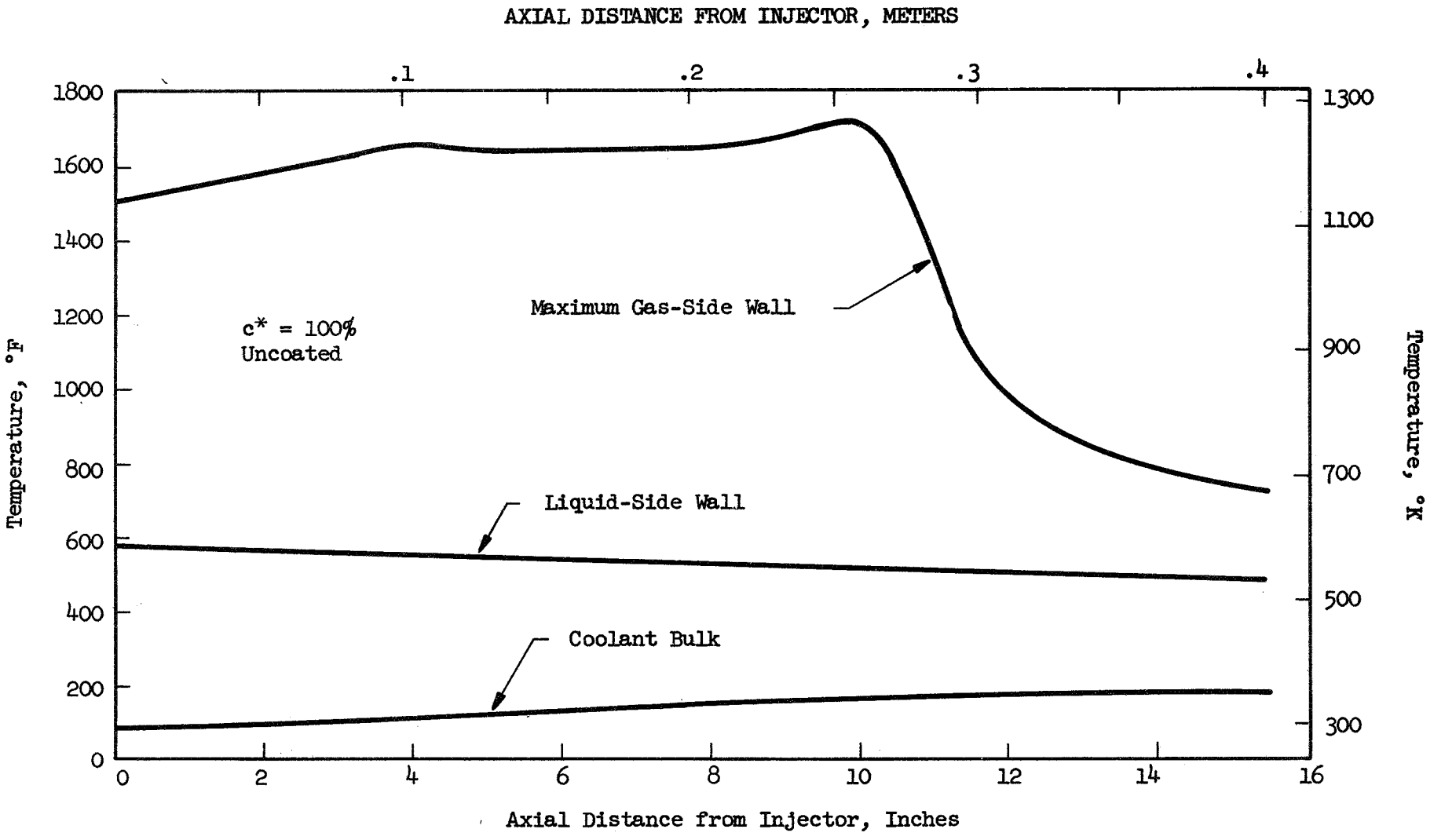

Figure 27. Tubular Test Panel Design Point Temperature Profiles

c* and with a 3500°F (2200°K) coating surface temperature, the best estimate throat heat flux is 12.9 Btu/sec-in.^{2} as compared to a design point value of 33.5. The best estimate gas-side wall temperature predicted for the coated nickel panel is 1080°F (856°K) and 1400°F (1034°K) for the uncoated panel.

V. FLOX/METHANE COATING EVALUATION

The flox/methane coating evaluations were made using the combustor components described in the previous section. In addition to these components, an uncooled copper heat-sink chamber of the same dimensions as the water-cooled hardware was fabricated for the checkout tests.

A. TEST FACILITY

Testing of the flox/methane combustor was accomplished with the equipment shown on Figure No. 28. The oxidizer supply system depicted consisted of standard feed system components, including redundant flowmeters for flow rate measurement. It also included the necessary passivation system with three points for introducing GF_2 to the flox system; a burn-off system for fluorine vents and bleeds; and a helium pressurization system.

The methane was fed from a cascade of methane tanks into a pressurized 5 gal (18.9×10^{-3} m^3) run tank. Facility piping, a remotely-controlled pressure regulator, redundant flow meters, remote shut-off valves, and purge as well as venting systems comprised the complete system for supplying the gaseous fuel to the hardware thrust chamber valves.

The coolant water system contained a run tank, remote shutoff valves, a turbine flow meter, and a GN_2 pressurization system.

The flox required for the tests was mixed by introducing liquid fluorine into the LN_2-jacketed, 50 gal (189×10^{-3} m^3) weigh tank in a predetermined amount and then bubbling a measured amount of gaseous oxygen through the dip tube into the tank. After stabilization of the mixed fluids in the jacketed vessel, it was ready for transfer to the adjacent 12 gal (45.5×10^{-3} m^3) run vessel. The composition of the flox was determined by reacting a known volume and pressure of gaseous flox with mercury. This reaction (mercuric fluoride) resulted in a pressure drop and the ratio between this pressure drop and the original pressure was used to establish the fluorine content.

All primary functions were measured and recorded during the combustor tests, including chamber, manifold, and tank pressures; oxidizer, fuel, fuel film coolant and coolant water flow rates; and propellant and coolant water bulk temperatures.

Both analog and digital recorders were used to record test data. The analog recorders include strip charts, oscillographs, and time-event recorders. The digital system is made up of the analog-to-digital converter (ADC) and the digital tape recorder.

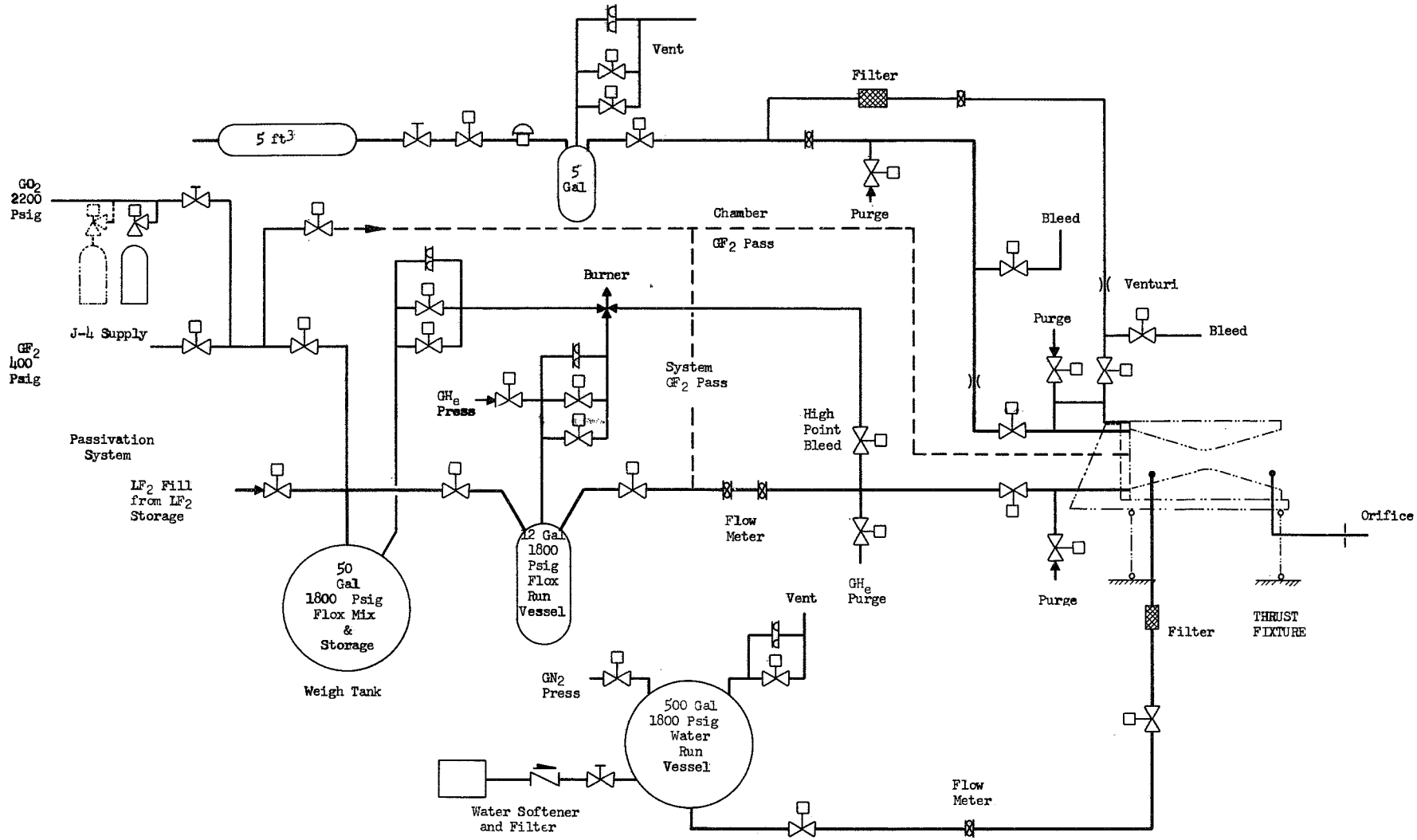

Figure 28. Flox/Methane Flow System Major Components - Test Stand J2A

B. FLOX/METHANE CHECKOUT TESTS

Fifteen flox/methane tests were made in the program. Nine of these were used to checkout the system and injectors while the remaining six tests were used to expose coatings to the exhaust stream.

The first three checkout tests were made with the 36-element injector (36-1) (see Figure No. 7) and a copper heat-sink chamber (see Figure No. 29). This injector was designed for high performance without face cooling and, therefore, a heat transfer problem was possible. However, it was intended to provide data for the system checkout without jeopardizing the hardware in the rest of the system. The injector was instrumented with two thermocouples to obtain surface temperature while the chamber was instrumented with three, water-cooled calorimeters to provide heat transfer data. The results of these first three tests are shown on Table VI.

The injector face overheated in all three tests. Visual examination of the injector and copper chamber after the first test revealed carbon combustion products, but no melting or material degradation. After the second test, melting was observed around the outside edges of the injector in three areas on the face of the injector (see Figure No. 30). The flame surface of the copper chamber after the second test was not degraded as evidenced by visual examination.

Tests 004, 005, 006, and 007 were made using the 20-element injector (20-1) which was fabricated with N155 rigimesh on the injector face. After test No. 004, which was programmed for 0.9 sec, visual examination of the injector revealed eroded areas in the rigimesh at the weld corners in the center of the injector and between the outside elements (see Figure No. 31). Prior to test No. 005, eight bleed holes were drilled in the rigimesh face to increase the cooling on the injector face. Four of these holes, 0.020-in. (5×10^{-4} m) diameter, were placed at the corners of the welds in the center of the injector and the other four holes, 0.015-in. (3.8×10^{-4} m), were located between the outboard elements of the injector. The copper chamber had carbon deposits on the flame surface but no evidence of melting. Streaked areas, approximately 0.75-in. (0.019 m) wide were observed in three areas on each face of the chamber.

Test No. 005 was conducted with the modified injector face. Its duration was 1.5 sec and visual examination revealed that the rigimesh had no additional erosion but three heat-marked areas now existed in the center of the injector. The copper chamber contained carbon deposits but no evidence of melting. The heat flux data obtained from water-cooled calorimeters positioned in the thrust chamber are shown on Figure No. 32. A maximum heat flux of 15.8 Btu/in.^{2}-sec (25.9×10^6 J/m^2 sec) was measured with the calorimeter positioned 0.4-in. (0.0102 m) upstream from the throat of the chamber. A conservative maximum heat flux of 33.5 Btu/in.^{2}-sec (55×10^6 J/m^2 sec) was used in the design of the water-cooled hardware. The best estimate of the maximum heat flux at the throat was 20 Btu/in.^{2}-sec (32.8×10^6 J/m^2 sec). In view of the

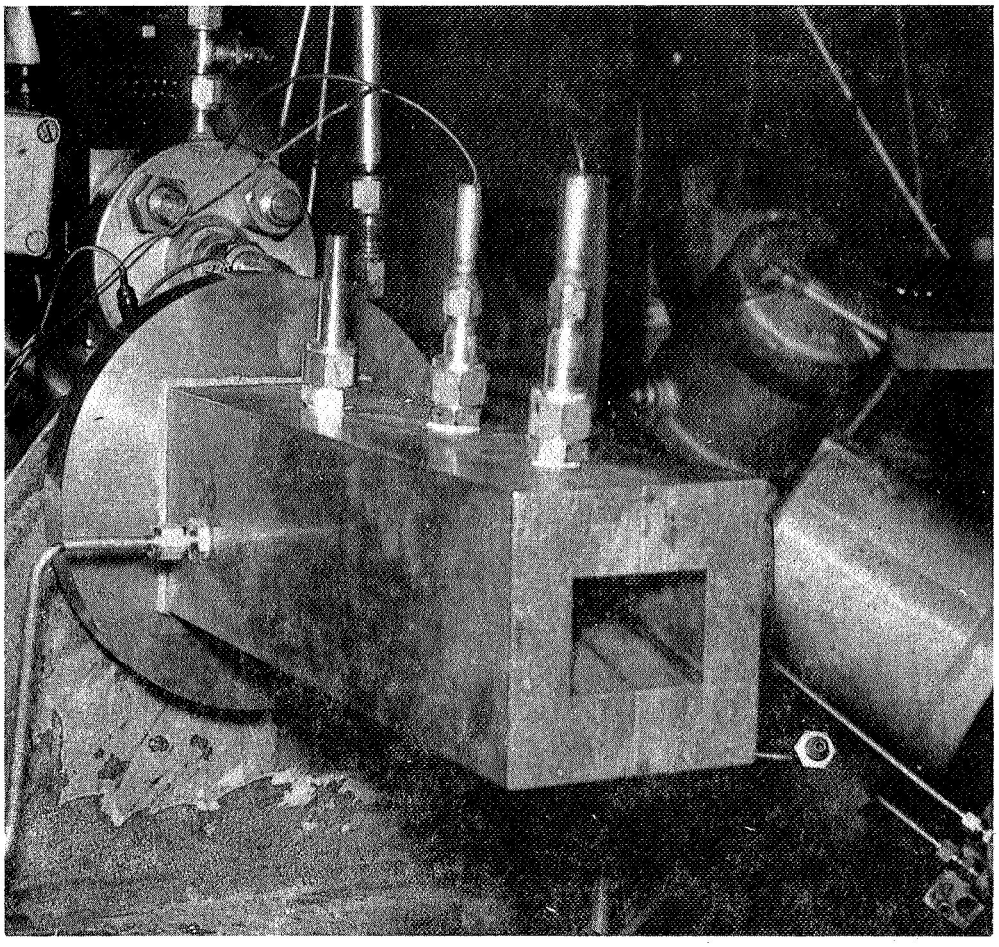

Figure 29. Copper Heat-Sink Chamber used for Flox/Methane Checkout Tests

Figure 30. Post-Fire Condition of 36-Element Injector Face

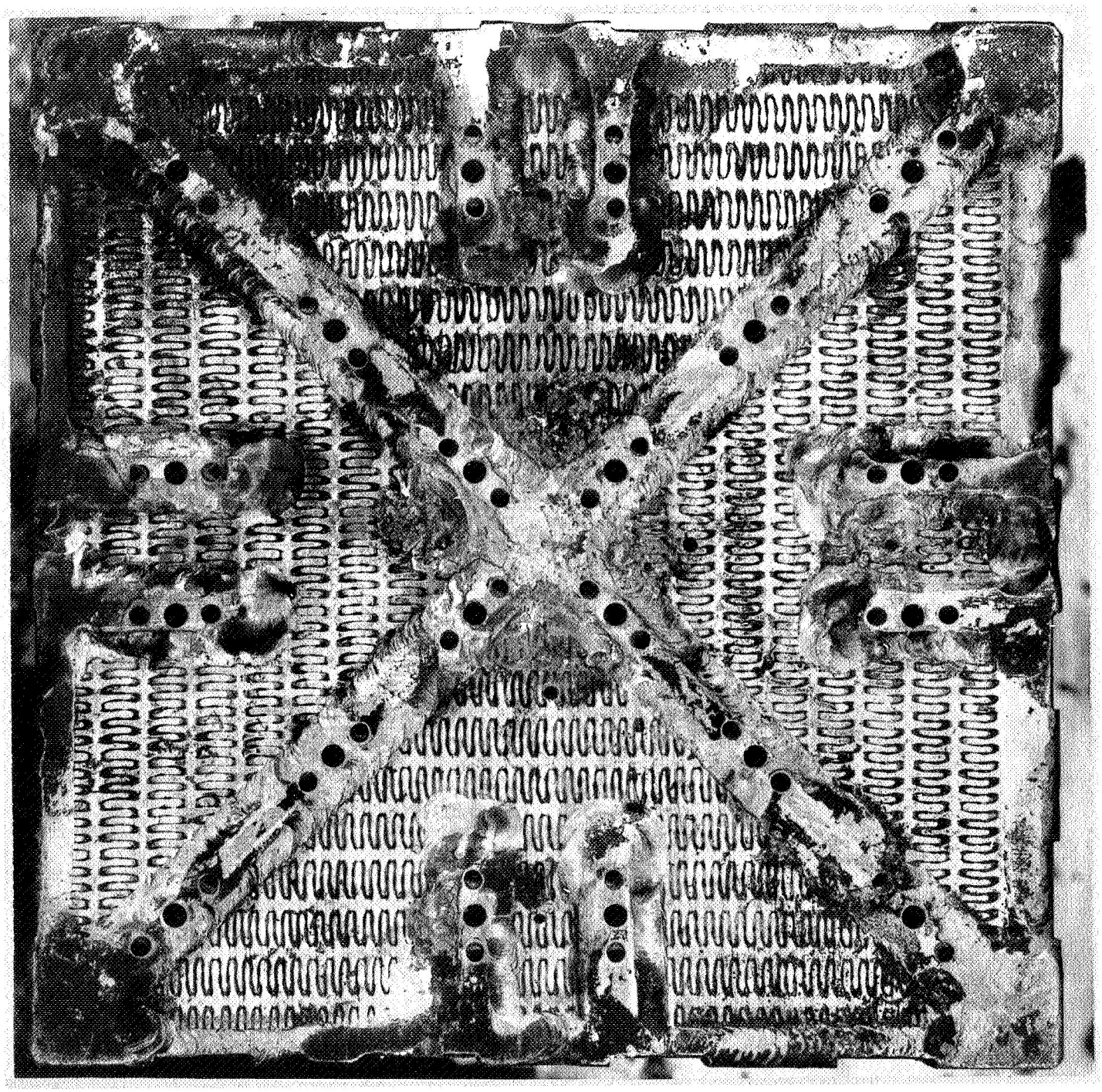

Figure 31. Post-Fire Condition of 20-Element Injector Face

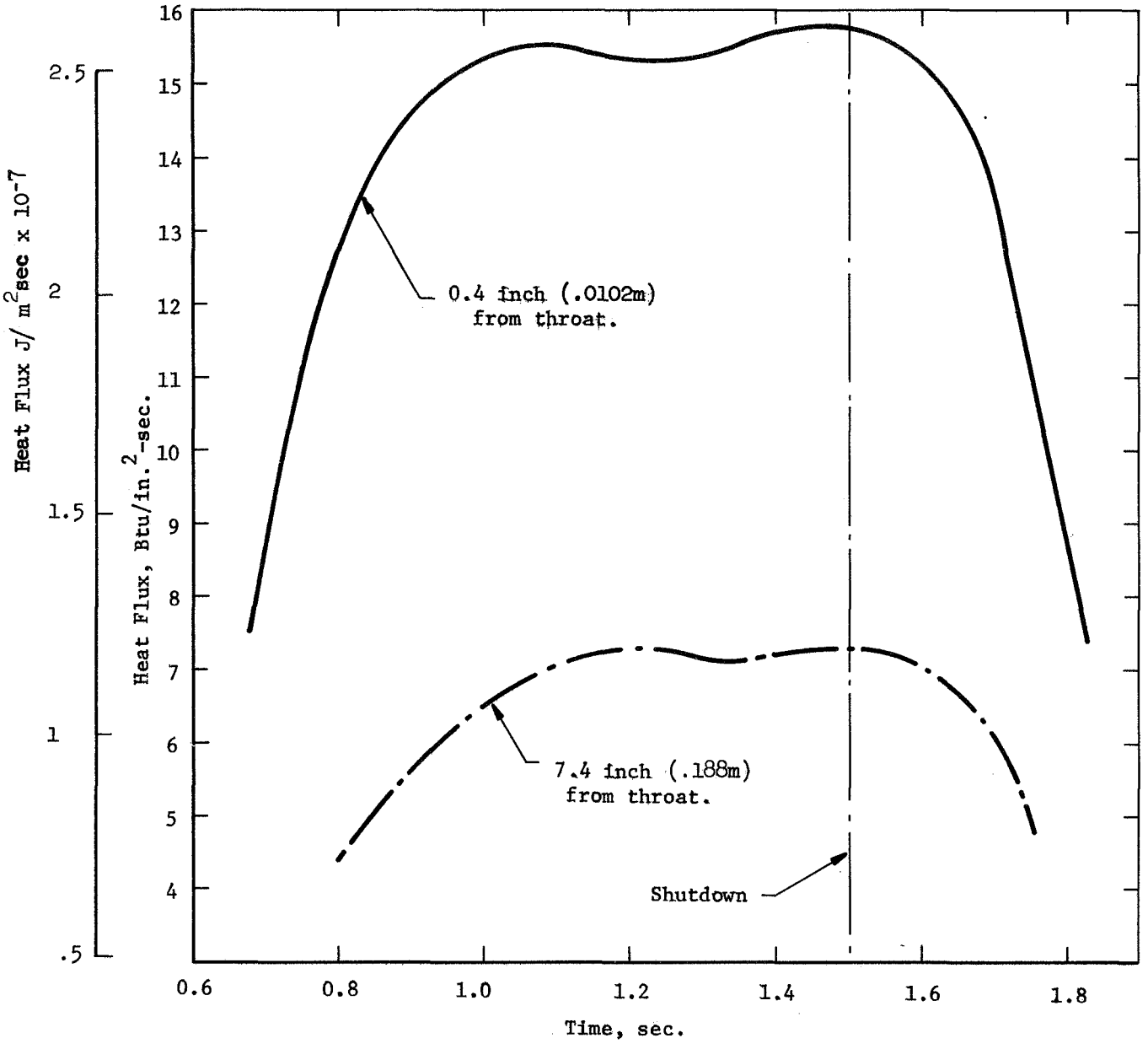

Figure 32. Heat Flux Data from Test 005

calorimeter data having been obtained 0.4-in. (0.0102 m) upstream from the throat, the estimated 20 Btu/in.^{2}-sec (32.8 x 10^6 J/m^2 sec) data appears reasonable.

Two additional checkout tests (006 and 007) were made with the copper heat-sink chamber and the 20-1 injector. Nine additional holes were machined into the rigimesh face to provide further cooling on the injector face. Eight of these holes were placed around the center near the corners of the welds and one was placed in the center of one of the outboard elements.

Test 006 was programmed for 2.5 sec and visual examination of the injector after the test revealed no damage or heat marks. Test 007 was programmed for 4-sec and again, post-test examination revealed that the injector face was in a satisfactory condition. From these tests, it was projected that the injector was satisfactory for the 15 sec duration tests.

Tests 008 and 009 were coating evaluation tests with injector 20-1.

Two flox-methane checkout firings (tests 010 and 011) were made with the nickel-rigimesh face injector (20-2) without the mixing section. The results of these two tests are shown on Table VI. The injector face was satisfactory, as shown on Figure No. 9 without any evidence of damage. Based upon these tests, the nickel-rigimesh-faced injector was deemed satisfactory for long duration firings. Moderate carbon deposition was observed on the injector face and on the inside diameter of the chamber. However, a single 0.75-in. (0.0191 m) oxidizer streak was observed extending from the injector face to the exit. This injector was used for four of the coating tests discussed below.

C. FLOX/METHANE COATING TESTS

Six flox/methane coating tests were made with the water-cooled chamber: two with injector 20-1 and four with injector 20-2. The chamber without the test panel is shown on Figure No. 33. Contoured blocks hold the test panels in position with through bolts. Figure No. 34 illustrates a plasma-sprayed test panel ready for testing. The assembled chamber ready for the test firing is shown on Figure No. 35.

The water flow rate in all of the tests was nominally 6.8 lb/sec (3.1 Kg/sec) in each panel with an inlet pressure of 1150 psia (7.9 x 10^6 N/m^2) and an exit pressure of 430 psia (2.96 x 10^6 N/m^2). The water temperature in the panels increased from 32°F (273°K) to 40°F (278°K) during the test. The predicted exit temperature, based upon the calorimeter data, was 45°F (281°K).

1. Hardware Evaluation

Tests 008 and 009 were made using the N155 rigimesh faced injector (20-1) and the water-cooled thrust chamber. Visual examination of the hardware after test 008 (5.94 sec duration) revealed that the injector

Figure 33. Water-Cooled Chamber without the Test Panels

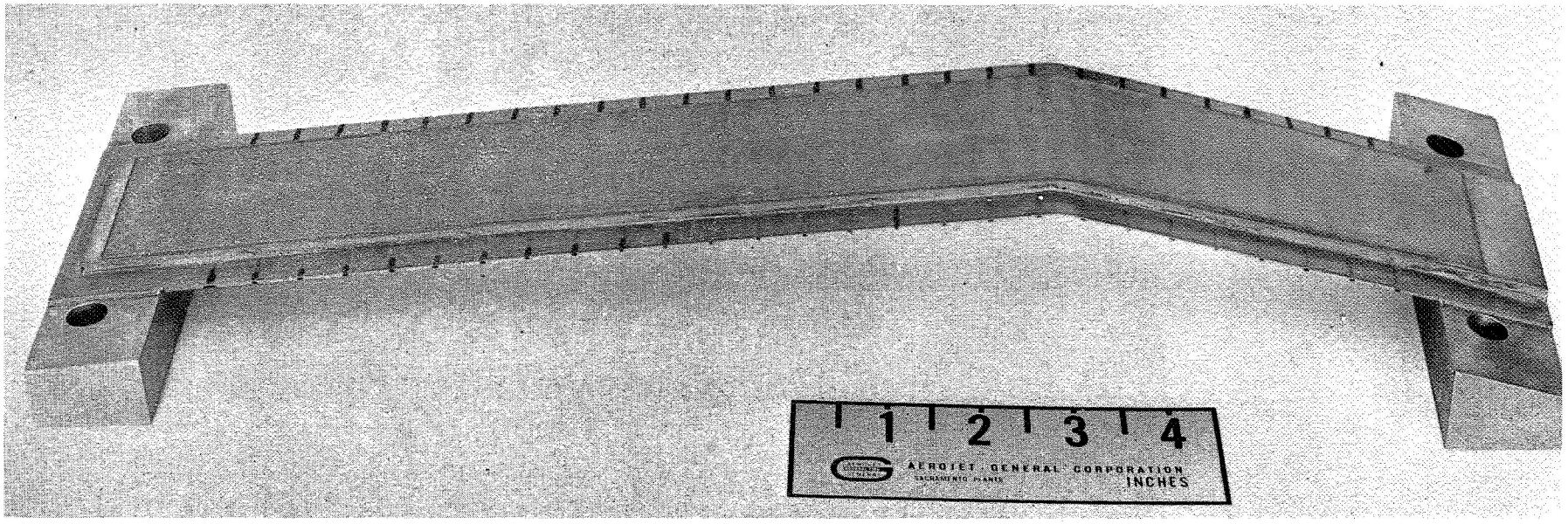

Figure 34. Plasma-Sprayed Test Panel

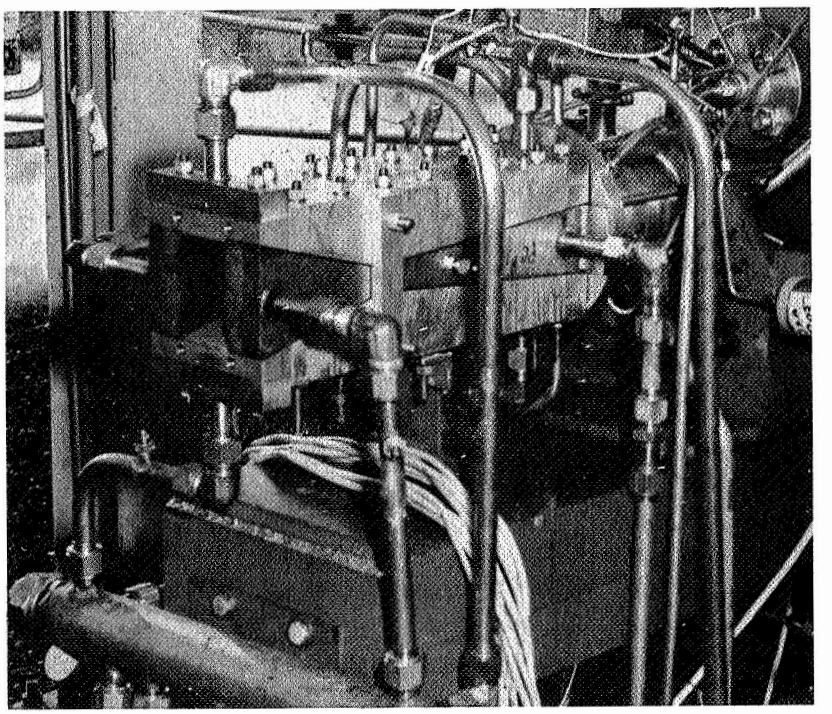

Figure 35. Assembled Test Chamber Prior to Test Firing

face appeared satisfactory with the usual carbon build-up over the entire face. The side panels had oxidizer streaks approximately 5/8-in. (0.0159 m) wide and 5-1/4-in. (0.134 m) long extending from the face of the injector downstream along the chamber (see Figure No. 36). No measurable material loss occurred on the copper side plates in these areas.

Because of the oxidizer streaks, the injector was modified by machining five, 0.015-in. (3.8×10^{-4} m) diameter holes along each side to minimize streaking. The modified injector was evaluated in test 009 (2.5 sec duration). Visual examination of the hardware revealed that melting occurred on the rigimesh in the center of the injector. The rigimesh in these areas apparently had received inadequate gas coolant because of the added holes to prevent streaking. The melted areas were of sufficient size to limit further use of the injector without replacing the rigimesh.

Examination of the hardware after the test revealed that the oxidizer streaks were still apparent indicating that the bleed holes did not eliminate the streaking.

Tests 012 and 013 were made with the Nickel rigimesh faced injector (20-2) which had been previously checked out in tests 010 and 011. The mixing section also was used for these tests. Examination of the hardware on the stand after 012 (8 sec duration) revealed that the injector was in excellent condition and there was no evidence of erosion. The normal carbon build-up occurred on the face during each test. The chamber section had a slight carbon deposit on the inside diameter surface of the chamber and no streaks were observed either on the coated panels or on the copper side plates.

After the visual examination, a retest (013) was made with the same hardware. Post-test examination revealed that there was no apparent streaking on either the chamber section or coated specimens. Also, the injector was in excellent condition. However, a localized water leak occurred at an unknown time during test 013 in the downstream section of the mixer and impinged upon the inside diameter of the chamber walls. Attempts to repair the leak for subsequent tests were not successful and the last two coating tests were conducted without the mixer section.

Tests 014 and 015 were made with a second, water-cooled chamber. Examination of the hardware on the test stand after test 014 (15 sec duration) revealed that the hardware was in excellent condition, but streaking was apparent on the chamber hardware. Next, test 015 was made (30 sec duration) and hardware remained in excellent condition after this test.

2. Coating Evaluation

Plasma-sprayed coatings, consisting of 5 mils (12.7×10^{-5} m) of 55% W and 45% Al_2O_3 and a flame liner of 10 mils (25.4×10^{-5} m) of tungsten were evaluated in the tester. The W-Al_2O_3 layer provided a thermal resistance of 180 in.^{2}-sec-°F/Btu (612×10^{-8} m^2 sec°K/J). With this thermal resistance, the coating operated at a surface temperature of 3000°F (1920°K).

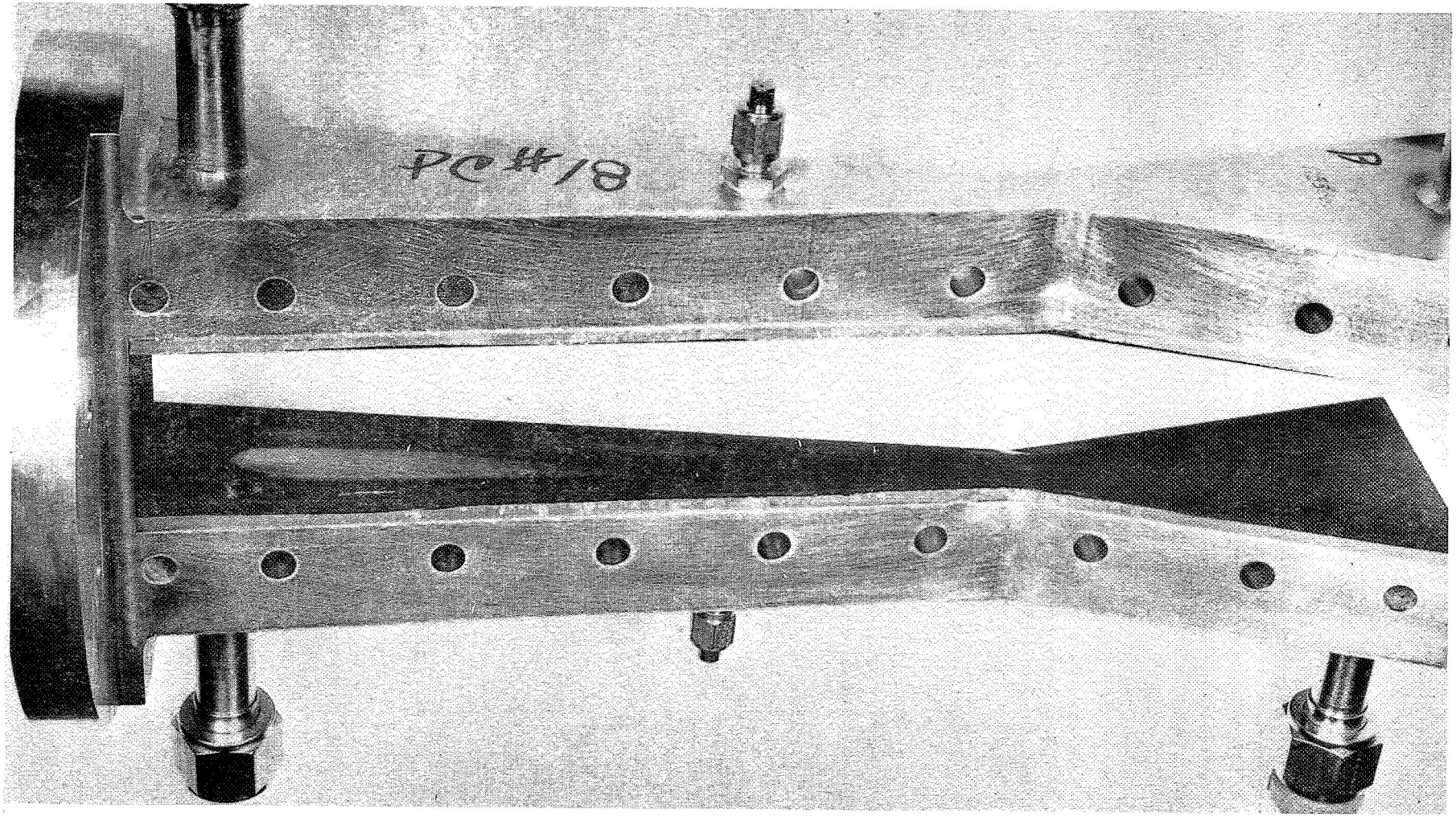

Figure 36. Oxidizer Streak on the Copper Flame Surface of the Flox/Methane Test Chamber

Visual examination of the plasma-sprayed coated panels after test 008 (5.94 sec duration) revealed streaks along the panels in three locations (see Figure 37). The W and W-Al_2O_3 coating in the streaked areas was completely eroded through to the primer. In the non-streaked areas, no measurable material loss was observed. The coated panels were retested for 2.5 sec in test 009. The streaks were extended during this test, but no measurable regression occurred in the non-streaked areas.

The coatings evaluated in tests 012 and 013 consisted of the W-Al_2O_3 undercoat for thermal resistance. In one specimen (No. 17), the tungsten flame liner was plasma-sprayed at Aerojet with a density of 80% to 85%, and the other specimen (No. 7), the tungsten flame liner was plasma-sprayed at Union Carbide with a density of >95%.

Examination of these coatings on the test stand after test 012 (8 sec duration) revealed that Specimen No. 17 was in excellent condition with no visual evidence of cracking or spalling. The coating on Specimen No. 7 was satisfactory except for an approximate 1-in. (0.0254 m) square section at the throat which spalled off during the test. Streaks were not visible on the coated test panels. The coated panels were retested in test 013 (15 sec duration). Coating performance was affected by a water leak in the mixer which flowed into the chamber during the test. Examination of the coatings after the test revealed transverse cracks approximately 1-in. (0.0254 m) apart in the chamber area of both specimens down to the throat. The coatings in both specimens spalled. In Specimen No. 7, approximately 3.0-in. (0.0762 m) of the coating extending upstream from the throat was missing after the test. In Specimen No. 17, a section approximately 1-in. (0.0254 m) wide was spalled from the throat (see Figure No. 38). The remainder of the coating on both specimens was intact.

The total regression of the coating remaining on the Union Carbide specimen (No. 7) was 0.1 mil/sec (2.54×10^{-6} m/sec). For the Aerojet specimen (No. 17), it was 0.13 mil/sec (3.3×10^{-6} m/sec). The water leak in the chamber significantly affected the regression of the tungsten flame liner on both panels.

Tests 014 and 015 were conducted using a second water-cooled chamber consisting of two coated specimens (No. 4-Aerojet and No. 6-Union Carbide) fabricated by the same procedure as were the specimens used in tests 012 and 013. The water-cooled mixer was not used in either test 014 or 015.

Test 014 had a 15 sec duration. The coatings on both specimens contained an oxidizer streak approximately 1-in. (0.0254 m) wide which extended from the injector face down the center of the panel to the exit region (see Figure No. 39). However, apparent regression was observed on the remaining coating and there was no cracking or spalling seen.

Test 015 was a repeat of test 014 except that the duration was increased to 30 sec. Examination of the coated panels again revealed oxidizer streaks extending from the injector face downstream through the throat

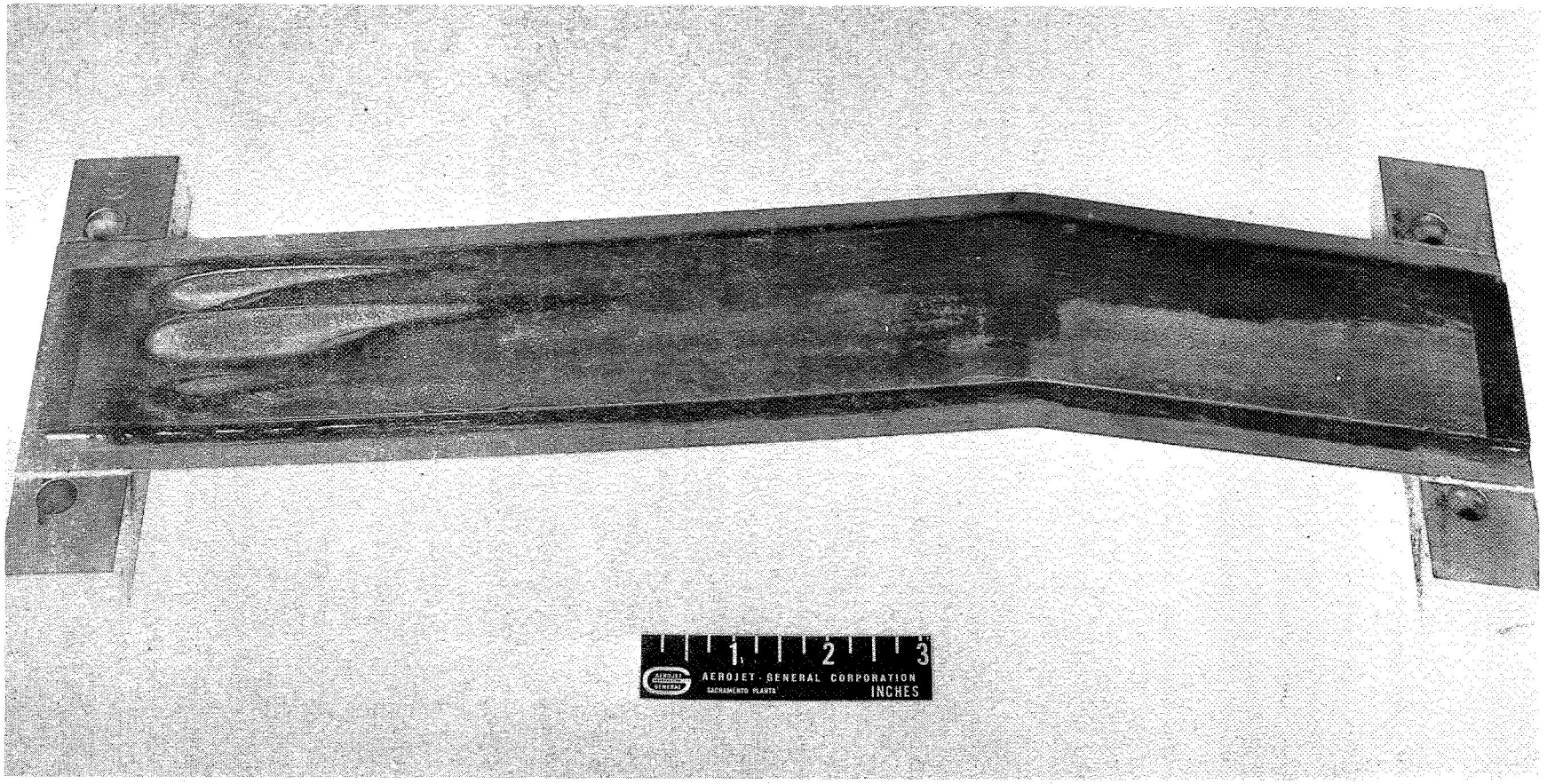

Figure 37. Post-Fire Condition Specimen No. 3 after Exposure to Test 008

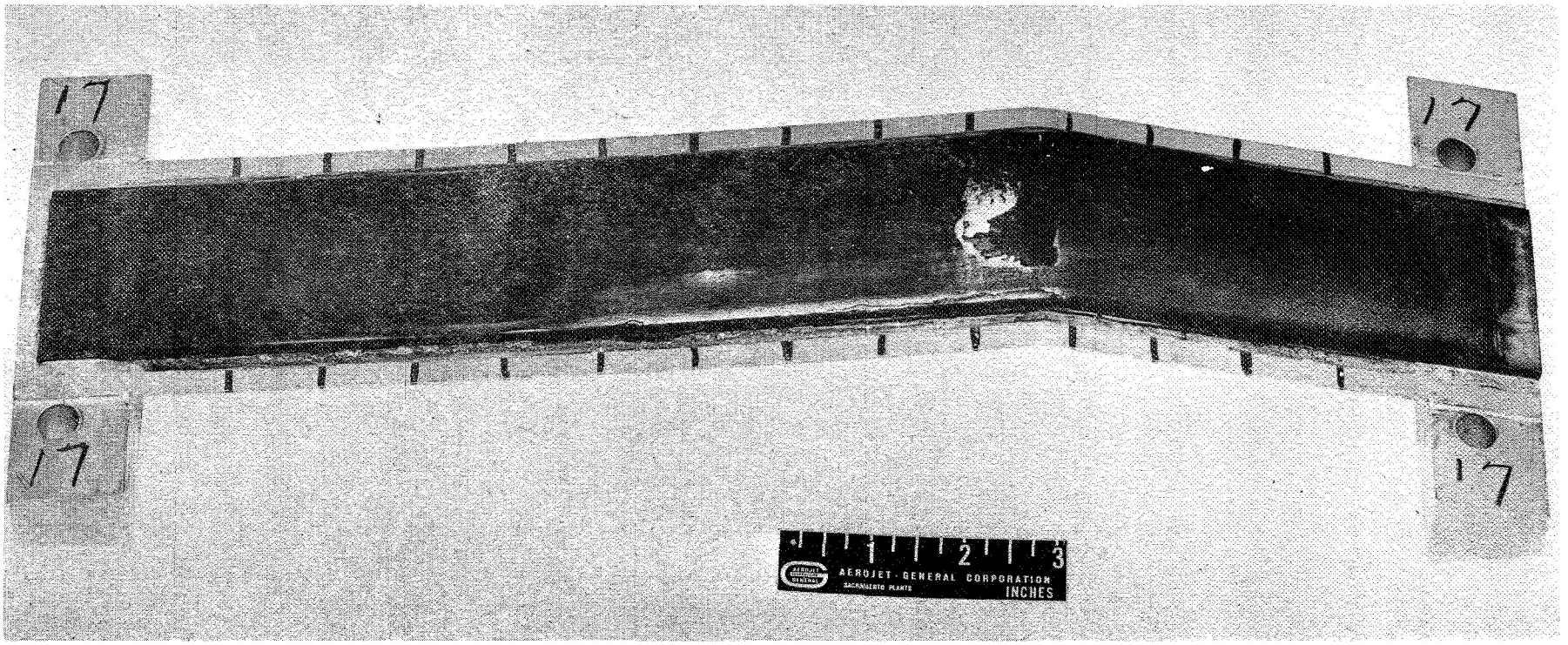

Figure 38. Post-Fire Condition of Specimen No. 17 after Exposure to Tests 012 (8 sec) and 013 (15 sec)

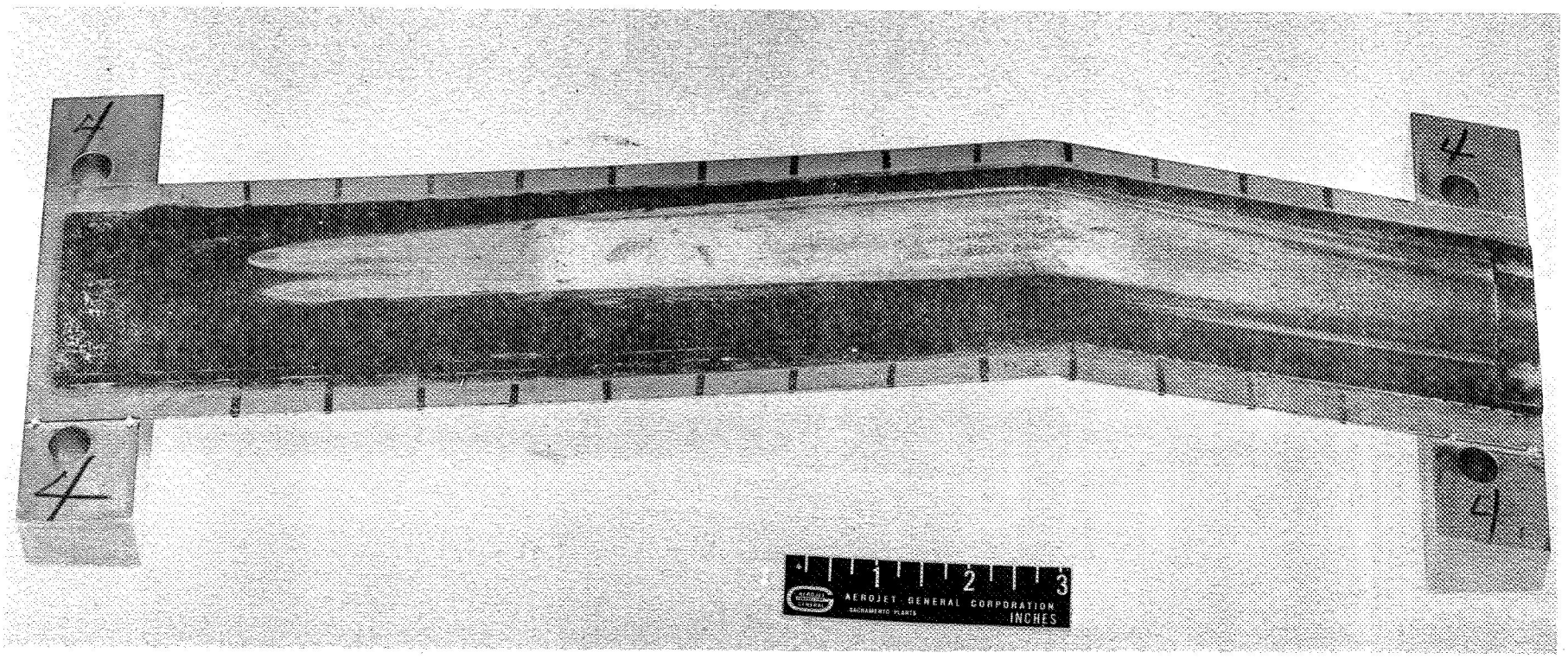

Figure 39. Post-Fire Condition of Specimen No. 4 after Exposure to Tests 014 (15 sec) and 015 (30 sec)

and exit area. In the streaked area, the tungsten and tungsten Al_2O_3 mixture were completely eroded down to the primer on the specimen, but on each side of the streak, the coating was intact. Total regression for the coating in the areas away from the streak for the 45 sec duration was 1 mil (2.54×10^{-5} m) or a regression rate of 0.02 mils/sec (5.08×10^{-7}m/sec) for Specimen No. 4 and 5 mils for Specimen No. 6 or a regression rate of 0.11 mils/sec (28×10^{-7}m/sec).

VI. CONCLUSIONS AND RECOMMENDATIONS

The evaluation of the modified coatings previously described revealed that increasing the density of the tungsten flame liner from 85% to 95% resulted in a decrease in the regression rate of 0.4 mils/sec (1×10^{-5} m/sec) to less than 0.1 mils/sec (2.54×10^{-6} m/sec). The other modifications did not improve regression resistance.

Plasma-sprayed thermal barriers consisting of 5 mils (12.7×10^{-5} m) of 55% W and 45% Al_2O_3 for thermal resistance with a flame liner of tungsten were evaluated in the previously described tester for durations of 8 sec to 30 sec. The coatings operated at a surface temperature of 3000°F (1920°K) and a thermal resistance of 180 in.^{2}-sec-°F/Btu (612×10^{-8} m^2 sec°K/J).

The regression of the tungsten liner in non-streaked areas was 0.02 mils/sec (5×10^{-8} m/sec) for the 95% dense tungsten and 0.1 mils/sec (2.54×10^{-6} m/sec) for 80% dense tungsten. In the streaked areas, the flame liner and undercoat were completely eroded. Spalling also was observed on the coatings.

Based upon these results, further studies are recommended to evaluate improved coatings in the rectangular tester. Coating refinement should be conducted to decrease the spalling observed in the tests. This spalling occurred because of the poor adherence of the tungsten flame liner on the metal-ceramic substrate. At this interface, the tungsten liner is deposited on the sublayer consisting of 55% tungsten by weight, which is actually only 20% tungsten by volume. In plasma-sprayed coatings, the metal does not adhere as well to ceramic substrate as to metal substrates. To minimize spalling, a gradated coating is recommended with increasing metal content from the substrate to the flame surface. This would provide a metal-rich substrate for the application of the tungsten flame liner. Also, the use of a ductile flame liner would minimize the flame liner cracking, but most plasma-sprayed materials are not ductile at room temperature because of the discontinuity in as-sprayed deposits. However, it is estimated that there are differences between the ductile-brittle transition temperature of the various plasma sprayed materials. These differences would be expected to follow the trend in the wrought condition. For example, a ductile-brittle transition temperature for wrought rhenium has not been observed below -300°F (89°K) compared to a transition temperature of 700°F (644°K) for wrought tungsten. Because of the inherent ductility of the rhenium, it would be expected to have usable ductility at a lower temperature than tungsten even in the plasma-sprayed conditions. Therefore, rhenium should be able to withstand the thermal stresses at lower temperatures better than tungsten. It is recommended that rhenium coatings be evaluated for flame liners and compared to tungsten.

REFERENCES

1. Johnson, J. R., et al., Performance of Rocket Nozzle Materials with Several Solid Propellants, NASA Technical Note TND 34228 C.1., May 1966.

2. Coatings for Regenerative Engines, Final Report No. 1, Aerojet-General Corp., Contract NAS 3-7955, NASA CR-72413, 12 July 1968.

3. McIntyre, R. D., Tungsten-Nickel-Copper Ternary Alloys for High Temperature Applications, NASA TND-3015, September 1965.

4. Schmidt, H. W., Fluorine and Fluorine-Oxygen Mixtures in Rocket Systems, NASA SP-3037, 1967.

DISTRIBUTION LIST FOR FINAL REPORT NO. 2

CONTRACT NAS 3-7955

COATINGS FOR REGENERATIVE ENGINES

Report Copies R	D	Recipient	Designee
		National Aeronautics & Space Administration Lewis Research Center 21000 Brookpark Road	
1		Attn: Contracting Officer, MS 500-313	
5		Liquid Rocket Technology Branch MS 500-209	
1		Technical Report Control Office, MS 5-5	
1		Technology Utilization Office, MS 3-16	
2		AFSC Liaison Office, MS 501-3	
2		Library	
1		Office of Reliability & Quality Assurance MS 500-111	
1		D. L. Nored, Chief, LRTB, MS 500-209	
6		R. A. Duscha, Project Manager, MS 500-209	
1		E. W. Conrad, MS 500-204	
1		J. W. Gregory, MS 500-209	
1		S. J. Grisaffe, MS 49-1	
1		A. N. Curren, MS 500-204	
2		Chief, Liquid Experimental Engineering RPX Office of Advanced Research & Technology NASA Headquarters Washington, D.C. 20546	
2		Chief, Liquid Propulsion Technology, RPL Office of Advanced Research & Technology NASA Headquarters Washington, D.C. 20546	
1		Director, Launch Vehicles & Propulsion, SV Office of Space Science & Applications NASA Headquarters Washington, D.C. 20546	
1		Chief, Environmental Factors & Aerodynamics Code RV-1 Office of Advanced Research & Technology NASA Headquarters Washington, D. C. 20546	
1		Chief, Space Vehicles Structures Office of Advanced Research & Technology NASA Headquarters Washington, D.C. 20546	

Report Copies R	D	Recipient	Designee
1		Director, Advanced Manned Missions, MT Office of Manned Space Flight NASA Headquarters Washington, D.C. 20546	
6		NASA Scientific & Technical Information Facility P.O. Box 33 College Park, Maryland 20740	
1		Director, Technology Utilization Division Office of Technology Utilization NASA Headquarters Washington, D.C. 20546	
1		National Aeronautics & Space Administration Ames Research Center Moffett Field, California 94035 Attn: Library	Hans M. Mark Mission Analysis Division
1		National Aeronautics & Space Administration Flight Research Center P.O. Box 273 Edwards, California 93523 Attn: Library	
1		National Aeronautics & Space Administration Goddard Space Flight Center Greenbelt, Maryland 20771 Attn: Library	Merland L. Moseson, Code 620
1		National Aeronautics & Space Administration John F. Kennedy Space Center Cocoa Beach, Florida 32931 Attn: Library	Dr. Kurt H. Debus
1		National Aeronautics & Space Administration Langley Research Center Langley Station Hampton, Virginia 23365 Attn: Library	Ed Cartwright, Director
1		National Aeronautics & Space Administration Manned Spacecraft Center Houston, Texas 77001 Attn: Library	J.G. Thiobodaux, Jr. Chief, Propulsion & Power Division

Report Copies R	D	Recipient	Designee
1		National Aeronautics & Space Administration George C. Marshall Space Flight Center Huntsville, Alabama 35812 Attn: Library	Keith Chandler Hans G. Paul Leon J. Hastings James Thomas E. H. Hyde I. G. Yates Clyde Nevins Robert E. Shannon J. Blumrich
1		Jet Propulsion Laboratory 4800 Oak Grove Drive Pasadena, California 91103 Attn: Library	Henry Burlage, Jr. Duane Dipprey
1		Defense Documentation Center Cameron Station Building 5 5010 Duke Street Alexandria, Virginia 22314 Attn: TISIA	
1		Office of the Director of Defense Research & Engineering Washington, D.C. 20301 Attn: Office of Asst. Dir. (Chem. Technology)	
1		RTD (RTNP) Bolling Air Force Base Washington, D.C. 20332	
1		Arnold Engineering Development Center Air Force Systems Command Tullahoma, Tennessee 37389 Attn: Library	Dr. H. K. Doetsch
1		Advanced Research Projects Agency Washington, D.C. 20525 Attn: Library	
1		Aeronautical Systems Division Air Force Systems Command Wright-Patterson Air Force Base, Dayton, Ohio Attn: Library	D. L. Schmidt Code ARSCNC-2

Report Copies R	D	Recipient	Designee
1		Air Force Missile Test Center Patrick Air Force Base, Florida Attn: Library	L. J. Ullian
1		Air Force Systems Command Andrews Air Force Base Washington, D.C. 20332 Attn: Library	Capt. S. W. Bowen SCLT
1		Air Force Rocket Propulsion Laboratory (RPR) Edwards, California 93523 Attn: Library	
1		Air Force Rocket Propulsion Laboratory (RPM) Edwards, California 93523 Attn: Library	
1		Air Force FTC (FTAT-2) Edwards Air Force, Base, California 93523 Attn: Library	Donald Ross
1		Air Force Office of Scientific Research Washington, D.C. 20333 Attn: Library	SREP, Dr. J. F. Masi
1		Space & Missile Systems Organization Air Force Unit Post Office Los Angeles, California 90045 Attn: Technical Data Center	
1		Office of Research Analyses (OAR) Holloman Air Force Base, New Mexico 88330 Attn: Library - RRRD	
1		U.S. Air Force Washington, D.C. Attn: Library	Col. C. K. Stambaugh, Code AFRST
1		Commanding Officer U.S. Army Research Office (Durham) Box CM, Duke Station Durham, North Carolina 27706 Attn: Library	

Report Copies R	D	Recipient	Designee
1		U.S. Army Missile Command Redstone Scientific Information Center Redstone Arsenal, Alabama 35808 Attn: Document Section	Dr. W. Wharton
1		Bureau of Naval Weapons Department of the Navy Washington, D.C. Attn: Library	J. Kay Code RTMS-41
1		Commander U.S. Naval Missile Center Point Mugu, California 93041 Attn: Technical Library	
1		Commander U.S. Naval Weapons Center China Lake, California 93557 Attn: Library	W. F. Thorm Code 4562
1		Commanding Officer Naval Research Branch Office 1030 E. Green Street Pasadena, California 91101 Attn: Library	
1		Director (Code 6180) U.S. Naval Research Laboratory Washington, D.C. 20390 Attn: Library	H. W. Carhart J. M. Krafft
1		Picatinny Arsenal Dover, New Jersey 07801 Attn: Library	I. Forsten
1		Air Force Aero Propulsion Laboratory Research & Technology Division Air Force Systems Command United States Air Force Wright-Patterson AFB, Ohio 45433 Attn: APRP (Library)	R. Quigley C. M. Donaldson

Report Copies R	D	Recipient	Designee
1		Electronics Division Aerojet-General Corporation P.O. Box 296 Azusa, California 91703 Attn: Library	W. L. Rogers
1		Space Division Aerojet-General Corporation 9200 East Flair Drive El Monte, California 91734 Attn: Library	S. Machlawski
1		Ordnance Division Aerojet-General Corporation 11711 South Woodruff Avenue Downey, California 90241 Attn: Library	
1		Propulsion Division Aerojet-General Corporation P.O. Box 15847 Sacramento, California 95803 Attn: Technical Library 2484-2015A	R. Stiff
1		Aeronutronic Division of Philco Ford Corp. Ford Road Newport Beach, California 92663 Attn: Technical Information Department	Dr. L. H. Linder
1		Aerospace Corporation 2400 E. El Segundo Blvd. Los Angeles, California 90045 Attn: Library-Documents	J. G. Wilder
1		Arthur D. Little, Inc. 20 Acorn Park Cambridge, Massachusetts 02140 Attn: Library	A. C. Tobey
1		Astropower Laboratory McDonnell-Douglas Aircraft Company 2121 Paularino Newport Beach, California 92163 Attn: Library	

Report Copies R	D	Recipient	Designee
1		AFML (Mane, G. F. Schmitt, Jr.) Wright-Patterson AFB, Ohio 45433	
1		ARO, Incorporated Arnold Engineering Development Center Arnold AF Station, Tennessee 37389 Attn: Library	
1		Susquehanna Corporation Atlantic Research Division Shirley Highway & Edsall Road Alexandria, Virginia 22314 Attn: Library	Dr. Ray Friedman
1		Battelle Memorial Institute 505 King Avenue Columbus, Ohio 43201 Attn: Report Library, Room 6A	
1		Beech Aircraft Corporation Boulder Facility Box 631 Boulder, Colorado Attn: Library	Douglas Pope
1		Bell Aerosystems, Inc. Box 1 Buffalo, New York 14205 Attn: Library	T. Reinhardt W. M. Smith
1		Bendix Systems Division Bendix Corporation 3300 Plymouth Street Ann Arbor, Michigan Attn: Library	John M. Brueger
1		Bellcomm 955 L'Eufant Plaza, S.W. Washington, D.C. Attn: Library	H. S. London
1		Boeing Company Space Division P.O. Box 868 Seattle, Washington 98124 Attn: Library	J. D. Alexander C. F. Tiffany

Report Copies R	D	Recipient	Designee
1		Boeing Company 1625 K Street, N.W. Washington, D.C. 20006	
1		Boeing Company P.O. Box 1680 Huntsville, Alabama 35801	Ted Snow
1		Chemical Propulsion Information Agency Applied Physics Laboratory 8621 Georgia Avenue Silver Spring, Maryland 20910	Tom Reedy
1		Chrysler Corporation Missile Division P.O. Box 2628 Detroit, Michigan Attn: Library	John Gates
1		Chrysler Corporation Space Division New Orleans, Louisiana Attn: Librarian	
1		Grumman Aircraft Engineering Corporation Bethpage, Long Island, New York Attn: Libary	Joseph Gavin
1		Hercules Powder Company Allegheny Ballistics Laboratory P.O. Box 210 Cumberland, Maryland 21501 Attn: Library	
1		Honeywell Inc. Aerospace Division 2600 Ridgeway Road Minneapolis, Minnesota Attn: Library	Gordon Harris
1		IIT Research Institute Technology Center Chicago, Illinois 60616 Attn: Library	C. K. Hersh

Report Copies R	D	Recipient	Designee
1		Kidde Aer-Space Division Walter Kidde & Company, Inc. 567 Main Street Belleville, New Jersey	R. J. Hanville
1		Ling-Temco-Vought Corporation P.O. Box 5907 Dallas, Texas 75222 Attn: Library	
1		Lockheed Missiles and Space Company P.O. Box 504 Sunnyvale, California 94087 Attn: Library	
1		Lockheed-California Company 10445 Glen Oaks Blvd., Pacoima, California Attn: Library	
1		Lockheed Propulsion Company P.O. Box 111 Redlands, California 92374 Attn: Library, Thackwell	H. L. Thackwell
1		Marquardt Corporation 16555 Saticoy Street Box 2013 - South Annex Van Nuys, California 91409	L. R. Bell, Jr.
1		Martin-Marietta Corporation (Baltimore Division) Baltimore, Maryland 21203 Attn: Library	
1		Denver Division Martin-Marietta Corporation P.O. Box 179 Denver, Colorado 80201 Attn: Library	Dr. Morganthaler F. R. Schwartzberg
1		Orlando Division Martin-Marietta Corporation Box 5827 Orlando, Florida Attn: Library	J. Fern

Report Copies R	D	Recipient	Designee
1		Western Division McDonnell Douglas Aircraft Company, Inc. 3000 Ocean Park Blvd. Santa Monica, California 90406 Attn: Library	R. W. Hallet G. W. Burke Paul Klevatt
1		McDonnell Douglas Aircraft Corporation P.O. Box 516 Lambert Field, Missouri 63166 Attn: Library	R. A. Herzmark
1		Rocketdyne Division North American Rockwell Inc. 6633 Canoga Avenue Canoga Park, California 91340 Attn: Library, Department 596-306	Dr. R. J. Thompson S. F. Iacobellis
1		Space & Information Systems Division North American Rockwell 12214 Lakewood Blvd. Downey, California Attn: Library	
1		Northrop Space Laboratories 3401 West Broadway Hawthorne, California Attn: Library	Dr. William Howard
1		Purdue University Lafayette, Indiana 47907 Attn: Library (Technical)	Dr. Bruce Reese
1		Radio Corporation of America Astro-Electronics Products Princeton, New Jersey Attn: Library	
1		Rocket Research Corporation Willow Road at 116th Street Redmond, Washington 98052 Attn: Library	F. McCullough, Jr.
1		Stanford Research Institute 333 Ravenswood Avenue Menlo Park, California 94025 Attn: Library	Dr. Gerald Marksman

Report Copies R	D	Recipient	Designee
1		International Harvester Company Solar Division 2200 Pacific Highway San Diego, California 92112 Attn: Library	J. V. Long
1		Thiokol Chemical Corporation Redstone Division Huntsville, Alabama Attn: Library	John Goodloe
1		TRW Systems Inc. 1 Space Park Redondo Beach, California 90278 Attn: STL Tech. Lib. Doc. Acquisitions	Dr. H. Lee
1		TRW Incorporation TAPCO Division 23555 Euclid Avenue Cleveland, Ohio 44117	P. T. Angell
1		United Aircraft Corporation Corporation Library 400 Main Street East Hartford, Connecticut 06108 Attn: Library	Dr. David Rix Erle Martin Frank Owen Wm E. Taylor
1		United Aircraft Corporation Pratt & Whitney Division Florida Reasearch & Development Center P.O. Box 2691 West Palm Beach, Florida 33402 Attn: Library	R. J. Coar Dr. Schmitke
1		United Aircraft Corporation United Technology Center P.O. Box 358 Sunnyvale, California 94038 Attn: Library	Dr. David Altman
1		Vickers Incorporated Box 302 Troy, Michigan	

Report Copies R	D	Recipient	Designee
1		Vought Astronautics Box 5907 Dallas, Texas Attn: Library	
1		Plasmadyne Giannini Scientific Corp. Santa Ana Division 3839 South Main Street Santa Ana, California 92702	J. W. Rosenbery
1	1	Monsanto Research Corp. 1515 Nicholas Road Dayton, Ohio 45407 Attn: Library	R. Janowiecki
1		Union Carbide Corporation Materials System Division 1245 Main Street Indianapolis, Indiana, 46224 Attn: Library	R. L. Wolff